Unsaturated Zone Hydrology for Scientists and Engineers

James A. Tindall, Ph.D.

United States Geological Survey, National Research Program
Department of Geography and Environmental Sciences, University of Colorado Denver

James R. Kunkel, Ph.D., P.E.

Knight Piésold, LLC, Denver, Colorado;
Department of Geology and Geological Engineering, Colorado School of Mines

with

Dean E. Anderson, Ph.D.

United States Geological Survey, National Research Program

PRENTICE HALL
Upper Saddle River, New Jersey 07458

9

Transport of Heat and Gas in Soil and at the Surface

INTRODUCTION

Plant and animal life depend upon the physical processes that govern soil heating, spatial distribution of water, and gaseous exchange between the soil and atmosphere. These interrelated processes are responsible for determining the following: plant and microbial growth rates; rates of decomposition; soil temperature and moisture content; temperature and moisture distribution; evaporation; transpiration; and the gaseous composition of both the soil-air and that of the overlying atmosphere. While soil heating and cooling affect the distribution and movement of water in the unsaturated zone through the processes of condensation and evaporation, soil temperature and moisture can indirectly determine the rate of gaseous exchange between the soil and the atmosphere, thereby influencing the gaseous composition of both soil and atmosphere.

Soil temperature, moisture, and gaseous composition have a tremendous impact on agricultural operations. The rate of soil heating, as well as both the spatial distribution and temporal trends of soil temperature, determines planting and subsequent agronomic schedules. Planting too early (when soils are cool) can delay germination, thereby resulting in a higher potential of seed rot, while planting much later than normal can lead to a shortened growing season, likely decreasing yields. The composition of soil-air can influence biological activity, including plant and root growth. For example, productivity of agricultural crops and forests depends upon soil aeration, that is, the movement of oxygen (O_2) into the soil and subsequent release of carbon dioxide (CO_2) from the soil into the atmosphere. Respiration by plant roots and soil heterotrophs (the microbiological community living within the soil) consumes O_2 and generates CO_2. Typically, plant productivity and root growth are reduced when the volume fraction of O_2 is less than 15 percent and the volume fraction of CO_2 is greater than 5 percent or 50,000 ppm (Rosenberg, Blad, and Verma 1983). In fact, it appears that for well-watered and fertilized crops, the major limitation to attaining optimal growth rates is lack of sufficient soil aeration (Hillel 1982).

"Greenhouse gases" in the atmosphere prevent some of the heat that is radiated upward by the Earth's surface from escaping to space by absorbing it, and then re-radiating some of this energy back toward the Earth's surface. As a result, with solar radiation nearly constant, the total amount of radiant energy received at the surface increases, causing increased surface temperature. Biophysical processes within soil also play an important role in determining climate, by affecting atmospheric concentrations of most greenhouse gases, either through consumption or generation of these gases. While evaporation of soil water can affect water availability for plant growth, it also is an important component of the hydrologic

cycle. Water vapor released into the atmosphere during evaporation from soils can affect climate as a greenhouse gas and by determining the amount of water vapor available for cloud formation and precipitation. Other important greenhouse gases include CO_2, methane (CH_4), and nitrous oxides (NO, N_2O). Although both the burning of fossil fuels and forest clearing result in the greatest proportion of CO_2 in the atmosphere, warm, fertile soils in agricultural use also release significant amounts of CO_2 to the atmosphere (Houghton 1995). It is well documented that saturated soils, such as those found in rice paddies, beaver ponds, and areas seasonally flooded, host production of globally significant amounts of CH_4 (Conrad 1989). While arable lands consume substantial amounts of CH_4, the conversion of forest and pasture lands to intensive agriculture often decreases the strength of this sink (Goulding et al. 1995). Additionally, conversion of forest to agriculture usually results in a several-fold increase in the release of nitrous oxides; emissions of these gases are enhanced following the application of N-based fertilizers (Firestone and Davidson 1989).

As a final point of introduction, radon gas is produced by radioactive-decay reactions in a number of uranium-bearing geologic environments. This gas can diffuse through rock fractures or soil pores, and can enter dwellings via cracks in building foundations. Radon is a suspected carcinogen at low concentrations, and hence poses a public-health risk. Understanding its transport has led to building methods that divert the gas away from buildings, thereby lowering gas concentrations in occupied spaces.

This chapter introduces basic physical principles governing soil heat and gaseous transport, and their mathematical descriptions. Soil heating, evaporation, and gaseous transport are presented together for these reasons: (1) temperature and moisture are linked thermodynamically in both the soil-air and the atmosphere; and (2) soil–gas transport, as well as the generation (or consumption) of soil gases by biological activity, is affected by both soil temperature and moisture distribution. This chapter initially begins with an examination of the modes of energy transfer and the surface-energy budget of the Earth's surface, driven by solar radiation. This radiant energy is responsible for heating the soil, and determines both the spatial and temporal distribution of temperature and water in soil, as well as surface evaporation rates. Its influence is also important in determining the types of vegetation supported by soils. In this vein, the mechanisms responsible for heat and gaseous transport (as well as evaporation) are detailed; this includes an introduction to some of the models used to quantify heat and mass transport in soil. We also examine the role of vegetation in determining soil temperature and moisture. The chapter then proceeds with a discussion of the role of biology (plants and microbes) in the development of soil-air composition, describing the instrumentation and methodologies that help us quantify temperature distribution as well as the fluxes of heat, water vapor, and other gases.

9.1 BASIC CONCEPTS AND DEFINITIONS

Energy Transfer and Heat Content

Energy may be transferred from place to place by some combination of the following three processes:

1. **Conduction**—kinetic energy is transferred from molecule to molecule through physical contact;
2. **Convection**—a mass having some level of kinetic energy is transported from one place to another;
3. **Radiation**—electromagnetic energy is emitted from one object, transmitted through space, and is then received by another.

All three of these processes are relevant to the study of heat transport in soil. The Sun's radiant energy heats the soil's surface; surface heat is transferred to the subsurface by conduction, and to the air by convection.

Any mass composed of molecules that have kinetic energy is considered to have heat. If an object with an initially warmer temperature (T_i) is placed in contact with an object that has a cooler temperature (T_o), heat will flow from the warmer object to the cooler object until an equilibrium is reached, such that both objects are at the same temperature, T_f (where $T_i > T_f > T_o$). The initially warmer object loses a quantity of heat, ΔH:

$$\Delta H = -C(T_f - T_i) \tag{9.1}$$

where C is the heat capacity (J K^{-1}). C is considered either on a per-unit-mass or per-unit-volume basis; that is, mass (J kg^{-1} K^{-1}) or volume-specific heat capacity (J m^{-3} K^{-1}). Specific heats of common materials and soils are given in table 9.1.

Evaporation and Condensation

The term evaporation generally refers to the volatilization of water, in which the phase change from liquid to vapor occurs. For example, consider a body of water consisting of molecules in a constant state of random motion. These molecules are bound by a weak physical attraction between them that diminishes with the sixth power of the distance known as Van der Waal's forces. At any given moment, the kinetic energy of these water molecules results in a certain number of molecules gaining enough energy to leave the surface of the body of water. In order to do so, they must gain energy equivalent to their mass times the latent heat of vaporization (L_v) from the water. These molecules are now in a gaseous state, called water vapor; the pressure exerted by this gas is called vapor pressure. At the same time, a certain number of water molecules that are in the air are driven to the water's surface when they collide with other air molecules; subsequently, they lose their energy to liquid water molecules when they release a quantity of heat (mass times L_v). If the number of molecules that leave the water equals the number of molecules that return, the system is in equilibrium, and the overlying air is considered saturated with water vapor at that temperature. The pressure exerted by water vapor at equilibrium is the saturated vapor pressure. The evaporation rate is zero in this case, but would be nonzero if more molecules left the water than returned. Condensation is the reverse of evaporation—more molecules leave the gaseous state than enter it. Thus, both evaporation and condensation are continuous processes.

TABLE 9.1 Thermal Properties of Common Materials and Soils

Substance	Density (kg m^{-3})	Specific heat capacity (J kg^{-1} K^{-1})	Volumetric heat capacity (J m^{-3} K^{-1})	Thermal conductivity (W m^{-1} K^{-1})
Air (20 °C)	1.2	1.0×10^3	1.2×10^3	0.025
Water (20 °C)	1.0×10^3	4.2×10^3	4.2×10^6	0.58
Ice (0 °C)	9.2×10^3	2.1×10^3	1.9×10^6	2.2
Quartz	2.66×10^3	8.0×10^2	2.0×10^6	8.8
Mineral clay	2.65×10^3	8.0×10^2	2.0×10^6	2.9
Soil organic matter	1.3×10^3	2.5×10^3	2.7×10^6	0.25
Light soil with roots	4.0×10^2	1.3×10^3	5.0×10^5	0.11
Wet sand ($\theta = .4$)	1.6×10^3	1.7×10^3	2.7×10^6	1.8

Source: Data from de Vries (1963) and Rosenberg, Blad, and Verma (1983).

There are four requirements that must be met for soil evaporation to occur: (1) a supply of water; (2) a supply of heat to enable the phase change of water to vapor; (3) a vapor-pressure gradient such that the overlying air contains fewer vapor molecules than if the air were saturated; and (4) turbulence in the overlying atmosphere that carries vapor away from the surface, thus maintaining a vapor-pressure gradient between the soil and the atmosphere.

At times, in both temperate and arctic soils, water can be found in all three phases. As previously described, for water to become water vapor, a quantity of energy (mass of water times L_v) must be supplied to the water body ($L_v = 2.5$ [MJ kg^{-1}] $- 2.37 \times 10^{-3}\ T$[MJ · kg^{-1} °C^{-1}]; where T is temperature (°C)). This heat is obtained from the water and its surroundings, thereby cooling them. For ice to melt, energy equivalent to the latent heat of fusion ($L_m = 0.34$ MJ kg^{-1}) is needed; however, water molecules in the solid phase do not necessarily have to make the transition to liquid, to become vapor. At temperatures below freezing, solid-phase water molecules can obtain sufficient energy to reach the vapor phase, but in order to do this they have to obtain the latent heat of sublimation ($L_s = L_m + L_v$), which at 0 °C is 2.84 MJ kg^{-1}. As shown in a phase diagram such as figure 9.1, at 273 K and a vapor pressure of 0.611 kPa (the "triple point," point A in the diagram), all three phases of water can exist at the same time. Water can exist as a liquid (if it is pure) at temperatures as low as −40 °C, provided it does not come into contact with a solid of a crystalline structure similar to ice; below about −40 °C, water undergoes spontaneous self-crystallization to ice. Curve segment *A–B* (see figure 9.1, inset) shows the distinction between saturation vapor pressure over water and over ice. Note that below freezing, the saturation vapor pressure over water (solid line) is greater than that over ice (dotted line). Above 273 K, curve segment *A–C* becomes the saturation-vapor pressure curve discussed earlier. At the boiling point of water (100 °C at sea level), saturation vapor pressure is 1 atmosphere (101.325 kPa). By increasing the pressure of an enclosed system, equilibrium saturation vapor pressure and boiling point may be increased. Curve segment *A–D* is the latent heat of fusion (melting/freezing), showing the dependence of water's phase on pressure.

The phase diagram of figure 9.1 helps us to realize the significance of phase changes (determined by temperature) as an important variable in controlling the movement of water in soil. Consider the following: Due to the net loss of longwave radiation at night, the soil's surface cools to the dew-point temperature (T_{DP}), the temperature at which air in contact

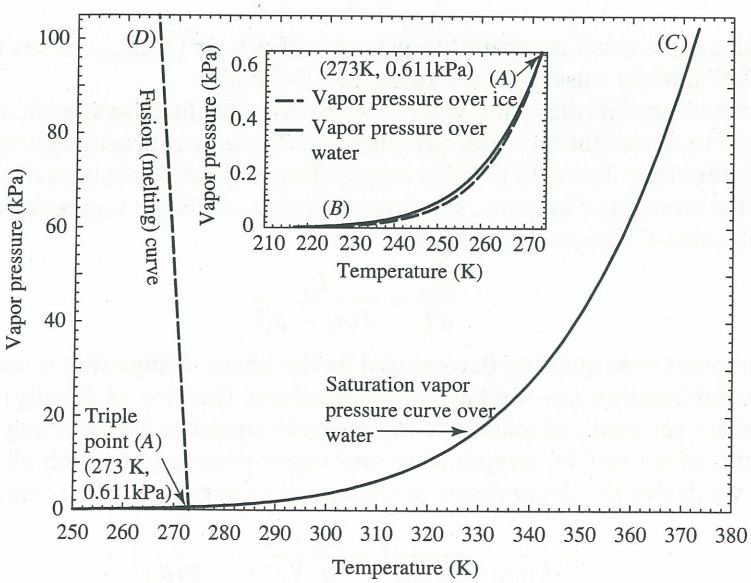

Figure 9.1 Phase diagram for water at standard pressure (101.325 kPa). Saturation vapor pressure curve (segment *A–C*) extends from the "triple point" (273 K) to the boiling point (373 K), and theoretically extends below freezing (segment *A–B*) to 0 K. The saturation vapor pressure curve over ice (segment *A–B*, dotted line) extends below that for vapor, along which sublimation occurs. Melting (or freezing) occurs along curve segment *A–D*.

with the soil cools to the saturation vapor pressure. As the soil continues to cool, water vapor from the atmosphere condenses onto the soil, forming dew and releasing heat to the soil; soil-air also has a dew-point temperature that can be different from that of the atmosphere. Given sufficient permeability of the soil crust, water vapor from within the soil can condense onto the subsurface of the crust, or even further below the crust if the soil temperature becomes cool enough. If the soil's surface cools enough to freeze, water tends to migrate by vapor-phase transport from the liquid water mass (below the ice) to the ice at the surface, because the saturation vapor pressure over ice is lower than that over water. However, it should be noted that, in contrast to the liquid phase, water vapor can move just as easily in any direction—vertical or horizontal—and that the direction of its movement is determined solely by the gradient in vapor pressure.

To summarize, water and heat are almost always in a state of transition. They are thermodynamically linked via water's ability to change phase through some combination of the following: evaporation; condensation; melting; freezing; or sublimation. Each change of phase involves a release or absorption of energy between water and its surroundings. For instance, energy needed for evaporation within soil is derived from the soil mass, thereby cooling it. Finally, we stress that the movement of water vapor is driven by gradients of both humidity and temperature.

QUESTION 9.1

In a closed soil column having a temperature of −10 °C at one end and 5 °C at the other, soil-water content (in the form of ice) was observed to increase at one end while moisture content, at the other end, decreased. Explain why.

Quantifying Water Content in Air

So far, we have described water vapor qualitatively. Using the terms discussed in the following text, we obtain the means for quantifying water vapor.

Water vapor is a component of ambient air; we speak of its partial pressure as vapor pressure. We can write Dalton's Law of partial pressures (discussed in detail in section 9.7) as:

$$P_{\text{total}} = P_{\text{dryair}} + e \tag{9.2}$$

Vapor pressure (e) is small compared to pressure of dry air (P_{dryair}). At sea level, P_{total} averages 101.325 kPa, while e usually has a range of 0.5–3.0 kPa.

Water vapor equilibrates with water in a steady-state closed system at a vapor pressure; this is referred to as saturation vapor pressure (e_s). There is a direct physical dependence of e_s on temperature (see figure 9.1), which can be derived from basic laws of thermodynamics by invoking the concept of entropy. The rate of change of e_s with temperature (T) is quantified in the Clausius–Clapeyron equation:

$$\frac{de_s}{dT} = \frac{L_x}{T(a_2 - a_1)} \tag{9.3}$$

where L_x is a latent heat quantity determined by the phase change that is occurring—vaporization (v) or sublimation (s)—and a is specific volume (inverse of density), with subscripts identifying phase (or state) of matter. If we integrate equation 9.3, inserting the constants at the triple point of water (the temperature and vapor pressure at which all three phases of water exist), we derive the dependence of saturation vapor pressure on temperature:

$$\ln\left(\frac{e_s}{0.6108[\text{kPa}]}\right) = \frac{L_x}{R_v}\left(\frac{1}{273} - \frac{1}{T[\text{K}]}\right) \tag{9.4}$$

where R_v is the gas constant for water vapor (461.5 J kg^{-1} K^{-1}), derived by dividing the universal gas constant (R^* = 8.3144 J mol^{-1} K^{-1}) by the molecular weight of water (m_v = 0.018016 kg mol^{-1}). The solution for e_s in equation 9.4 may be approximated (above 80 kPa total pressure) with Teten's empirical formula (1930):

$$e_s[\text{kPa}] = 0.6108 \times 10^{7.5T[°\text{C}]/(T[°\text{C}]+237.3)} \tag{9.5}$$

We find somewhat better accuracy for a range of temperatures (−50 to +50 °C) using Buck's relation (1981):

$$e_s\,[\text{kPa}] = 0.61365\, exp\,(17502T[°\text{C}]/(240.97 + T[°\text{C}]) \tag{9.6}$$

Where exp is the exponential function.

The consideration of saturated conditions gives us a relative basis for gauging humidity or water content in air. The ratio of vapor pressure in air to saturated vapor pressure at the same temperature is known as relative humidity (rH):

$$\text{rH}(\%) = \frac{e}{e_s} \times 100 \tag{9.7}$$

Note that for any fixed rH there exists a range of water contents (or vapor pressures), if the temperature is allowed to vary (see figure 9.2). That is, relative humidity is a function of vapor pressure and temperature; it does not quantify the amount (mass) of moisture in air. One way of expressing the amount of water-vapor mass in air is by using absolute humidity

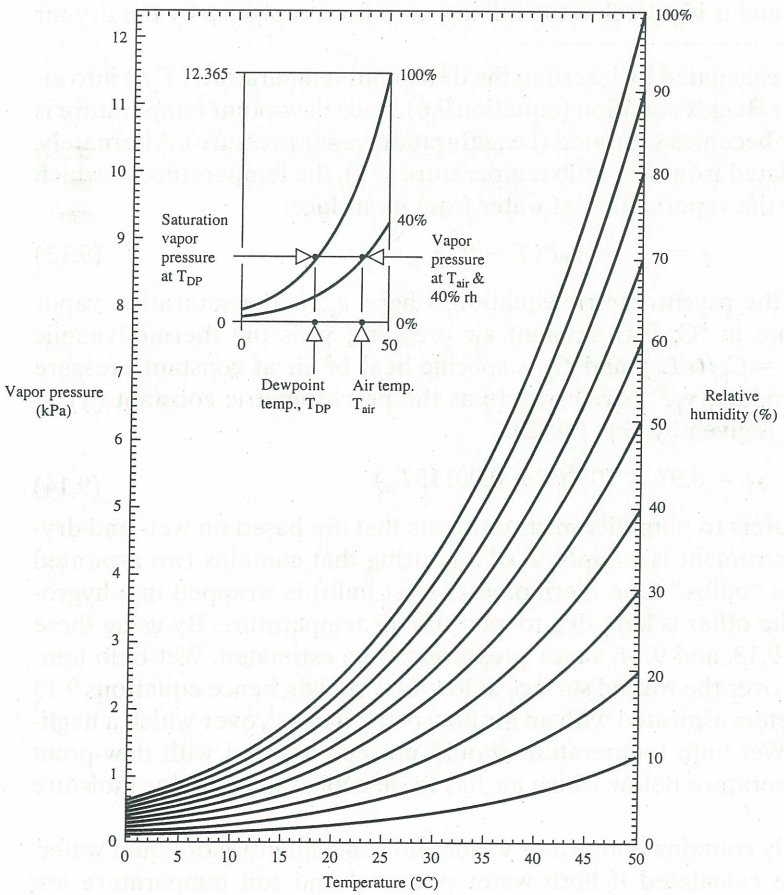

Figure 9.2 Psychrometric chart depicting the relation between relative humidity, vapor pressure, temperature, and dew-point temperature

or vapor density (kg m^{-3}):

$$\rho_v = \frac{e}{R_V T} = \frac{m_v e}{R^* T} = \frac{\varepsilon e}{RT} \tag{9.8}$$

where

$$\varepsilon = \frac{m_v}{m_d} \tag{9.9}$$

R (R^*/m_d) is the dry-air gas constant and m_d is the molecular weight of dry air (0.028996 kg mol^{-1}). If vapor pressure is known, absolute humidity can be calculated from

$$\rho_v[\text{kg m}^{-3}] = \frac{e[\text{Pa}]}{461.5[\text{J kg}^{-1}\text{K}^{-1}] \times (T[\text{K}])} \tag{9.10}$$

A related quantity, specific humidity (unitless), is given by this ratio:

$$q = \frac{\rho_v}{\rho} \tag{9.11}$$

where

$$\rho = \frac{mP_{\text{total}}}{R^* T} \tag{9.12}$$

and m is the molecular weight of moist air. Specific humidity is approximately equal to the mixing ratio of vapor in air, and is identical to the mixing ratio if we replace ρ by the dry-air density in equation 9.11.

Vapor pressure can be calculated by inserting the dew-point temperature (T_{DP}) into either Teten's (equation 9.5) or Buck's equation (equation 9.6), since dew-point temperature is the temperature at which air becomes saturated (i.e., saturation vapor pressure). Alternately, vapor pressure can be calculated from wet-bulb temperature (T_{w}), the temperature to which a wetted object cools due to the vaporization of water from its surface:

$$e = e_{\text{sw}} - \gamma_T P(T - T_{\text{w}}) \tag{9.13}$$

Equation 9.13 is known as the psychrometric equation, where: e_{sw} is the saturation vapor pressure at T_{w}; T and T_{w} are in °C; P is ambient air pressure; γ_T is the thermodynamic psychrometric constant ($\gamma_T = C_{\text{p}}/(\varepsilon L_v)$, and C_{p} is specific heat of air at constant pressure (1.005 kJ kg^{-1} K^{-1}). The product, $\gamma_T P$, is referred to as the psychrometric constant (γ). A handy approximation for γ_T is given by Gay (1972):

$$\gamma_T = 6.97 \times 10^{-4}(1 + 0.00115T_{\text{w}}) \tag{9.14}$$

The term "wet bulb" refers to humidity measurements that are based on wet- and dry-bulb psychrometers. This instrument is composed of a housing that contains two aspirated thermometers, referred to as "bulbs." One thermometer (wet bulb) is wrapped in a hygroscopic, wetted cloth, while the other is kept dry, to measure air temperature. By using these readings and equations 9.6, 9.13, and 9.14, vapor pressure can be estimated. Wet-bulb temperature varies with air flow over the wetted surface at low-flow speeds, hence equations 9.13 and 9.14 apply to psychrometers aspirated with an air flow of 4–10 m s^{-1}, over which a negligible change in T_{w} occurs. Wet-bulb temperature should not be confused with dew-point temperature (T_{DP}), the temperature below which air has to be cooled in order for moisture to condense out of it.

Unsaturated soil usually contains both water vapor and some quantity of liquid water. Water-vapor content can be calculated if both water potential and soil temperature are

known. Vapor density can be calculated directly from:

$$\rho_v = \rho_{vs} exp(\psi / R_v T) \tag{9.15}$$

where ρ_{vs} is saturation vapor density, and ψ is water potential (J kg^{-1}). More often we want to know ψ, having some measure of humidity. Solving equation 9.15 for ψ yields the Kelvin equation:

$$\psi = R_v T \ln\left(\frac{e}{e_s}\right) \tag{9.16}$$

A deep, uniform soil that is initially wetted and allowed to drain for several days typically has a ψ of about -30 J kg^{-1}. The permanent wilting point of many plants is typically below $-2{,}000$ J kg^{-1} (equivalent to $-2{,}000$ kPa or -2 MPa), and is about $-1{,}500$ J kg^{-1} for agricultural crops. Even at this point, soil air is humid compared to that usually found in the atmosphere; at the permanent wilting point, soil air at 25 °C has a relative humidity of about 99 percent. Relative humidities sometimes fall below 95 percent in soils, but only in arid regions (Loskot, Rousseau, and Kurzmack 1994). Therefore, over typical soil-moisture ranges, equation 9.16 can be closely approximated by:

$$\psi[\text{J kg}^{-1}] = 461.5 \times T[\text{K}]\left(\frac{e}{e_s} - 1\right) \tag{9.17}$$

QUESTION 9.2

For a fixed amount of moisture in the air, how does rH change with increasing T?

Measurement of soil-air temperature Temperature is often measured with either a thermistor, RTD (resistance-temperature device), or thermocouple. In choosing a sensor, there are a number of factors to consider: sensor stability (i.e., minimal drift in output or calibration); resolution; accuracy; and cost.

Thermistors are specialized variable resistors whose electrical resistance varies strongly with temperature, in a predictable way; voltage drop across the thermistor is calibrated to temperature. Thermistors have an advantage over RTDs or thermocouples because of their adjustable-voltage output and low cost. A brief description of these sensors is given below, details are given in Fritschen and Gay (1979).

RTDs are of two types: thin metal film, or wire-wound (usually platinum wire). Resistance of RTDs strongly varies with temperature; therefore, the principle of temperature measurement with RTDs is similar to that of thermistors. However, in contrast to thermistors, RTDs are quite stable, generally offer a larger temperature measurement range, but are somewhat more expensive.

Thermocouples are welded junctions of dissimilar metals, across which a weak electrical potential develops as a function of temperature (see tables 9.2 and 9.3). Thermocouple

TABLE 9.2 Thermocouple Sensitivity to Temperature

Thermocouple	ISA symbol	Sensitivity (μV °C^{-1})
Chromel (P)–constantan	E	6.32
Iron–constantan	J	5.27
Chromel (P)–alumel	K	4.10
Copper–constantan	T	4.28

TABLE 9.3 Elemental Composition of Metals Used in Thermocouples

Alumel	95% nickel, 2% manganese, 2% aluminum
Chromel	90% nickel, 10% chromium
Constantan	55% copper, 45% nickel
Evanohm	75% nickel, 20% chromium, 2.5% copper, 2.5% aluminum

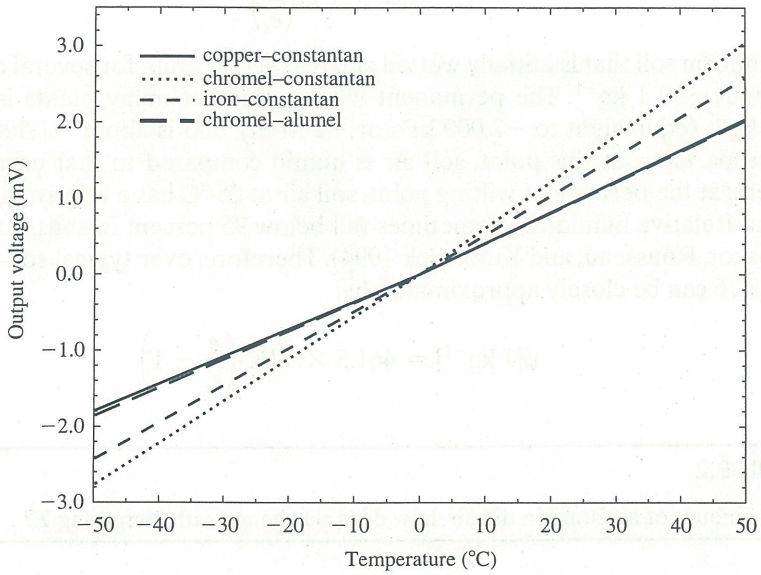

Figure 9.3 Voltage output as a function of temperature for commonly used thermocouples

junctions can be built using a variety of metals whose sensitivities to temperature differ (see figure 9.3). To measure temperature, two thermocouples are connected in series. A reference junction is maintained at 0 °C, to yield a constant voltage. Voltage across the sample-sensing junction increases with temperature when measured with respect to the reference junction in the same circuit. More often, a precision microvolt source is used rather than a reference junction, to produce the required reference voltage. Due to very weak thermocouple output (on the order of microamps and microvolts), a high-impedance, high-precision, voltmeter is needed to measure output accurately. In addition, the sampling junction must be electrically isolated from soil (usually encased in a Teflon shield), to prevent electrical-ground loops. While most thermocouples are inexpensive and can be built with minimal equipment costs, they also have the potential to provide measurements with high accuracy and resolution.

Measurement of humidity (water potential) Soil-air humidity is difficult to measure accurately in situ, yet its determination is often essential in interpreting water potential in unsaturated soil; this assumes the vapor phase of moisture is in equilibrium with the liquid phase. Frequently, a soil psychrometer, as shown in figure 9.4 (see Spanner 1951; Rawlins and Campbell 1986), or a soil dew-point hygrometer (Neumann and Thurtell 1972) is used to obtain water potential. Both instruments employ thermocouples and are unaspirated; however, their procedures for obtaining water potential differ.

Calculating water potential from a soil psychrometer involves the measurement of both dry- and wet-bulb temperatures. Typically, one of the psychrometer's thermocouple junctions is cooled by the Peltier effect (i.e., the current flow through a thermocouple junction is reversed), thereby water condenses onto it; temperature of the wetted thermocouple is the wet-bulb temperature. However, the evaporation of water droplets from the unaspirated pyschrometer's wet bulb is a function of both droplet shape and size, and in turn somewhat

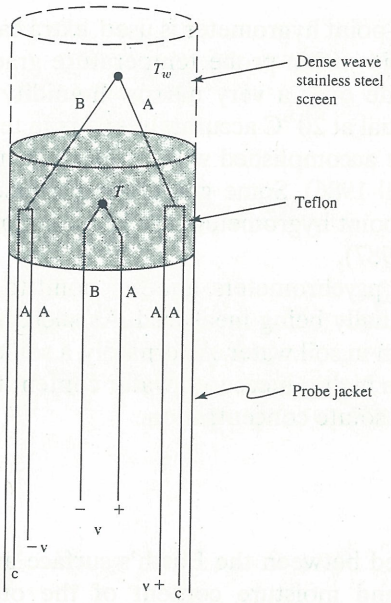

Figure 9.4 Diagram of a soil psychrometer for measurement of soil-air humidity. Thermocouples are used to measure air temperature (dry bulb, T), and wet-bulb (T_w) or dew-point temperature (T_{DP}), from humidity is calculated. Wires A (usually copper) and B differ in elemental composition. The screen is of high density, to prevent the entrance of water; the Teflon block helps to eliminate temperature differences between dry junctions. Switchable voltage is applied to the wet bulb thermocouple loop at points C so that current runs opposite to that of the thermocouple circuit, cooling the T_w junction and condensing water onto it. Voltage is read off of loops at points $v(+, -)$.

dependent upon soil-air humidity. Thus, wet-bulb depression ($T - T_w$) cannot readily be used to determine humidity and water potential when using the combination of equations 9.13 and 9.16. Instead, a strictly empirical approach is usually employed.

Following the procedure of Loskot, Rousseau, and Kurzmack (1994), the psychrometer probe (with both dry- and wet-bulb thermocouples) is outfitted with a tightly woven metal screen that prevents water seepage into the thermocouples. Since saturation vapor pressure varies as a function of osmolality and temperature, normally this instrument is calibrated by immersing it in a series of salt solutions with varying molality. Alternately, the probe can be enclosed in a small, sealed chamber that contains the forementioned solutions, and the procedure is duplicated at various temperatures. The final product is a family of calibration curves spanning a range of humidities that encompass the anticipated range of environmental conditions; humidity is found by interpolating between these calibration curves with psychrometer voltage. A procedure outlined in Rawlins and Campbell (1986) substantially reduced the number of humidity calibrations required when using the empirical approach described above. This reduction is achieved by using equation 9.16 as well as a semi-empirical equation based on the conventional psychrometer equation. When this approach is followed, water potential can be calculated directly from the psychrometer voltage without the necessity for interpolation between calibration curves. Details of some salt-solution preparations can be found in Brown and Van Haveren (1971), Rawlins and Campbell (1986), or Loskot, Rousseau, and Kurzmack (1994).

Neumann and Thurtell (1972) introduced a modification of the wet-bulb psychrometer (called a thermocouple dew-point hygrometer), that improved the accuracy of humidity measurements. This instrument measures dew-point temperature in an iterative process. First, a thermocouple is cooled until moisture condenses onto it. Next (as with the psychrometer), the wetted thermocouple's temperature is measured until all the water on it is reevaporated. During several more cycles, the junction is allowed to cool and warm repeatedly, but in each iteration cooling and heating cycles are shortened, thereby approaching the precise temperature of condensation, the dew point. The dew-point hygrometer has the advantage of negligibly disturbing the natural soil-moisture distribution, and is 2 to 5 times more accurate than soil psychrometers (Brunini and Thurtell 1982; Rawlins and Campbell 1986).

Whether a soil psychrometer or dew-point hygrometer is used, extra care is essential to measure temperature accurately and avoid within-probe temperature gradients, since humidity measurements are frequently made over a very narrow humidity range (99% to 100%). To resolve a 10 J kg^{-1} water potential at 20 °C accurately, errors in temperature measurement must be < 0.001 °C. This can be accomplished with proper selection of materials and probe design (Rawlins and Campbell 1986). Some guidelines for assessing errors involved with soil psychrometers and dew-point hygrometers are given in Savage, Cases, and de Jager (1983), and Savage and Wiebe (1987).

When measuring soil moisture with psychrometers, another point to keep in mind is that it is the osmotic potential that is actually being measured. As such, humidity will decrease with increasing solute concentration in soil water. Alternately, a soil containing water with a low solute concentration will have a higher measured water content than one with an identical amount of water but with higher solute concentration.

9.2 ENERGY EXCHANGES AT THE SURFACE

Heat and water are continually exchanged between the Earth's surface and the overlying atmosphere; each influences the heat and moisture content of the other (Entekhabi, Rodriguez-Iturbe, and Castelli 1996). Solar energy heats the Earth's surface, including the soil. Heat, water vapor (from evaporation of surface and subsurface water), and other gases are transported to (or from) the surface by a variety of air motions. Transport from the surface occurs across two distinct air layers. Adjacent to every surface is a layer (a few millimeters thick) called the laminar sublayer in which heat, water vapor, and other gases are carried to and from the surface by molecular motions. Laminar flow is well organized, but both heat and mass transfer within it are slow compared to the turbulent sublayer immediately above (see figure 9.5(a)), that is dominated by turbulent motions (eddies). Together, the laminar

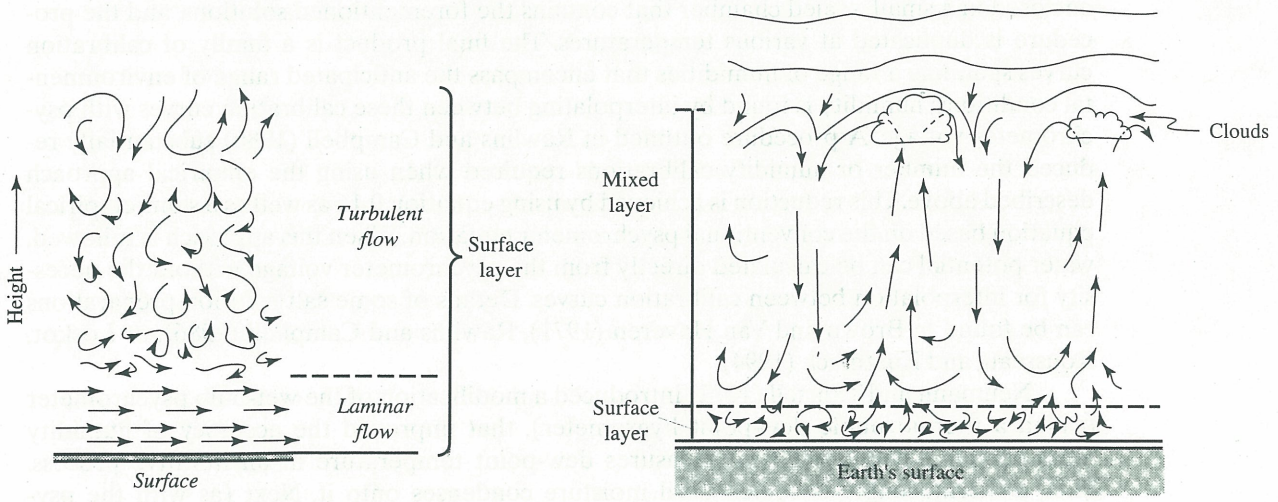

Figure 9.5 Conceptual diagram of the surface layer (a), divided into laminar and turbulent sublayers. Arrows indicate characteristics and direction of air movement. The laminar sublayer is characterized by molecular transport of heat and gas, and is only millimeters thick. The surface layer is of the order of tens of meters deep, and the atmospheric-boundary layer (ABL) or mixed layer (b) is of the order of a kilometer deep. Motion in the ABL is dominated by large-scale convection that carries surface energy and moisture through the atmosphere.

and turbulent sublayers comprise the surface layer, typically on the order of tens of meters thick. Above the surface layer is the mixed layer (see figure 9.5(b)), dominated by large-scale convection. The top of the mixed layer defines the top of the atmospheric-boundary layer, approximately one or more kilometers deep.

Solar energy is absorbed differentially by the mosaic of surfaces covering the Earth. Thus, the atmosphere is heated and humidified differentially by these surfaces. Consequently, density variations occur in the atmosphere, from which pressure patterns develop. Since it tends to flow down pressure gradients, air flow (wind) over the mosaic of Earth's surfaces carries warm air over cold surfaces, and vice versa. Additionally, storms embedded in the atmospheric circulation carry moisture from one area to another.

Near-surface soils are heated by a combination of solar radiation, sensible (i.e., thermal energy) and latent heat exchanges (described later in this chapter), and to a lesser extent, geothermal sources. Soils are cooled by the loss of radiant energy at night (see the next section) or by contact with cold air advected from another region of the Earth's surface by the atmosphere. Averaged spatially and temporally on a global basis, solar radiation is by far the greatest source of heat, supplying more than 99 percent of the energy that heats soil. Some tens of meters below the surface, geothermal heating from the Earth's core (in excess of 3,000 °C) begins to determine temperature substantially, with rate-of-increase with depth of about 2–4 °C/100 m (Foster 1969; Sorey 1971; Sass et al. 1988). It is believed that core heat is due to residual heat of creation and radioactive decay.

An aside of historical interest regarding soil heating: in the 1800s Lord Kelvin of England used measurements of the rate-of-heat flow to the Earth's surface to estimate its age, assuming the Earth was molten at the time of its formation and had been cooling ever since. Kelvin's assumptions led him to estimate the Earth's age at less than 100 million years. Geologists immediately dismissed the estimate based upon their understanding of the rates of sedimentation; scientists of Kelvin's time were unaware of radioactive decay.

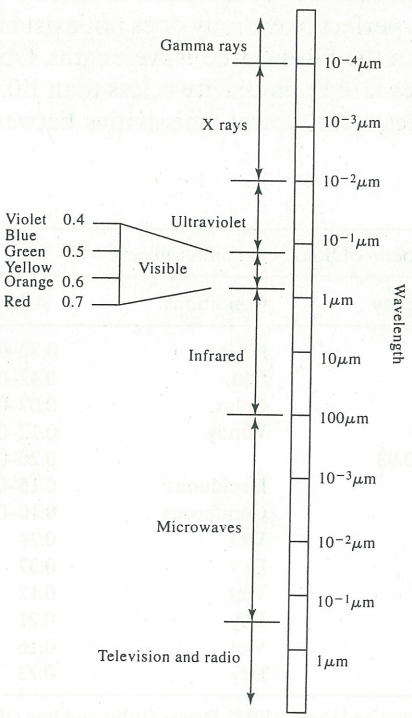

Figure 9.6 The electromagnetic spectrum

Radiation Balance

Our examination of radiation at the Earth's surface concerns just a small fraction of the electromagnetic spectrum (shown in figure 9.6), ranging in wavelength from ultraviolet (0.01 μm) through the far-infrared (100 μm); the range encompasses almost all radiation emitted as solar and terrestrial radiation. The discussion following concerns this region but first, let us consider some basic concepts.

Wavelength (λ) is related to frequency (ν) by:

$$\lambda = \frac{c}{\nu} \tag{9.18}$$

where c is the speed of light (3.0×10^8 m s^{-1}). A portion of radiation, of a certain wavelength that is incident upon an object, can be absorbed while passing through it. The ratio of the amount absorbed to that incident is the monochromatic (single wavelength) absorptivity, $\alpha(\lambda)$. Radiation not absorbed can be reflected or transmitted, or both. When described with respect to incident radiation, these terms are called reflectivity (r) and transmissivity (τ), respectively. Summing all three terms, we account for the fate of all monochromatic radiation:

$$\alpha(\lambda) + r(\lambda) + \tau(\lambda) = 1 \tag{9.19}$$

All bodies at temperatures above absolute zero (0 K) possess molecular kinetic energy and emit radiation in the thermal or far-infrared wavebands, due to specific molecular vibrations (Williamson 1973). Bodies that emit radiation at shorter wavelengths (higher frequencies) have to derive this energy from electron activity at the atomic level.

In the thermal waveband, Kirchhoff's law states that absorptivity of a mass (α, ratio of energy absorbed to that incident) is equal to its emissivity (ε) at that wavelength:

$$\alpha(\lambda) = \varepsilon(\lambda) \tag{9.20}$$

A mass that is both a perfect emitter and absorber of radiation is called a blackbody. For its surface, $\alpha(\lambda) = 1$ and $r(\lambda) = \tau(\lambda) = 0$. A perfect blackbody does not exist in nature, although many natural objects come quite close in the far-infrared wavelengths. Objects that are not blackbodies are referred to as greybodies if their emissivity is less than 1.0, or whitebodies if their emissivity is 0. Soils are greybodies, with typical emissivities between 0.90–0.98 (see table 9.4).

TABLE 9.4 Emissivity and Albedo of Some Common Objects

Substance	Emissivity	Conditions	Albedo
Snow	0.99	Fresh	0.80–0.95
		Old	0.42–0.70
Water body	0.97	Calm	0.07–0.08
		Windy	0.12–0.14
Crops	0.96–0.98		0.20–0.26
Forests	0.97	Deciduous	0.15–0.20
		Coniferous	0.10–0.15
Soil: sandy	0.949	Wet	0.24
		Dry	0.37
Soil: silty clay	0.966	Wet	0.12
		Dry	0.21
Soil: loam	0.967	Wet	0.16
		Dry	0.23

Source: Data from Rosenberg, Blad, and Verma (1983), Davies (1979), and Idso (1969).

Any body will emit energy at an intensity (I) as a function of its surface temperature (T), and emissivity as given by Stefan's law:

$$I(\lambda) = \varepsilon(\lambda)\sigma T^4 \tag{9.21}$$

where σ is the Stefan–Boltzmann constant (5.67×10^{-8} W m^{-2} K^{-4}) and I is in W m^{-2}. Stefan's law also applies to emissions from liquid and gas bodies. However, since there is no definable surface of a region or parcel of gas (such as the atmosphere), an effective temperature is used that is determined from a density and composition profile of the gas parcel (Fleagle and Businger 1963).

The radiation budget at the Earth's surface (see figure 9.7) may be partitioned into two components: incoming (received by the surface) and outgoing (leaving the surface); net radiation is the sum of these components. Incoming solar radiation of short wavelengths (0.15–3.0 μm) dominates during the day, heating the Earth; outgoing terrestrial radiation at long wavelengths (3–100 μm) dominates at night, cooling the Earth.

Solar radiation that reaches the top of the atmosphere has a magnitude of 1367 W m^{-2} as projected on a flat surface. The annual average over the curved surface of the Earth is 339 W m^{-2}. Approximately 47 percent of solar radiation is in the visible portion (0.36–0.75 μm) of the electromagnetic spectrum and 48 percent in the near infrared (0.75–3.0 μm). Of the remaining 5 percent of solar radiation, about 3 percent occurs in ultraviolet (> 0.3 μm) and 2 percent in far-infrared (> 3 μm) spectrums. At the Earth's surface, the 50: 50 clear-sky ratio of visible to infrared radiation becomes a 60: 40 ratio under overcast conditions.

Some portion of solar radiation received at the surface is reflected; the ratio of reflected to incoming solar radiation (within visible or infrared wavebands) is called the albedo. The distinction between albedo and reflectivity of a surface is that reflectivity is wavelength-specific, while albedo pertains to wavebands. Materials that compose the Earth's surface have a wide range of albedos (see table 9.4). The albedo of some objects can differ for different wavebands. For example, snow has a high, visible albedo that exceeds its near-infrared value.

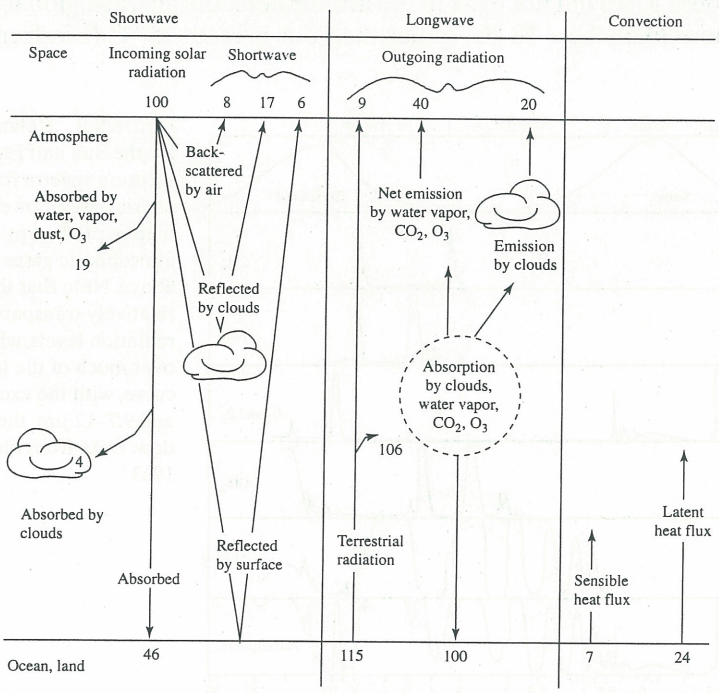

Figure 9.7 Earth's energy balance (from an annual global average), depicting the fate of solar and terrestrial radiation at the surface and in the atmosphere. All values expressed as percent of incoming solar radiation (339 W m^{-2}); data from MacCracken and Luther (1985)

Most soils exhibit a range of albedos depending upon mineral, organic, or water content of the crust; values range from about 5–45 percent. For the same soil, an increase in soil water content decreases albedo. For example: Idso, Asae, and Jackson (1975) provided the following relation between albedo (a) and fractional water content (w/w_s; w is water content and w_s is field capacity) of a soil:

$$a = 0.31 - 0.34\left(\frac{w}{w_s}\right); \quad \frac{w}{w_s} \leq 0.5 \tag{9.22a}$$

$$a = 0.14; \quad \frac{w}{w_s} > 0.5 \tag{9.22b}$$

Thus, as near-surface soil moisture can vary with time, so can albedos, for the same surface.

Terrestrial radiation is also referred to as thermal or longwave radiation, and occurs in the far-infrared region (3–100 μm). It is emitted by the Earth's surface at an intensity determined by temperature (see equation 9.21). Under clear skies, surface temperature—and hence outgoing terrestrial radiation—usually reaches a maximum just after midday, and a minimum shortly before sunrise. As shown in figure 9.7, about 80 percent of the upward-component of terrestrial radiation from the surface is absorbed by the atmosphere then returned to the surface. Returned energy is emitted at an intensity that is determined by the effective temperature of the atmosphere, and specifically related to its radiating components: clouds, aerosols, water vapor, and other greenhouse gases (these are listed further on, in table 9.8). Increasing atmospheric concentrations of these important radiative atmospheric constituents also increases the amount of energy re-radiated back to the Earth's surface, which in turn, can cause increases in surface temperature. We often experience the effect of increased terrestrial re-radiation at night, under calm winds and changing sky conditions. Under a clear sky, the air cools rapidly as net radiation typically reaches about -40 to -60 W m^{-2}. As cloud cover appears, the rate of cooling decreases rapidly, due to increased re-radiation from the atmosphere; net radiation often approaches 0 under these circumstances.

Greenhouse gases also play an important role in thermal regulation of the Earth's surface. If greenhouse gases did not exist in the atmosphere, the average global-surface temperature would more likely be -18 °C, rather than our present 15 °C (Lindzen, 1990). Surface

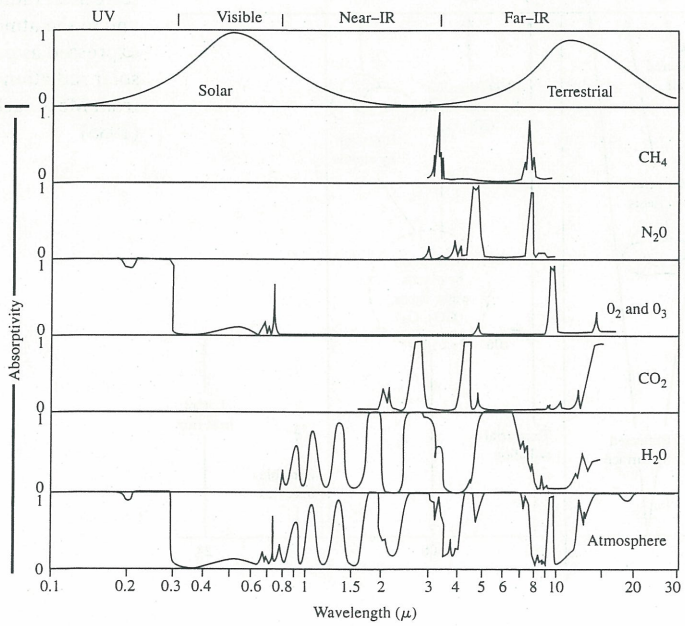

Figure 9.8 Relative emission spectra for the Sun and Earth (top), and absorption spectra for major atmospheric gases. Lowest panel is the summation of absorption by all atmospheric gases listed in panels above. Note that the atmosphere is relatively transparent near peak solar radiation levels, while it is opaque over much of the terrestrial radiation curve, with the exception of 8.5–9.5 and 9.7–12 μm, the atmospheric window. Data from Fleagle and Businger 1963

temperatures could even be warmer if not for the "atmospheric window"—a split region in the far-infrared (8.5–9.5 and 9.7–12 μm)—where absorption by greenhouse gases is markedly minimal (see figure 9.8); about 8 percent of terrestrial radiation escapes to space through these wavebands. The split in the atmospheric window around 9.6 μm is due to a strong absorption peak by O_2 and O_3. Strong absorption of far-infrared radiation by water vapor (at shorter wavelengths), and by CO_2 (at longer wavelengths) borders this window. Among greenhouse gases, water vapor usually occurs in the greatest concentration in the atmosphere, and accounts for the largest portion of reradiated energy.

Incoming energy not reflected or emitted by the surface is absorbed by the soil and ground cover. Here it is converted into kinetic energy, then released into the atmosphere as sensible (kinetic energy) and latent heat. On an annual global basis, these two convective terms account for 31 percent of solar energy. Note that no net energy goes into conduction; it is assumed that the Earth is not warming measurably, so the net flux of heat into the solid Earth (soil-heat flux) is negligible. We also note that incoming solar energy is balanced by that outgoing, which prevents the Earth from warming or cooling.

Net radiation exchange at the soil's surface is complicated by the presence of vegetation. Vegetation type, vigor, age, height, and density can all be significant factors in determining shortwave absorption and longwave emission, thereby affecting net radiation; vegetation can also reduce net radiation at the surface substantially. Baldocchi et al. (1984) report that net radiation at the floor of a closed-canopy, deciduous forest is only a few percent of that above-canopy during the growing season, but during winter months, floor values are much closer to above-canopy values. Methods for calculating and measuring net radiation at the soil's surface, at the floor of a stand of vegetation, can be found elsewhere (Baldocchi et al. 1984; Norman 1979).

QUESTION 9.3

Examining equation 9.21, a surface temperature increase from 20 °C to 22 °C leads to what size increase in I for a wet, sandy soil?

QUESTION 9.4

Referring to the value at the bottom of the center panel (longwave) of figure 9.7, terrestrial radiation is 115 percent of incoming solar energy. Explain how terrestrial radiation leaving the Earth's surface can exceed the value of incoming solar radiation (100 percent).

Energy Balance

Bare soil The net radiation (R_n) received by a bare-soil surface is partitioned into heating the soil and atmosphere, and evaporating water. Under steady-state conditions (i.e., time-invariant, horizontally homogeneous), the energy budget of the surface can be written as:

$$R_n = H + L_v E + G \tag{9.23}$$

where H is sensible-heat flux, G is soil-heat flux, and $L_v E$ is latent-heat flux—a product of the latent heat of vaporization (L_v) and mass flux of water vapor (E). The term 'flux' as used here refers to the amount of energy (or matter) that passes through a unit area per unit time and is alternately known as flux density. Sign convention for fluxes in equation 9.23 varies in the literature, although frequently (as here), the favored convention considers fluxes toward the surface as positive. Fluxes are commonly expressed in W m^{-2} units; therefore, the units of E are typically [kg m^{-2} s^{-1}], and L_v units are [MJ kg^{-1}]. The partitioning of energy derived from the radiation balance is shown in figure 9.9. Parts (a) and (b) of this figure show the energy-

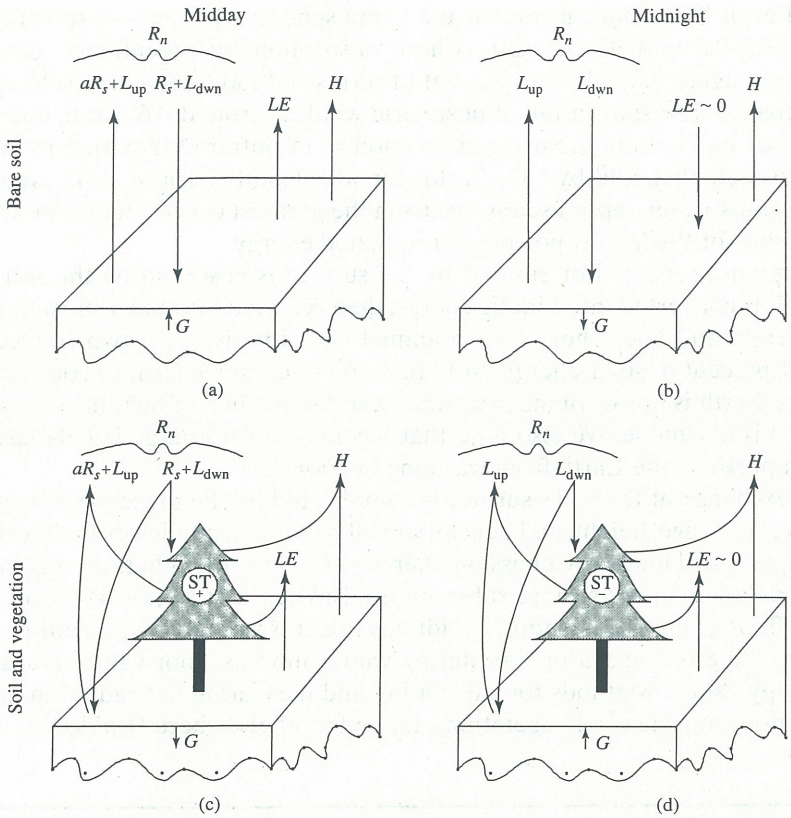

Figure 9.9 Energy-budget components for bare soil and soil with vegetation for both daytime and night-time conditions under clear skies. Radiation is decomposed into shortwave (R_s), reflected shortwave (aRs), and longwave (L) components. H, LE, and G are sensible, latent, and soil-heat fluxes, respectively. Storage (ST) is positive during the day before solar noon, as the canopy vegetation (including air within it) lags ambient temperature. ST becomes negative late in the day and at night as the canopy releases stored energy.

balance terms of bare soils and how these change as time-of-day functions. Energy gain during the day at the surface from solar radiation (figure 9.9(a)) is used to heat the air through sensible heat (H), in evaporation as the latent heat of evaporation (L_vE), and in heating the soil (G). At night, the soil's surface cools because net radiation (incoming minus outgoing longwave) is negative; heat flow in the soil is upward since the subsurface soil layers are warmest.

The energy derived from net radiation and from that of soil that heats the air (through sensible and latent heat) are sometimes lumped together as available energy (A):

$$A = (R_n - G) = H + L_vE \tag{9.24}$$

In order to appreciate the partitioning presented in equation 9.24 more fully, we should examine data gathered on a warm, clear day (figure 9.10). Environmental measurements were taken hourly over a dry desert lake bed, where $L_vE \sim 0$. As indicated in the figure, soil-heat flux roughly tracked net radiation in the early morning hours. Sensible-heat flux lagged behind that of soil, since it depended upon atmospheric turbulence to transport heat away from the surface. During these hours, mechanical transport by turbulence was presumably weak, since wind speed was light. As a result, surface temperatures increased rapidly, which led to strong soil-heat flux to subsurface layers; by mid-morning, soil-heat flux had peaked. Past this time, the trend to decrease was likely due to increased wind-generated turbulent transport of heat (H) from the surface to the atmosphere. If the surface had sufficient moisture, L_vE would also have been expected to increase. Net radiation reached a maximum near noon, or near the time that peak solar radiation was expected. With increased wind speed, sensible-heat flux from the soil to the atmosphere continued to increase; its peak followed that of net radiation by two hours. Then, with declining input of solar radiation into the soil-

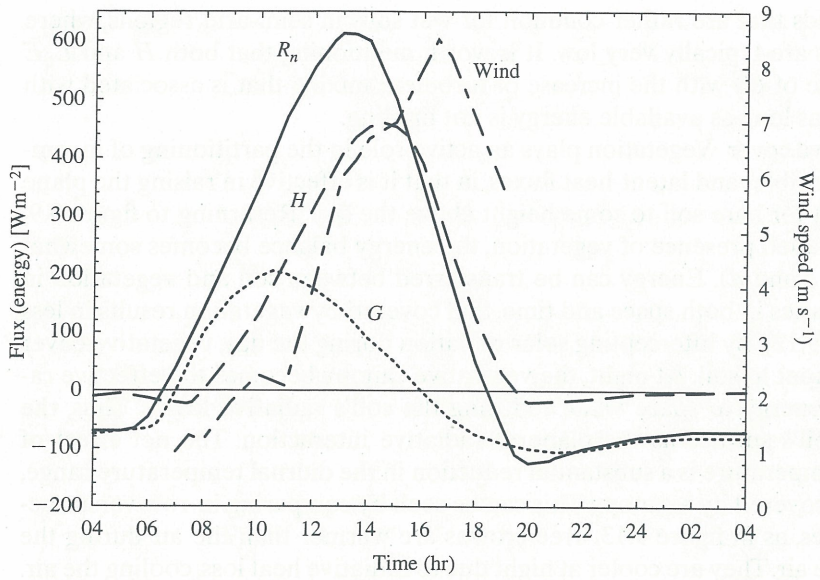

Figure 9.10 Principle energy-budget components of a dry, bare soil (e.g., dry desert lake bed), El Mirage, California, June 10–11, 1950 (data from Vehrencamp 1953)

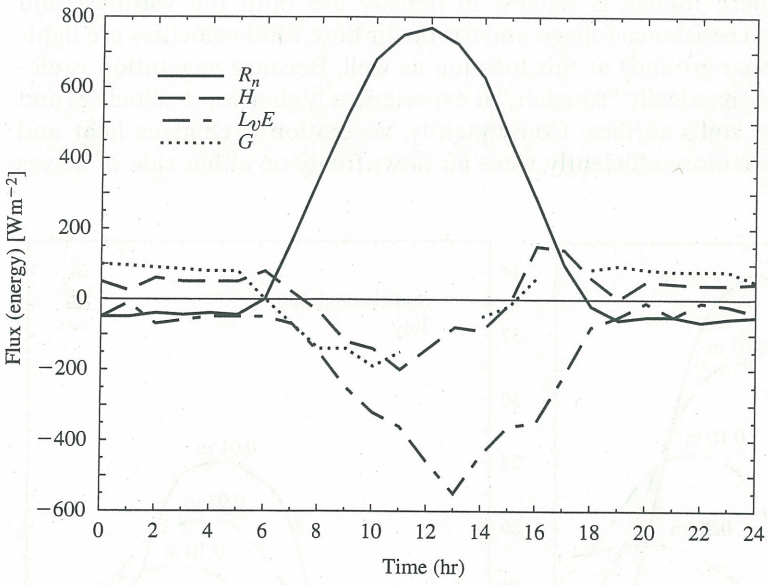

Figure 9.11 Diurnal trends of energy-balance components over a wet soil, Phoenix, Arizona (data from Fritschen and van Bavel 1962). Note sign convention; fluxes to the surface are positive.

atmosphere system, sensible-heat flux steadily declined, despite relatively strong winds. From 1600–2000 hours, sensible-heat flux exceeded net radiation, as it derived heat from the soil (note that soil-heat flux became upward, or negative). After 1800 hours, net radiation became negative since incoming solar radiation was low, and emission by the hot-soil surface that radiated in the far-infrared was high. After 2000 hours, net radiation remained a fairly constant negative value as the surface continued to lose heat, deriving energy from subsurface soil, and thereby lowering soil temperatures.

In the case of a moist soil as shown in figure 9.11, energy can be partitioned into soil-, sensible-, and latent-heat fluxes. The net radiation curve shown again depicts a smooth parabolic shape, indicative of a clear day. Latent-heat flux peaks near 1300 hours, at which time it consumes 80 percent of net radiation. Evaporative demand is so large that after 1500 hours, the energy that drives evaporation comes from net radiation, soil-, and sensible-heat fluxes.

This figure depicts trends that are rather common for wet soils in semi-arid regions, where atmospheric humidities are typically very low. It is worth mentioning that both H and L_vE increase (at the expense of G) with the increase of turbulent mixing that is associated with increasing wind speed, as long as available energy is not limiting.

Soil with vegetative cover Vegetation plays an active role in the partitioning of incoming solar energy into sensible- and latent-heat fluxes, in that it is effective in raising the plane of interaction from that for bare soil to some height above the soil. Returning to figure 9.9, we note that with the added presence of vegetation, the energy balance becomes somewhat more complex (panels *c* and *d*). Energy can be transferred between soil and vegetation in such a manner that it varies in both space and time. Soil covered by vegetation results in less soil heating (see figure 9.12); by intercepting solar radiation during the day, vegetative cover reduces the radiative input to soil. At night, the vegetative canopy becomes the effective radiative surface, losing energy to space while reducing the soil's radiative losses. Thus, the canopy replaces the soil's surface as the plane of radiative interaction. The net effect of canopy cover on soil temperature is a substantial reduction in the diurnal temperature range, in contrast to soils not covered by a canopy. This can be seen by comparing in-row versus between-row temperatures, as in figure 9.13. Tree crowns are warmer than the air during the day, thereby heating the air. They are cooler at night due to radiative heat loss, cooling the air.

Vertical profiles of temperature and humidity as measured in a forest (see figure 9.14) indicate that conditions where foliage is highest in density are both the warmest and moistest. Due to the frictional resistance foliage imparts on air flow, wind velocities are lightest (with the exception of near-ground) at this location as well. Because vegetation is elevated above soil and is aerodynamically "rougher," it experiences higher wind velocities and greater turbulence than the soil's surface. Consequently, vegetation exchanges heat and moisture with the atmosphere more efficiently, since air flows freely on either side of leaves

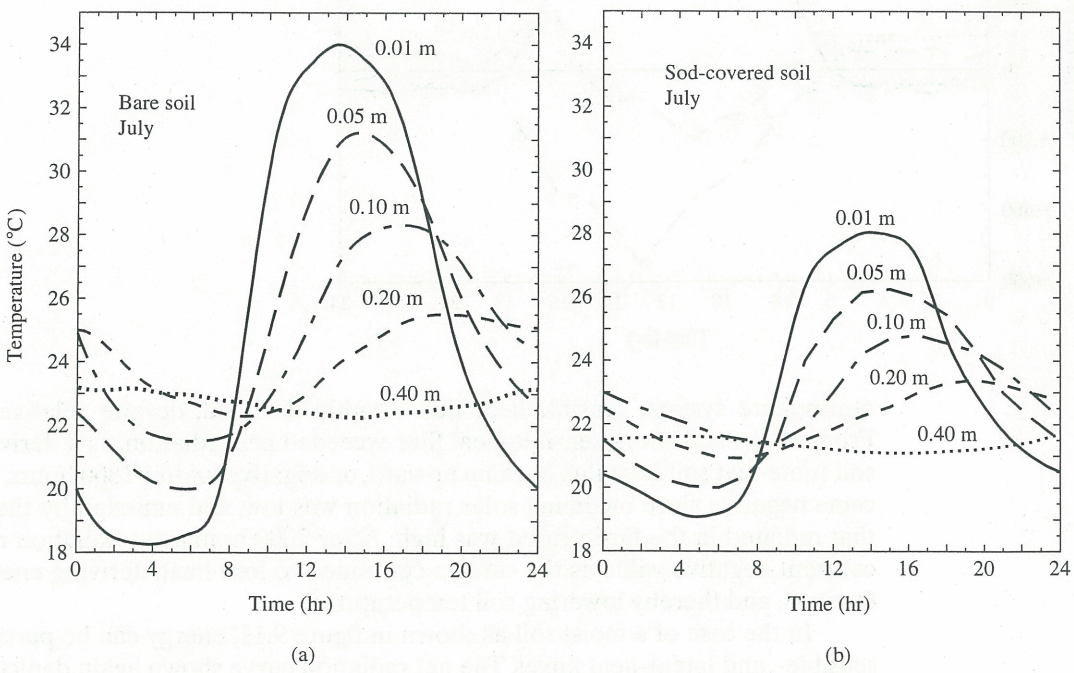

Figure 9.12 Typical diurnal patterns of soil temperature at various depths under clear skies for bare-soil surface (left) and sod-covered soil surfaces (right). The effect of lowering soil temperature in the presence of vegetation decreases with increasing soil depth (data from Backer 1965)

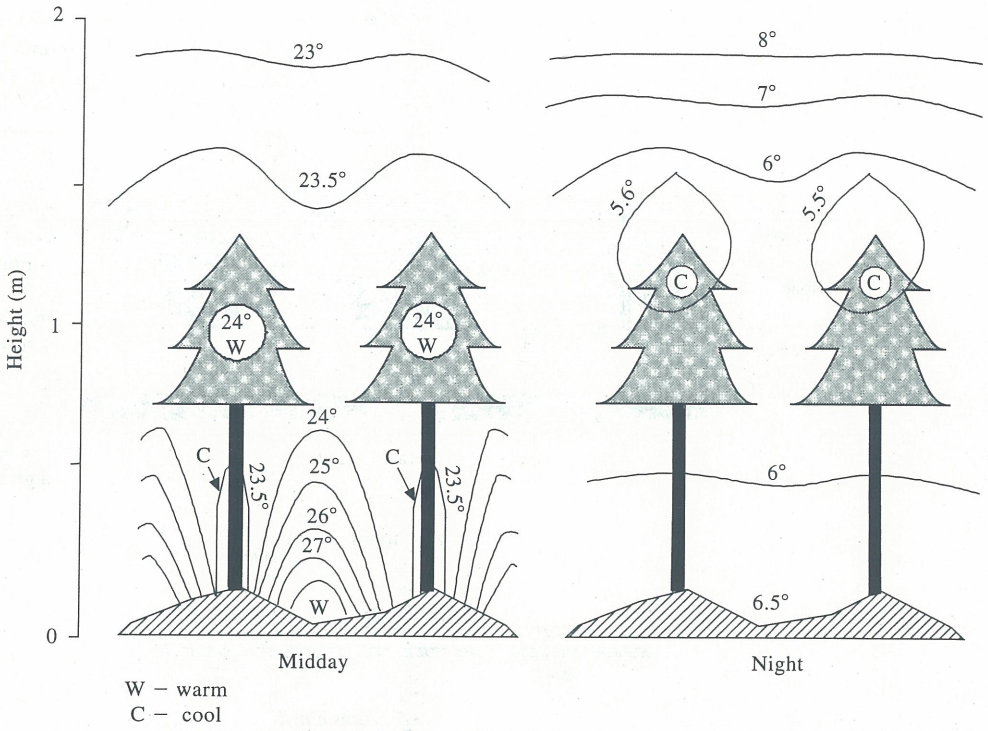

Figure 9.13 Distribution of temperature in an orchard (data from Geiger 1965) for typical conditions at mid-day, and at night under clear skies. Windy conditions tend to diminish temperature differences during the day or at night.

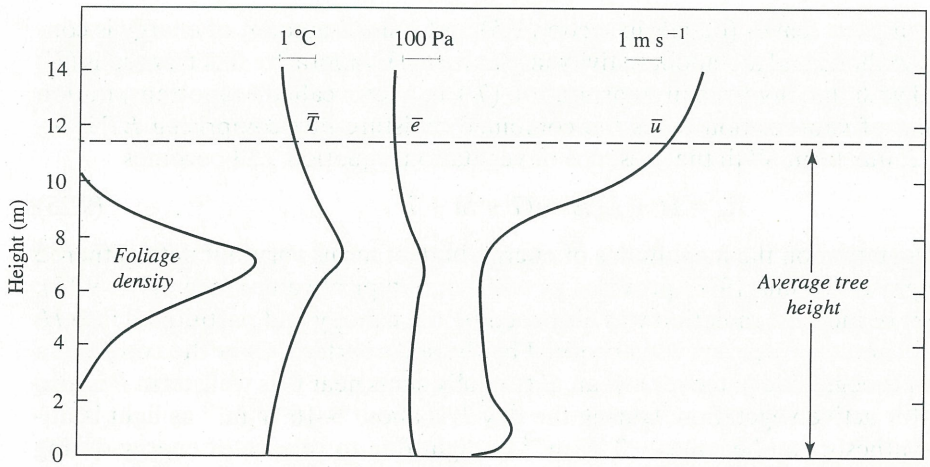

Figure 9.14 Typical profiles of relative foliage density (function of the amount of leaf area), air temperature, vapor pressure, and wind speed in a dense forest (data from Jarvis, James, and Landsberg 1976)

and other plant elements. Although much of our discussion involves tall canopies, the same statements generally apply to short canopies (such as grass) as well. In either case, under vegetative cover, the near-surface soil temperature range decreases and evaporation of soil moisture at the surface is reduced through a combination of decreased ventilation (lower wind speed) and lower available energy at the surface.

Referring once again to figure 9.9, we see that heat can be stored or released from vegetation (St) as a combination of sensible and latent heat. Some energy is consumed in

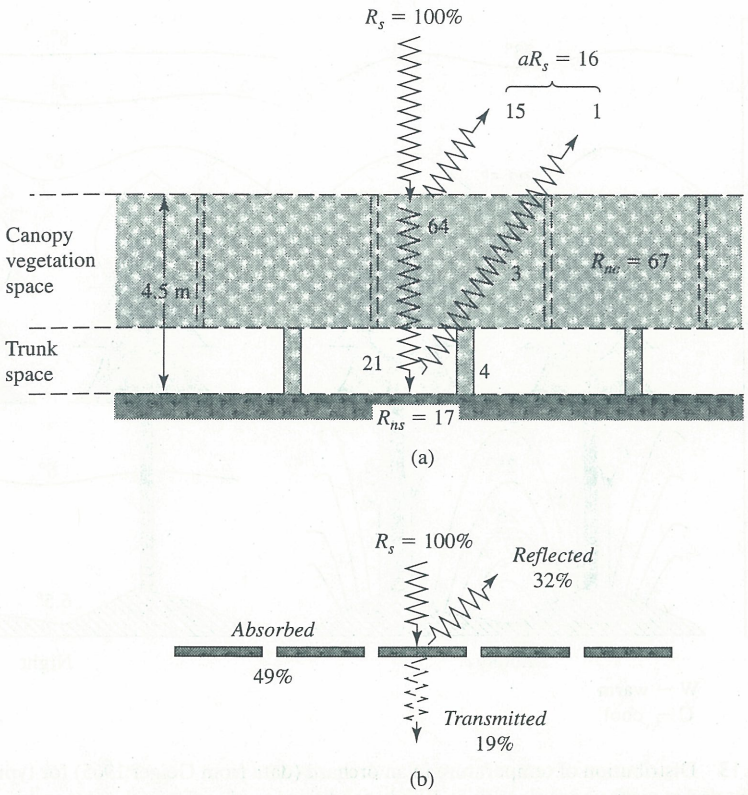

Figure 9.15 (a) Fate of radiant energy falling upon an orange grove (data from Kalma 1970). All values are expressed as a percent of incident radiation: R_s is shortwave (solar) radiation; R_{ns} is net shortwave radiant flux at the soil; and R_{nc} is net shortwave flux in the canopy. (b) Percentages of reflected, absorbed, or transmitted shortwave radiation for a single layer of orange-tree leaves. These numbers differ from those of a grove due to interactions between leaves, and varying leaf orientations within a grove.

transpiration from plant leaves (details in section 9.5) and a small amount of energy is consumed by photosynthetic and metabolic activity in plants (P). Evaporative flux from soils (E) can be combined with that involved in transpiration (T), in a term called evapotranspiration (ET). Latent heat of vaporization times the combined moisture flux comprising ET is included in the L_vE flux term. With the presence of vegetation, equation 9.23 becomes

$$R_n = H + L_vE + G + St + P \tag{9.25}$$

The effects of vegetation on the magnitudes of energy-budget terms vary, but data gathered from an orange grove (Kalma 1970) provides us with some typical values (see figure 9.15): About 67 percent of incident radiation was absorbed by the canopy and partitioned into H, LE, St, and P; and about 17 percent was absorbed by the soil's surface. Over the course of a day, the sum of St is negligible and over a year, G typically sums near 0 as well; term P is also negligible, even for active vegetation. During the day P is about 6–16 W m^{-2} as light is utilized for photosynthesis, and becomes -3 W m^{-2} at night due to release of energy during nocturnal respiration (Oke 1987). With respect to the shortwave radiation budget (equation 9.19), orange leaves absorbed 49 percent of incoming radiation, reflected 32 percent, and transmitted 19 percent.

The partitioning of R_n into H and LE over vegetation can vary in time due to changes in plant physiology, environmental conditions (notably wind speed), and availability of soil water. Van Bavel (1967) shows the influence of water availability in a semi-arid region on an alfalfa crop that was flood irrigated at the beginning of the month, receiving no water thereafter. Note how energy partitioning changes as soil-water availability declines during the month (see figure 9.16). For the first several days, H is negative since latent heat loss due to transpiration by plant leaves (the active surface), enables them to become cooler than the air. Later, L_vE

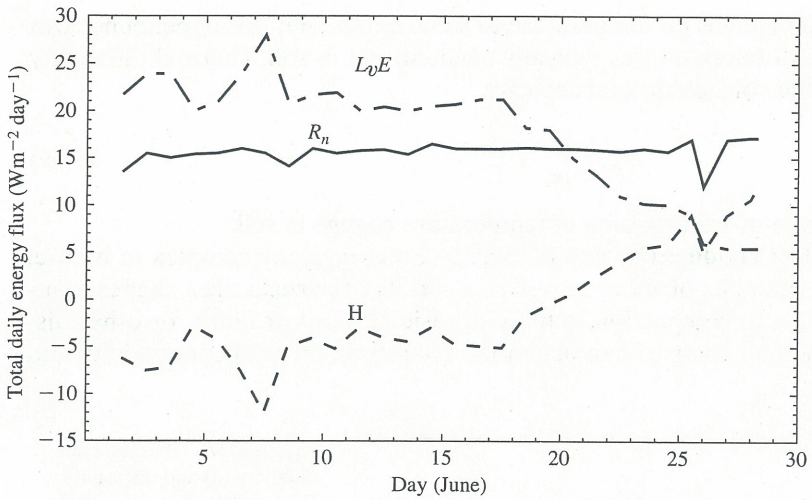

Figure 9.16 Daily sums of key energy-budget components measured over an alfalfa crop near Phoenix, Arizona, June, 1964. The crop was flooded in late May, and not watered in June (data from van Bavel 1967).

declines as soil water availability decreases, slowing transpiration. With decreased transpiration, latent heat loss declines, resulting in more energy to be partitioned into H.

9.3 SOIL-HEAT TRANSFER

Heat Capacity, Conductivity, and Diffusivity

The conduction of heat through soil depends on several factors: the soil's water content; texture; mineral composition; organic content; and compaction. These soil characteristics can affect heat transfer by changing the soil's heat capacity and thermal conductivity, and consequently, thermal diffusivity. Many of the factors that characterize a soil are interrelated. For instance, coarse-textured sandy soil usually has a high air-filled porosity (typically about 25 percent), and dry quickly since they have a high nonhygroscopic mineral content. When wet they conduct heat well, since particle sizes are large and water is a good conductor of heat.

Calculating heat capacity Heat capacity (c) was introduced on a per-mass basis earlier in this chapter. It is often more convenient to express it on a volumetric basis

$$C_i = \rho_i c_i \tag{9.26}$$

where ρ is density of soil constituent (i). Volumetric heat capacity for a soil (C_{soil}) can be expressed as

$$C_{soil} = \sum (f_i C_i)_s + \sum (f_j C_j)_w + (fC)_a \tag{9.27}$$

where f is the volume fraction and subscripts s, w, a refer to solids, water, and air, respectively. Solids can be divided into mineral and organic matter categories (subscript i), and water into liquid or ice (subscript j). For practical applications, it is not usually necessary to differentiate among minerals, since their heat capacity varies little when compared to the differences seen between minerals and organic material (see table 9.1). The heat capacity of water is almost twice as large as that of ice and should therefore be treated separately, as in equation 9.27.

Conductivity and diffusivity To predict heat flow and temperature changes in soil, the thermal conductivity and diffusivity of soil must be known. Soil thermal conductivity (κ_c) is simply the ability of a soil to conduct a quantity of heat in the presence of a temperature gradient.

$$\kappa_c = \frac{G}{\left(\frac{\partial T}{\partial x}\right)} \tag{9.28}$$

κ_c [W m^{-1} K^{-1}] of a solid depends on temperature to some extent, but this dependence can be ignored for the range of temperatures typically encountered in soil. Thermal diffusivity (D_h) is the ratio of κ_c to the volumetric heat capacity,

$$D_h = \frac{\kappa_c}{\rho c} = \frac{\kappa_c}{C} \tag{9.29}$$

D_h [m^2 s^{-1}] governs the rate-of-transmission of temperature change in soil.

Soil factors that affect conductivity and diffusivity Soils, typically complex in nature, are composed of varying amounts of water as well as a variety of particle sizes, shapes, composition, and densities (due to compaction, activity of resident flora or fauna, or other disturbance); the end result is an array of conductivities. Therefore, thermal conductivity and

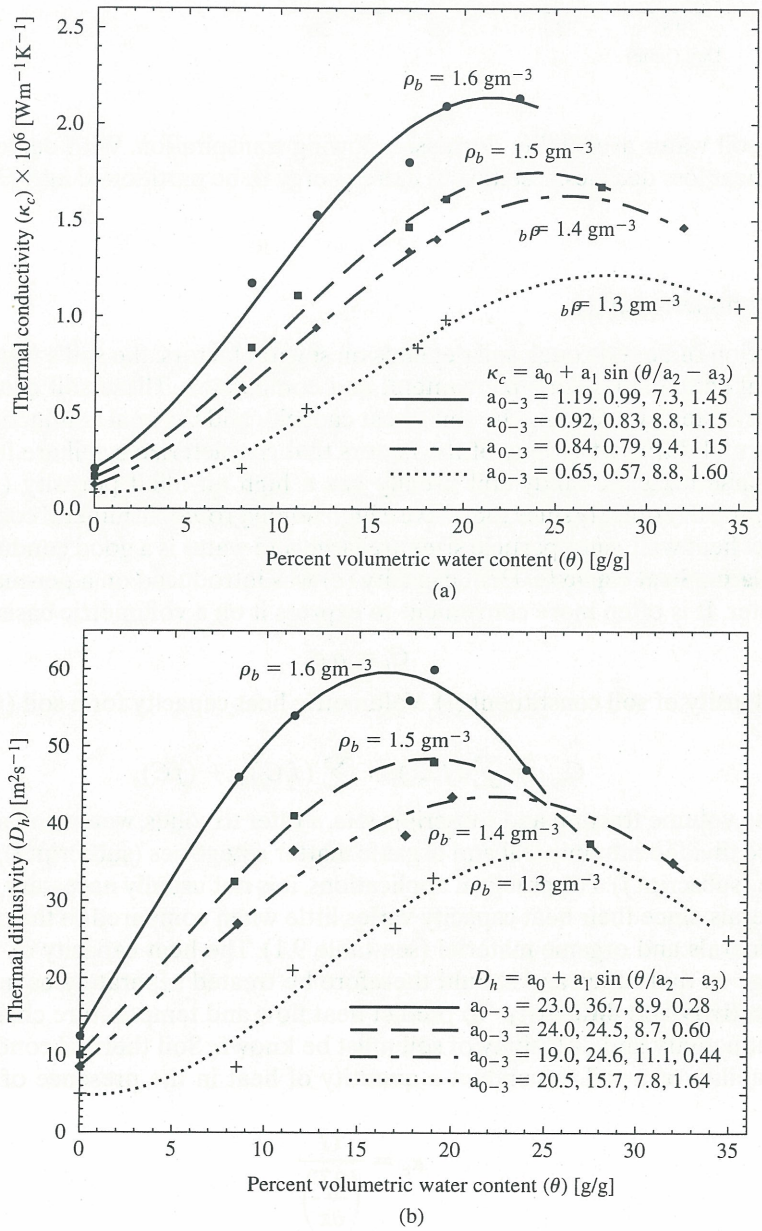

Figure 9.17 Thermal conductivity (a) and diffusivity (b) for soils of varying water content and bulk densities (values given on the curves). Data from Ghildyal and Tripathi 1987

thermal diffusivity can vary both spatially and temporally. κ_c and D_h depend greatly on soil-water content (see figure 9.17), and generally increase with it. This stems largely from water's greater thermal conductivity, 23 times larger than that of air (refer to table 9.1). Interestingly, the influence of water on conductivity and diffusivity is not linear, as depicted in the figure. An explanation for this is that at soil-water contents below ≃7 percent, a water film exists that merely coats soil particles. When soil-water content reaches between 7–20 percent, enough water fills soil pores to bridge the air-filled gaps between soil solids, thereby sharply increasing conductivity. Above ≃20 percent, further increases in soil-water content have little effect on increasing conductivity.

Thermal conductivity is higher for soils of coarser texture: sand > loam > clay. This can be due to a reduced area of contact between particles (Nakshabandi and Kohnke 1965), but thermal conductivities of these soils' dominant minerals can also be a factor. Increasing amounts of organic matter in the soil tend to decrease soil conductivity; organic matter' s thermal conductivity is less than that of mineral constituents and it tends to have a loose, friable structure that promotes granulation.

Finally, κ_c and D_h also increase with soil compaction or bulk density, as either air or water-filled porosity decreases (see figure 9.17). Note that the thermal conductivity of minerals is substantially higher than that of air or water, but not substantially different from that of ice.

Calculating conductivity Considering the variability of κ_c and the variety of soil constituents, de Vries (1975) and Hillel (1982) proposed the following in calculating it:

$$\kappa_c = \frac{\sum_{i=1}^{n} k_i f_i \kappa_i}{\sum_{i=1}^{n} k_i f_i} \tag{9.30}$$

where f is the volume fraction of particle class (i) having a conductivity κ_i , and k_i is the ratio of the average temperature gradient in particle class (i) versus the temperature gradient of the fluid medium (air or water; m) surrounding the particles, as defined by (de Vries 1975)

$$k = \frac{(dT/dz)_i}{(dT/dz)_m} \tag{9.31}$$

A more practical form of equation 9.30 is found by segregating the soil constituents into air (a), water (w), and solid (s) components (after Hillel 1982):

$$\kappa_c = \frac{k_a f_a \kappa_a + f_w \kappa_w + k_s f_s \kappa_s}{k_a f_a + f_w + k_s f_s} \tag{9.32}$$

where the conductive-media reference is water.

Soil-Heat Flux

First law of heat conduction (Fourier's law) For steady-state conditions (i.e., constant temperature gradient), the rate of heat flow (heat flux) through soil is described by the first law of heat conduction:

$$G = -\kappa_c \nabla T \tag{9.33}$$

or, for the vertical dimension only:

$$G = -\kappa_c \frac{\partial T}{\partial z} \tag{9.34}$$

where κ_c is considered constant. The flux is in the opposite direction of the gradient, hence the right side of the equation carries a minus sign. Equations 9.33 and 9.34 are commonly referred to as Fourier's Law, in honor of the French mathematician (1768–1830) who pioneered the analysis of heat conduction in solids, in 1822. These equations are analogous to Darcy's equation for the conduction of fluids in soils and to Fick's law for diffusion in fluids, which is discussed later in this chapter (see section 9.7).

When considering a specific volume of soil, we employ a continuity equation for heat similar to that for water (see equation 7.18), enforcing conservation-of-energy principles. As such, all energy is accounted for in a closed-volume of a conducting medium. The difference in the local time–rate-of-change in heat equals the divergence (or rate of change with distance), plus the contribution by sources and sinks (S) within the volume:

$$\rho c \frac{\partial T}{\partial t} = -\nabla \cdot G \pm S(x,y,z,t) \tag{9.35}$$

or (again), for the vertical direction only:

$$\rho c \frac{\partial T}{\partial t} = -\frac{\partial G}{\partial z} \pm S(z,t) \tag{9.36}$$

where ρc is the volumetric-heat capacity.

Combining the Fourier equation (equation 9.34) with the continuity equation for heat (9.36), we get an expression for the time-dependent change in heat flow, known as the second law of heat conduction:

$$\frac{\partial T}{\partial t} = \frac{\partial}{\partial z}\left(D_h \frac{\partial T}{\partial z}\right) \pm \frac{S(z,t)}{\rho c} \tag{9.37}$$

The source (or sink) term is often omitted for the sake of simplicity, yet it can be significant. Concurrent with the movement of kinetic energy as heat, phase changes of water can result in substantial transport of energy in the form of latent heat. Thus, evaporation and condensation can appear as substantial positive or negative S values; this phenomenon is examined in greater detail, later in this chapter. Oxidation of organic materials mediated by microbial activity can also be a source of energy in equation 9.37.

Sinusoidal Solution to the heat transport equation Initial and boundary values are chosen to represent steady-state, periodic conditions in the solution of equation 9.37. In approximation, the average annual and diurnal cycles of solar radiation that force surface temperature and soil heating are sinusoidal in character. We can assume: **(1)** an initial ($t = 0$) average temperature T_a at the surface with an isothermal profile such that the average soil temperature throughout the profile is the same (T_a); **(2)** a maximum soil-surface temperature that occurs just after solar noon ($\simeq$13:00 solar time); **(3)** a period (Π) of the temperature wave of 24 hours; and **(4)** a trend in surface temperature at the surface over the diurnal period given by:

$$T(z,t) = T_a + A_o \sin \omega t \quad \text{for } z = 0, t > 0 \tag{9.38}$$

where A_o is the temperature amplitude and ω is angular frequency given by

$$\omega = \frac{2\pi}{\Pi} \tag{9.39}$$

At $t = 13$ at the surface, equation 9.38 reduces to

$$T(0,13) = T_a + A_o \tag{9.40}$$

The solution to equation 9.37 (for simplicity, we ignore the term S), is a linear and homoge-

neous differential equation with constant coefficients, and has the form (details in Ghildyal and Tripathi 1987):

$$T(z,t) = ae^{(bt+cz)} \tag{9.41}$$

where b and c are constants. Substituting equation 9.41 into equation 9.37 (neglecting term S) and solving for $T(z,t)$, yields

$$T(z,t) = ae^{bt \pm z(b/D_h)^{1/2}} \tag{9.42}$$

where we require that $D_h = b/c^2$. In meeting the requirements of the boundary condition (a sine function must exist in t at $z = 0$), b must be defined as a complex value ($\pm i\beta$). Continuing, we apply boundary conditions in equation 9.42, to find

$$T(z,t) = b \exp\left[\pm i\beta t \pm z\left(\frac{\beta}{2D_h}\right)^{1/2}(1 \pm i)\right] \tag{9.43}$$

which can be decomposed into four solutions; of these four, the one realistic solution is

$$T(z,t) = T_a + A_o \exp\left[-z\left(\frac{\omega}{2D_h}\right)^{1/2}\right] \sin\left[\omega t - z\left(\frac{\omega}{2D_h}\right)^{1/2}\right] \tag{9.44}$$

Examining equation 9.44, we see that the amplitude of the diurnal temperature wave at the surface decreases with depth by a factor of $\exp(-z(\omega/2D_h)^{1/2})$; at that depth, it is out-of-phase, lagging surface temperature by the factor $-z(\omega/2D_h)^{1/2}$. The reciprocal of this factor, $(2D_h/\omega)^{1/2}$, is a constant (independent of z) known as the damping depth (Z_D), or the depth that the diurnal or annual temperature wave's amplitude decreases to, $1/e$ (~37 percent) of A_o. The amplitude decrease (with depth of the propagating temperature wave) is due to cumulative loss (or gain) of energy from the wave to a temperature-contrast in the soil, within which it penetrates. That is, a wave of warmer (or cooler) temperature loses (or gains) heat to the cooler (or warmer) soil it penetrates. Damping-depth increases with the period of the wave, such that the annual wave's penetration is about $(365)^{1/2} \sim 19$ times deeper than that of the diurnal wave. Diurnal and seasonal waves as seen in field data are examined in the next section.

We may rewrite equation 9.44:

$$T(z,t) = T_a + A_o \exp\left(-\frac{z}{Z_D}\right) \sin\left(\omega t - \frac{z}{Z_D}\right) \tag{9.45}$$

To satisfy condition (2) (maximum surface temperature occurring at $t_o = 13$ hours), a phase adjustment (Φ, a constant) is needed:

$$T(z,t) = T_a A_o \exp\left(-\frac{z}{Z_D}\right) \sin\left(\omega t - \frac{z}{Z_D} + \Phi\right) \tag{9.46}$$

We can solve for (Φ) by applying the boundary condition (equation 9.40; $T(0, 13)$) in equation 9.46

$$T_a + A_o = T_a A_o \sin\left(\frac{13\pi}{12} + \Phi\right) \tag{9.47}$$

which requires $\Phi = -7\pi/12$. Equation 9.45 can be extended to include prediction of the ensemble temperature-wave in soil arising from diurnal and annual forcing (Hillel 1982):

$$\begin{aligned} T(z,t) = T_a &+ A_d \exp\left(-\frac{z}{Z_{Dd}}\right) \sin\left(\omega t_d - \frac{z}{Z_{Dd}} + \Phi_d\right) \\ &+ A_y \exp\left(-\frac{z}{Z_{Dy}}\right) \sin\left(\omega t_y - \frac{z}{Z_{Dy}} + \Phi_y\right) \end{aligned} \tag{9.48}$$

Terms related to diurnal and annual periods are denoted by subscripts (d) and (y), respectively.

From equation 9.45, we can determine an expected temperature range (maximum–minimum) at a given level (z):

$$\text{Range}(z) = \text{Range}(0) \exp\left[-\frac{z}{Z_D}\right] \tag{9.49}$$

We can also predict when maxima and minima occur relative to their occurrence at some other level

$$t(z_2) = t(z_1) + \frac{z_2 - z_1}{2}\left(\frac{\pi}{D_h \Pi}\right)^{1/2} \tag{9.50}$$

where levels are denoted by subscripts (2) and (1), and where D_h and Π must be in the same units of time.

Semi-infinite slab solution to the heat transport equation Consider a soil column at a uniform initial temperature (T_o), heated by a source at the surface of a constant temperature (T_a). Initial conditions and boundary values are

$$T(z, 0) = T_o \quad \text{for } 0 \le z \le \infty \tag{9.51a}$$

$$T(0, t) = T_a \quad \text{for } t > 0 \tag{9.51b}$$

$$T(z, t) = T_a \quad \text{for } z \to \infty, t > 0 \tag{9.51c}$$

Details of the solution to equation 9.37 (second law of heat flow) with respect to the above conditions is given in Ghildyal and Tripathi (1987). Key steps include multiplying both sides of equation 9.37 (sink/source term S dropped for simplicity) by e^{-st} (s is a dummy parameter), and integrating over time:

$$\int_0^\infty e^{-st}\frac{\partial T}{\partial t}\,dt = D_h \int_0^\infty e^{-st}\frac{\partial^2 T}{\partial z^2}\,dt \tag{9.52}$$

If we apply the Laplace transformation to solve the integral, it yields a linear nonhomogeneous equation. After some algebra and application of boundary conditions, the following result can be obtained:

$$T = T_a + [T_o - T_a]\left[1 - \text{erf}\left(\frac{z}{2(D_h t)^{1/2}}\right)\right] \tag{9.53}$$

where erf is the error function (see appendix 3). Equation 9.53 can be used to determine temperature change with depth of confined-soil columns, or to determine thermal diffusivity of columns in a controlled (laboratory) environment.

Temperature Distribution in Soil

Temperature variability and its relevance The distribution of soil temperature and its temporal variability have important agronomic implications, particularly with respect to seed germination and plant development (Rosenberg, Blad, and Verma 1983). The warming of cool soil can accelerate seed germination and substantially increase root uptake of nitrogen, potassium, and phosphorous—all essential nutrients for plant growth. Kaspar, Wooley, and Taylor (1981) noted much deeper root penetration of soybeans in warm soils as opposed to that in cold soils, where the roots tend to spread laterally, almost paralleling the soil's surface. This tendency appears to be a trait characteristic of root-adaption to soils of cold climates (Kramer and Boyer 1995).

Earlier in this section, equations that described the penetration of diurnal and annual temperature waves were determined; these waves are identified easily in field data. For

example, diurnal patterns in soil temperature (with discernible amplitude dampening and phase shift) are found in a sandy soil (figure 9.18) beneath a boreal Jack pine forest in central Canada, just south of permafrost (data courtesy of D. I. Stannard, U.S. Geological Survey, Denver, Colorado). The solar-forcing responsible for the amplitude of the waves varies, in turn affecting soil temperature. Clear skies dominate the first two days (September 24 and 25), followed by two increasingly cloudy days (September 26 and 27). The character of the temperature-profile over the course of a 24-hour period for the same site on a clear day (see figure 9.19) indicates the speed and magnitude of the penetrating temperature wave through soil. The figure also shows null-points (zero heat-flux) for two of the profiles.

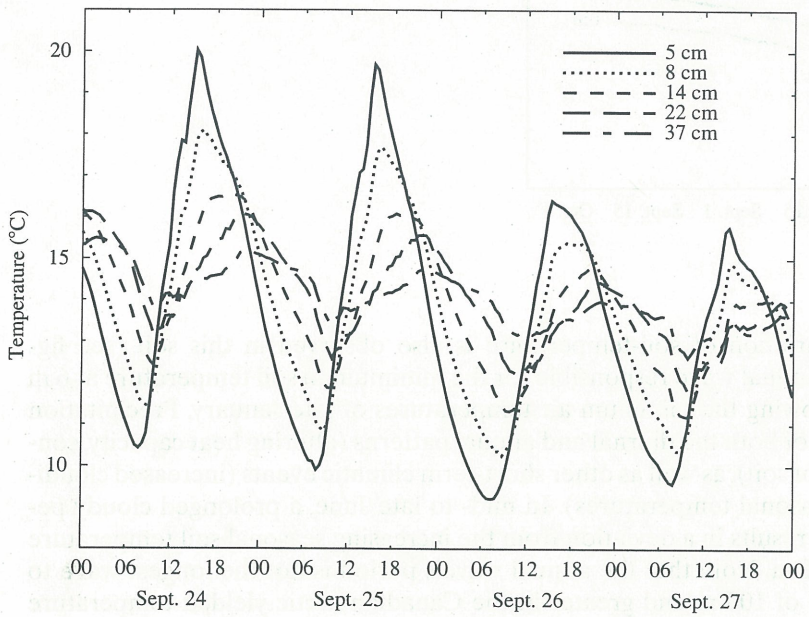

Figure 9.18 Diurnal variation of temperature in a sandy soil beneath a central Canadian forest. Various depths are given, illustrating both the dampening of the diurnal temperature wave with depth, and its increasing phase lag with respect to near-surface temperatures.

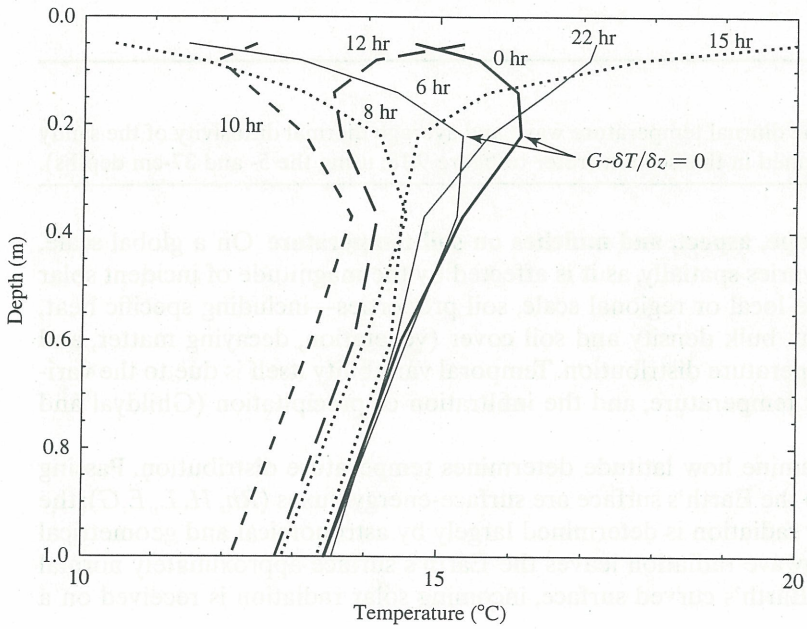

Figure 9.19 Soil-temperature profiles for various times of day, measured in the same soil as that of figure 9.18. Note location of soil-heat flux null-points (zero flux).

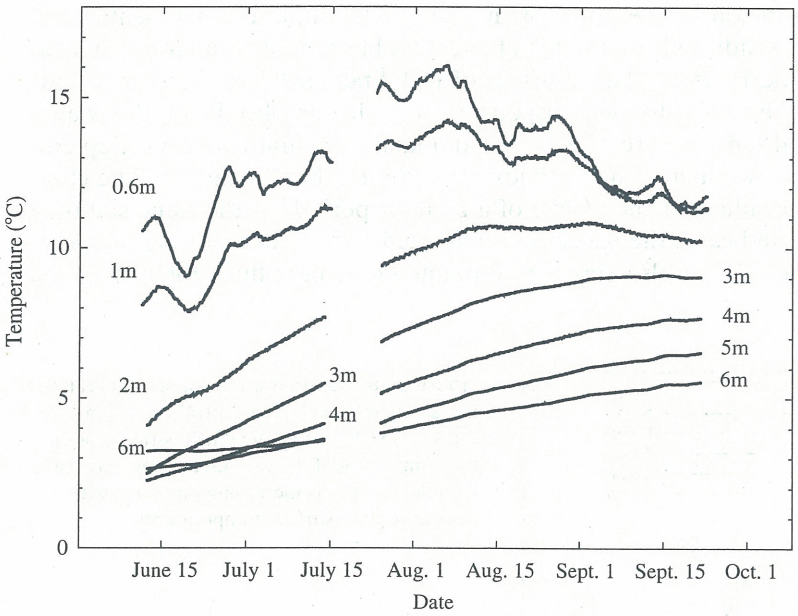

Figure 9.20 Seasonal variation of soil temperature at various depths, measured in the same soil as that of figures 9.18 and 9.19. Upper layers (0.6 m and 1 m) indicate peak soil temperatures in early August. The penetration of the annual temperature wave (winter temperatures) appears to reach the 6 m level in late June. Dips in the seasonal pattern at 0.6 m and 1 m in late June and mid-August are due to cloudy conditions and infiltration of cool rainwater. Data were missing from June 16–20 at all levels.

Strong seasonal variation of soil-temperature is also observed in this soil (see figure 9.20). Note that the annual wave responsible for the minimum in soil temperature at 6 m arrives in early July, following the minimum air temperatures of late January. Precipitation influences the amplitude of both the diurnal and annual patterns (altering heat capacity, conductivity, and diffusivity of soil), as well as other short-term climatic events (increased cloudiness, departures from seasonal temperatures). In mid- to late June, a prolonged cloudy period of nearly two weeks results in a deviation from the increasing seasonal soil temperature pattern, at 0.6 m and at 1 m. Note that the annual wave's period is not the longest wave to penetrate soil; boreholes of 100 m and greater in the Canadian arctic yielded temperature waves (forced by climate change) with periods in lengths varying from decades to 1,000 years (Wang 1992).

QUESTION 9.5

Find the damping depth of the diurnal temperature wave and average thermal diffusivity of the sandy soil in central Canada mentioned in this section (refer to figure 9.18, using the 5- and 37-cm depths).

Effect of latitude, slope, aspect, and mulches on soil temperature On a global scale, temperature distribution varies spatially, as it is affected by the magnitude of incident solar radiation (latitude). At the local or regional scale, soil properties—including specific heat, conductivity, water content, bulk density and soil cover (vegetation, decaying matter, and mulches)—determine temperature distribution. Temporal variability itself is due to the variability in solar-forcing, air temperature, and the infiltration of precipitation (Ghildyal and Tripathi 1987).

Now, we need to examine how latitude determines temperature distribution. Passing through a plane parallel to the Earth's surface are surface-energy fluxes (Rn, H, L_vE, G); the magnitude and sign of net radiation is determined largely by astronomical and geometrical considerations. While longwave radiation leaves the Earth's surface approximately normal to a plane tangent to the Earth's curved surface, incoming solar radiation is received on a

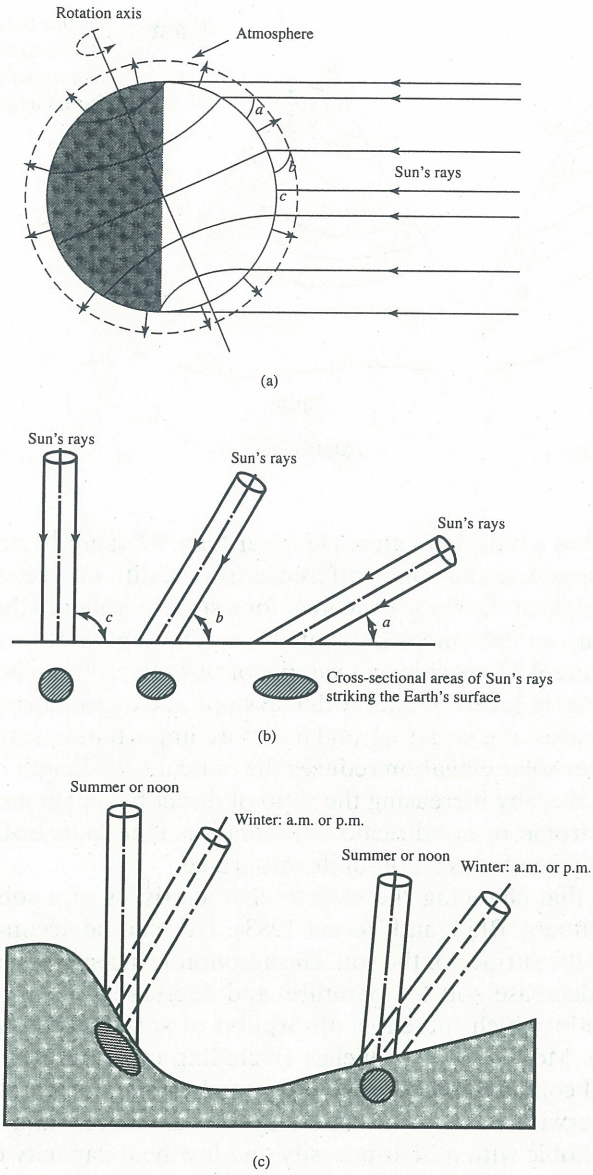

Figure 9.21 Variation of solar radiation incident upon the Earth's surface with latitude and season (a); terrestrial radiation symbolized by outgoing arrows. Cross-sections of solar beam (b) for three angles of incidence (a, b, c) correspond to positions in (a). Angles of incidence are also depicted for a solar beam incident upon hilly terrain (c).

plane normal to Earth's orbital plane (see figure 9.21a). Thus, the solar radiation received (per unit surface) generally decreases with the cosine of latitude (figure 9.21b and c), while longwave is not directly latitude-dependent. As a result, annual net radiation is greater in the tropics than in polar regions. The latitudinal difference is enhanced by a greenhouse-effect involving water vapor. Water vapor is a strong absorber of thermal longwave radiation. On average, it reradiates a greater percentage of outgoing radiation back to Earth at lower latitudes, than at higher latitudes, because it occurs at a higher density at lower latitudes. Water vapor occurs in greater density at lower latitudes largely because of a higher-saturation vapor pressure (higher temperature), and greater abundance of surface water.

With respect to slope, the solar radiation received on a hillside increases as the sine of the angle between the hills' slope and the Sun's rays increases (figure 9.21, c). In instances

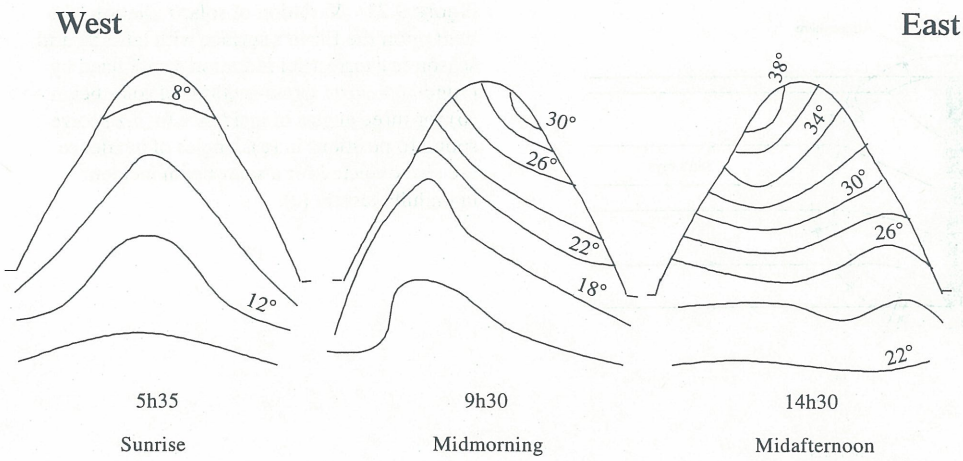

Figure 9.22 Temperatures (Celsius) of bare-soil furrows at various times of day (data from Geiger 1965)

when the solar beam strikes a hillside at an angle other than 90° (zenith), solar radiation received is expected to decrease, as the angle difference from zenith increases. Thus, soil heating varies with both the angle of the slope (maximal for a slope parallel to the Sun's rays) and aspect (cardinal direction), as field measurements show. The temperatures of furrows in a plowed field shown in figure 9.22 provide an example of this effect. To go beyond this example, we note that differences in received energy due to slope and aspect increase with latitude (being least-important nearest the equator), and are more important in summer, when solar elevation is highest. Higher solar elevation reduces the optical path-length of solar radiation through the atmosphere, thereby increasing the ratio of direct beam versus diffuse (also referred to as scattered, isotropic, or nondirectional) radiation. Due to its isotropic nature, diffuse radiation more evenly irradiates a non-uniform surface.

It is widely known that changing the surface characteristics of a soil can modify the soil's temperature (Rosenberg, Blad, and Verma 1983). This can be accomplished with the application of a mulch, to the surface of the soil. The agronomic incentive in applying a mulch is either to increase or decrease soil temperature, and decrease soil evaporation. A dark mulch can decrease albedo, which increases absorption of solar energy and generally increases soil temperature. Most organic mulches (including crop residues) have low heat capacity and low thermal conductivity. As such, they tend to dampen extremes of soil temperature that might otherwise have been experienced (van Doren and Allmaras 1978). Mulches that are hydrophobic with a high-porosity and low heat-capacity can decrease soil evaporation. Waggoner, Miller, and DeRoe (1960) and Rosenberg, Blad, and Verma (1983) present a comprehensive review of mulches and their applications.)

9.4 SOIL MOISTURE EVAPORATION AND THE STAGES OF SOIL DRYING

The evaporation of soil moisture is a much-studied process, considered to proceed along three stages of drying (Hillel 1980; 1982), identifiable in figure 9.23. Let us consider a scenario with soil moisture at field capacity, initially. At this point, evaporation proceeds at a rapid and constant rate, near that of potential evaporation, since the system approximates that of a free-water surface. Evaporation rate is determined by atmospheric transport in the boundary-layer above soil, and by available energy (A). The rate of evaporation increases as any of the following increase: wind speed, surface roughness (which increases turbulent transport), available energy at the surface, and vapor-pressure deficit ($e_s - e_a$). In some cases, the evaporation rate can exceed that of a free-water surface. This situation occurs more often over an

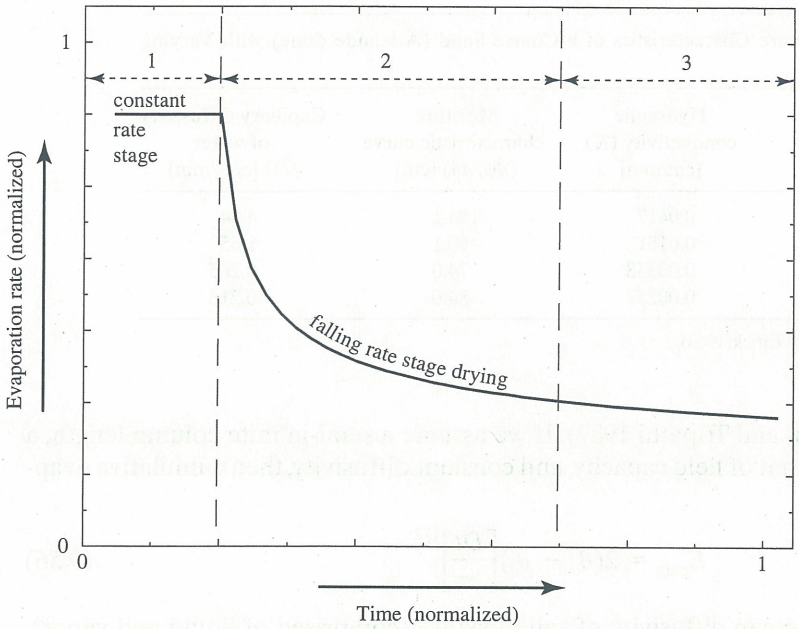

Figure 9.23 Conceptual diagram illustrating the three stages of soil drying over time

aerodynamically rough surface that increases the turbulent mixing of air. A rough, irregular surface can also have a greater amount of surface area (per horizontal distance) available for evaporation. The flow equation for a uniformly wet, isothermal soil-column of depth (Z) is:

$$\frac{\partial \theta}{\partial t} = \frac{\partial}{\partial z}\left[D(\theta)\frac{\partial \theta}{\partial z}\right] \tag{9.54}$$

where θ is water content [$cm^3\ cm^{-3}$], and D ($K(\theta)/(d\theta/d\psi)$) is soil-moisture (liquid) diffusivity [$cm^2\ s^{-1}$]. Conceptually, D is the ratio of hydraulic-conductivity to water-capacity of soil, as previously defined in chapter 8. We can derive a solution for the mean water-content in the column at the end of the first stage of drying, after successive integrations of equation 9.54 (Hillel 1980; Ghildyal and Tripathi 1987):

$$\bar{\theta} = \theta_a + \frac{1}{\beta}\ln\left(1 + \frac{\beta E z}{2D_a}\right) \tag{9.55}$$

where θ_a is soil-water content at air dryness (i.e., liquid water in equilibrium with air) and β is a soil-specific, dimensionless constant. D_a is the soil's hydraulic diffusivity at air dryness, related to $D(\theta)$ as: $D(\theta) = D_a \exp\{\beta(\theta - \theta_a)\}$. We assume: the supply of water required to meet the rate of evaporation (E) at the surface is constant with depth; there is no water flux out of the bottom ($d\theta/dz = 0$); and that evaporativity is determined by available energy. (Gardner and Hillel (1962) argue that θ varies little within the soil column, except at the surface.)

Transition to the second stage of drying occurs when the soil no longer can transmit enough water to the surface to meet evaporative demand; thus, the primary control on evaporation becomes the soil's hydraulic conductivity. As the soil dries, the plane of evaporation (i.e., source of water for evaporation) continues to move downward from the surface, and the water content of the surface layer eventually reduces to that of air (θ_a). Consequently, cumulative evaporation decreases (approximately) as the square root of the elapsed time (Gardner 1959), until it is about one-third the initial rate. Cumulative evaporation is derived from the flow equation (9.54), using the Boltzmann transformation (Kirkham and Powers

TABLE 9.5 Moisture Characteristics of a Coarse Sand (Adelaide dune) with Varying Water Content

Water content (θ) [cm^3/cm^3]	Hydraulic conductivity (K) [cm/min]	Moisture characteristic curve ($d\psi/d\theta$) [cm]	Capillary diffusivity of water (D) [cm^2/min]
0.293	0.0417	104.1	4.34
0.259	0.0181	90.1	1.65
0.150	0.00358	74.0	0.265
0.121	0.00257	84.0	0.216

Source: Data from Elrick(1963).

1972; Hillel 1980; Ghildyal and Tripathi 1987). If we assume a semi-infinite column length, a water content about half that of field capacity, and constant diffusivity, then cumulative evaporation is given by:

$$E_{\text{cum}} = 2(\theta_o - \theta_a)\left[\frac{\overline{D}t}{\pi}\right]^{1/2} \tag{9.56}$$

where $\overline{D}$ is the weighted-mean diffusivity of soil moisture (comprised of liquid and vapor), t is time, and subscript (o) refers to the initial conditions. Although Hillel (1980) presents a numerical method of calculating $\overline{D}$, empirical data are relied upon to set soil-specific constants. A more practical means of finding $\overline{D}$ is to solve for it using equation 9.56, expressing it in terms of slope S ($E_{\text{cum}}/t^{1/2}$). A rough estimate of S can be obtained in the literature (Jury, Gardner, and Gardner 1991; Tripathi and Ghildyal 1975). For instances requiring more precision and reliability, it is necessary to conduct laboratory or field measurements with the specific soil under study, to find S (Hillel 1980, 1982).

Historically, the soil-drying process was divided into constant-rate and falling-rate stages. Kimball and Jackson (1971) further divided the falling-rate stage into two phases. The first phase is controlled by liquid-water diffusivity ($D_l(\theta)$), which decreases exponentially with decreasing θ (Gardner 1959; Hillel 1980); $D_l(\theta)$ is defined (as above) by hydraulic conductivity. The second phase is determined increasingly by the diffusivity of vapor ($D_v(\theta)$), as θ decreases. This phase begins essentially when the surface layer of soil becomes so dry that liquid water no longer can be conducted through it. The transition from one phase to the other is not discrete but gradual, due to the coexistence of both diffusivities in soil ($D(\theta) \approx D_l(\theta) + D_v(\theta)$). The transport of moisture by $D_v(\theta)$ is rather complex, since it is affected by gaseous transport and the absorptive forces of soil particles. We emphasize that $D_v(\theta)$ controls the gaseous diffusion of vapor in soil, and is not a function of hydraulic conductivity.

Much of our discussion to this point is based on laboratory work. Field studies, such as that of Brutsaert and Chen (1995), indicate that the transition from constant-rate to falling-rate stages of drying is not as discrete as presumed in figure 9.23; they appear much smoother, and occasionally last from several days to a week or longer. Also, transition periods appear to lengthen with lower net radiation and also when soil water content well below the surface is high.

Another point to keep in mind with regard to figure 9.23 is that the curve shape is expected to vary among soil types. Much of the variability is due to hydraulic properties of soils, as defined by their physical structure and chemistry. Fine-textured soils (composed largely of clays and loams) tend to lose more water to evaporation than sandy soils, which drain faster. Consequently, sandy soils progress through the constant- and falling-rate stages of drying quickly, which results in lower cumulative evaporation. On the other hand, grummusol and vertisol soils contain smectite clay, which shrinks during drying. Dessication cracks in

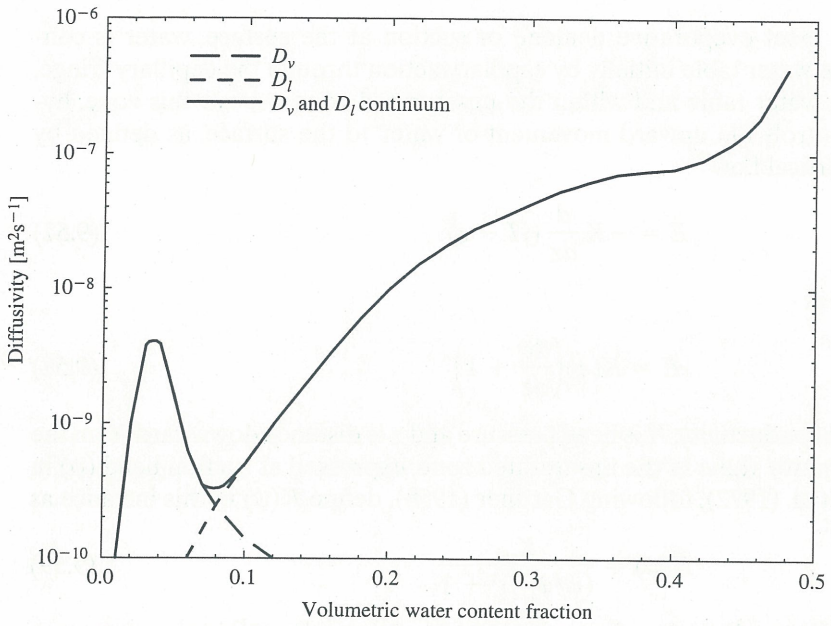

Figure 9.24 Relation between soil-moisture diffusivity (combination of liquid, l, and vapor, v) and water content for a Yolo light clay. Dashed lines illustrate extrapolations from liquid and vapor curves if only one phase of water is present in soil (data from Philip 1974; Hillel 1980)

these soils sometimes can reach several centimeters in width and a meter in depth. As these pores widen and deepen, a secondary plane of evaporation is created. In this case, soil drying can increase to 3 to 4 times that of a noncracking soil (Adams and Hanks 1964; Hillel 1980).

Soil evaporation is a dynamic, interactive process which we can appreciate in context of the material presented thus far, including the surface-energy balance. During stage-one drying, soil temperature varies little diurnally, due to the high heat capacity of soil with a high-water content. Low surface albedo of wet soil promotes absorption of radiant energy, which is partitioned into heating the surface, vaporizing water (latent-heat flux), and, in turn, humidifying the atmosphere. Following stage-one drying, the soil's albedo increases with progressive surface drying, lowering the soil's shortwave absorbence. However, the diurnal extremes of surface temperature increase due to the decrease in both heat capacity and thermal conductivity. This allows increasingly larger thermal gradients with decreasing water content to be established. The intensity of longwave radiation is expected to decrease slightly with decreasing soil-water content, since water's emissivity is slightly greater than that of minerals. However, the amplitude of the diurnal pattern of emitted longwave increases, with an increasing diurnal-temperature range of the surface. Recall that the intensity of this emitted longwave radiation increases with the fourth power of temperature. In turn, diurnal heating and cooling of near surface soil affects vapor transport by alternately vaporizing and condensing soil moisture within the soil column. A condition of soil-moisture hysteresis can develop that affects soil-moisture distribution, since sorption and desorption of soil moisture proceed at different rates.

QUESTION 9.6

Derive an equation for the evaporative flux using equation 9.56. Also using this equation, find $\overline{D}$ for a soil where $\theta_o = .35$ and a linear regression of E_{cum} versus $(\text{time})^{1/2}$ yields: $E_{cum}/t^{1/2} = 2.5$ cm/day$^{1/2}$.

Evaporation from a shallow water table Soils overlying a shallow water table rarely experience the latter stages of soil drying. Instead, their evaporation usually proceeds at the

constant-rate stage. To meet evaporative demand or suction at the surface, water is conducted upward from the water table initially by capillary action through the capillary fringe, immediately above the water table and within the unsaturated zone. Above this zone, hydraulic conductivity controls the upward movement of water to the surface, as defined by Darcy's equation for vertical flow

$$E = -K\frac{d}{dz}(H - z) \tag{9.57}$$

which can be rewritten as

$$E = K(\psi)\left(\frac{d\psi}{dz} + 1\right) \tag{9.58}$$

where $K(\psi)$ is hydraulic conductivity, H is head pressure and z is distance downward from the soil's surface. H is a negative value in the unsaturated zone, expressed as suction head (ψ) in equation 9.58. Ripple et al. (1972), following Gardner (1958), define $K(\psi)$ in this instance as

$$K(\psi) = \frac{K_{sat}}{(\psi/\psi_{1/2})^n + 1} \tag{9.59}$$

where K_{sat} is the hydraulic conductivity of saturated soil [m s^{-1}], $\psi_{1/2}$ [m s^{-1}] is a constant representing ψ when $K(\psi) = 1/2\ K_{sat}$, and n is an integer ranging from 2 (for clays) to 5 (for sands). Procedures for calculating evaporation from a soil column above a shallow water table are given in Ripple et al. (1972) where equations 9.58 and 9.59 are applied to describe soil's ability to meet evaporative demand.

Evaporative potential is determined by available energy, vapor pressure deficit, and turbulent transport at the surface. Soil-evaporation rates can reach that of potential evaporation at times (defined in the following section) but are typically less, since they are limited by the rate at which a soil can conduct water upward (hydraulic conductivity), through the unsaturated zone and to the surface. Ripple et al. (1972) derive the soil-limited evaporation rate (E_{lim}):

$$E_{lim} = K_{sat}\left[\frac{\psi_{1/2}}{Z}\right]^n \left[\frac{\pi}{n \sin(\pi/n)}\right]^n \tag{9.60}$$

where Z is the depth from the surface to the water table, and n is an integer value; it is assumed that $E_{lim} \ll K_{sat}$. We can see from equation 9.60 that E_{lim} decreases linearly with decreasing K_{sat}, but decreases nonlinearly with increasing water-table depth.

9.5 EVAPOTRANSPIRATION AND THE INFLUENCE OF VEGETATION ON SOIL MOISTURE

Plants play an important hydrologic role (see figure 9.25), in that they provide a rapid means of transporting large amounts of soil-water to the atmosphere. Plants have a biological need for water; most (terrestrial) plants obtain this water from unsaturated soil near their roots. Roots can access water over a wide and deep volume of soil, depleting water at rates far in excess of that by soil evaporation alone—especially in comparison with that of soil drying's latter stages. Tap roots can extend several meters in depth, at times reaching the water table.

Plant Physiology

To understand the spatial and temporal character of plants' demand on soil moisture more completely, we need to briefly examine some basic concepts of plant physiology (a com-

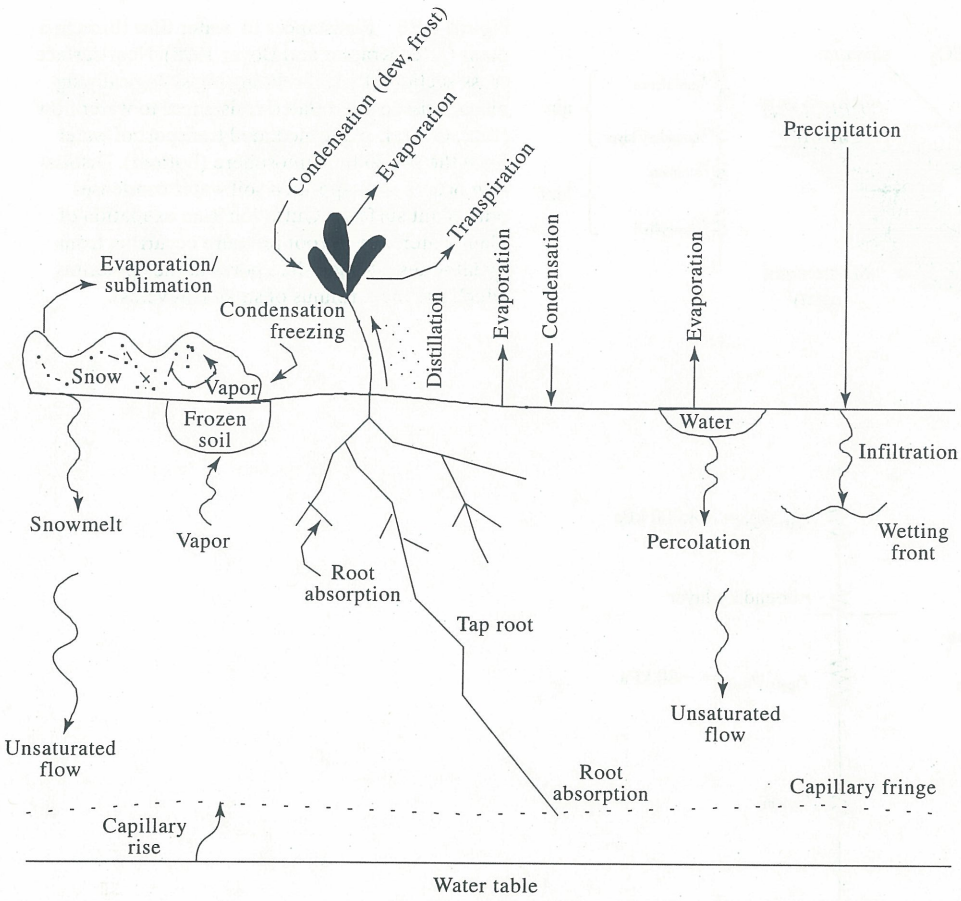

Figure 9.25 Fate of water in the soil–plant–atmosphere continuum, indicating the hydrologic importance of plants

prehensive discussion is given in Salisbury and Ross 1978). Plant growth and maintenance both depend on photosynthesis—a process in which CO_2 and water are combined (in the presence of light and chlorophyll) to produce simple sugars. The overall reaction of photosynthesis is

$$6CO_2 + 12H_2O + \text{Light} \rightarrow C_6H_{12}O_6 + 6O_2 + 6H_2O \qquad (9.61)$$

Soil moisture supplies the water needed in the reaction, as well as the O_2 that is released to the atmosphere (as determined by Ruben, Randall, and Hyde 1941, using oxygen isotopes). CO_2 is largely sequestered from the atmosphere, although a small percentage can be absorbed from soils (Higuchi, Yoda, and Tensho 1984; Wium-Andersen 1971). The energy needed for the reaction is derived from photon absorption by chlorophyll molecules, largely held in mesophyll cells (see figure 9.26, top) by chloroplasts.

Appearing among the leaf's epidermal cells are pores (openings) in the leaf interior called stomata. The size and shape of stomata are defined by guard cells that respond to light intensity, temperature, and leaf-water potential. The size of the stomatal opening directly affects the rate of diffusion of water vapor and CO_2 into (or out of) the stomatal cavity within the leaf.

In the soil–plant–atmosphere continuum, water exists at a variety of potentials (see figure 9.26, bottom). Vascular plants acquire water in the root zone, where it follows a gradient in chemical-energy potential from the soil into the roots through pores in the epidermis, and in the long peripheral cells on young roots (called root hairs). Water is absorbed along roots

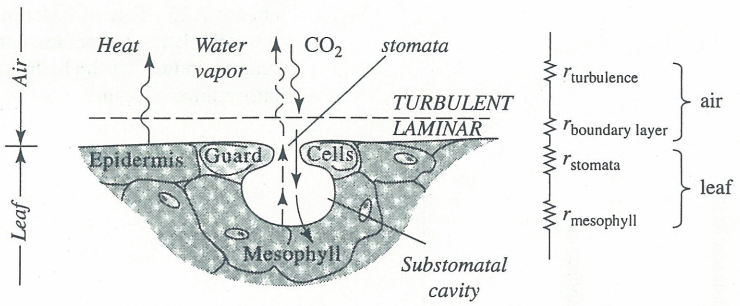

Figure 9.26 Resistances to water flow through a plant (after Kramer and Boyer 1995). Near-surface cross-section of a leaf relating physiologically significant tissue and related resistances to water flow (top). Overall-plant-mediated transport of water from the soil to the atmosphere (bottom). Distillation occurs as evaporated soil water condenses onto plant surfaces. Guttation is an exudation of plant water, due to root pressure occurring from hydathodes (stomate-like pores in the epidermis, which are the terminus of small leaf veins).

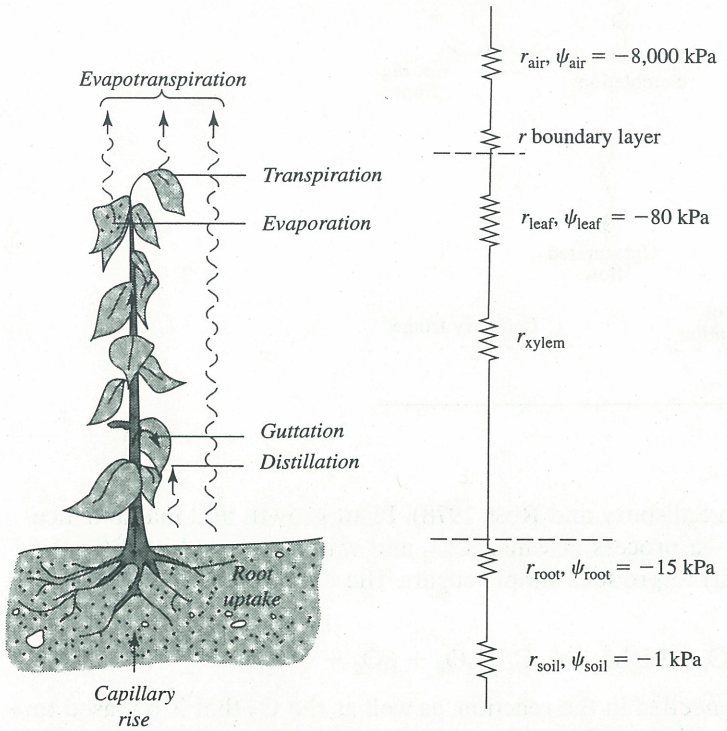

differentially, at rates that depend on cell structure and development (figure 9.27). Most of the water is absorbed where full root-cell structure develops in young cells; little water is absorbed at the root tips (for details, see Kramer and Boyer 1995). Once again, following the water-potential gradient (see figure 9.26, bottom), water is absorbed by roots and eventually reaches the root xylem; these are the fine, tubular structures near the center of roots and stems. Water in the xylem responds to water potential and consequently, it moves up the stems into the leaves. Continuing along the gradient, water passes through mesophyll cells and into the stomatal cavities, where it diffuses through stomata and into the atmosphere.

Transpiration is the process whereby water within plants is evaporated—either within stomata or at plant surfaces—and released to the atmosphere. Evapotranspiration is the combination of evaporation (including that from soil, soil cover, and plant surfaces) and transpiration. As a general rule, water loss to the atmosphere by transpiration is substantially

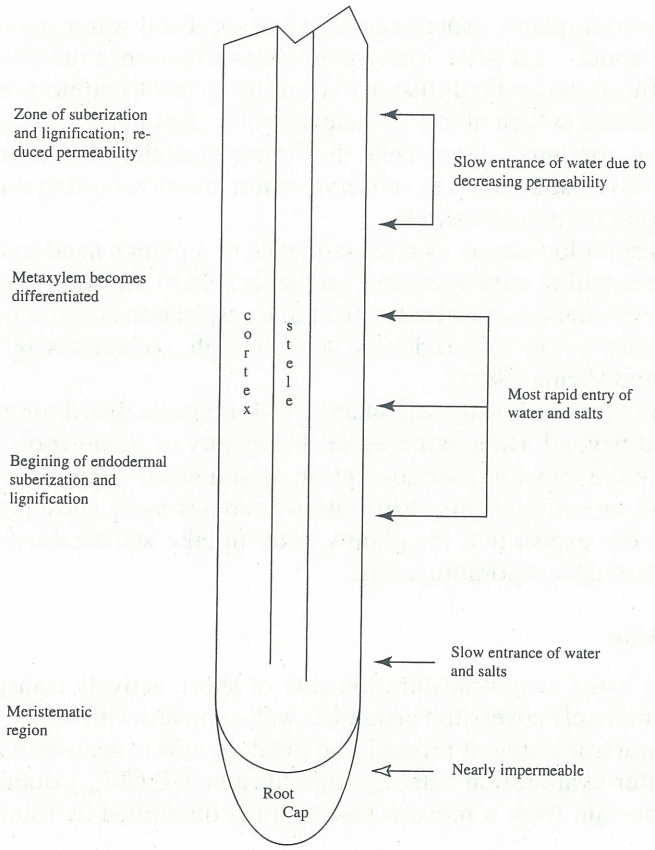

Figure 9.27 Diagram of a root cross-section indicating areas of water and solute absorption related to cell structure and development (after Kramer and Boyer 1995). Greatest absorption occurs where root xylem becomes fully functional, behind the meristematic region but before the older endodermal region, where suberization and lignification (corky and woody tissue) reduce permeability of water.

larger than that of soil evaporation alone. At the height of the growing season, crops typically extract ≃8 mm of water per day from soils, transpiring up to 5–10 times the amount of water they contain at any one time (Rosenberg, Blad, and Verma 1983). Over the course of a growing season, these rates account for substantial cumulative totals; for example, up to 1,000 kg of water is used in evapotranspiration to produce 1 kg of wheat. Citing corn growing in a semi-arid area, Salisbury and Ross (1978) found soil evaporation to be only one-fourth of the cumulative evapotranspiration over the growing season.

Among a variety of other factors (e.g., soil-moisture levels and plant physiology), the transpiration rate depends upon the number and size of stomata, their function, and the amount of leaf area (for details, see Gates 1980). Stomatal openings occupy only ≃1–3 percent of leaf surface area, yet about 90 percent of transpiration occurs through them. The remaining 10 percent of transpiration occurs by the diffusion of water through leaf epidermal cell walls and the overlying cuticle (a waxy covering). Resistance to diffusion through stomata normally is in the range of several hundred seconds/meter, while it is more than 1 to 2 orders of magnitude greater across the cuticle. Stomata tend to close under the following conditions: low-light intensity; temperature extremes; mechanical disturbance (such as wind); exposure to certain pollutants; and the lack of either sufficient soil moisture in the root zone or the ability of roots to uptake water sufficient to meet transpiration rates. When stomata close, the only source of transpiration is that of diffusion through the leaf cuticle (Gates 1980).

While stomatal function is the primary means for controlling transpiration and the subsequent movement of water from the root zone (rhizosphere) into the plant, it is not the only

control. Most (terrestrial) plants experience dehydration if soil-water potential (osmotic + matric) falls below about −1.5 MPa. Many plants also experience dehydration if soils become saturated; in this instance, O_2 diffusion to roots is too low to support metabolic activity, thus leading to a decrease in their ability to conduct water (Kramer and Boyer 1995). If water loss by transpiration continues, guard cells that sense declining leaf water-potential (i.e., larger negative values) close stomata to conserve water, thereby shutting down transpiration and, subsequently, photosynthesis as well.

Although transpiration occurs as a consequence of a plant's need to obtain CO_2 from the atmosphere, the resulting water-potential gradients help to transport dissolved soil-water nutrients to leaves. Another beneficial side-effect of transpiration is that it helps to cool plant leaves, when humidity is low and radiation load is high, sometimes by several degrees (Rosenberg, Blad, and Verma 1983).

Plant-root uptake of soil water can change soil-moisture distribution substantially in the rhizosphere and beyond. Data gathered in the vicinity of onion roots by Dunham and Nye (1973) illustrate the effect of root absorption on soil water and its distribution (see figure 9.28). The effect on soil-moisture distribution becomes more substantial at lower soil-moisture levels. We can expect that the plant's water uptake will accelerate the rate of soil drying, more than through evaporation alone.

Model Estimates of Evapotranspiration

Potential ET (ET_p) is the evapotranspiration rate of short, actively transpiring vegetation (e.g., grass) that: completely covers the ground; is well-supplied with water; and exerts negligible resistance to water movement through the plant. In arid to semi-arid regions, ET_p may exceed the free-water evaporation rate, E_o. Equilibrium ET (ET_{eq}) defines the minimum possible evaporation rate from a moist surface, and is quantified as (Slatyer and McIlroy 1961):

$$ET_{eq} = \left[\frac{s}{s + y}\right](R_n + G) \tag{9.62}$$

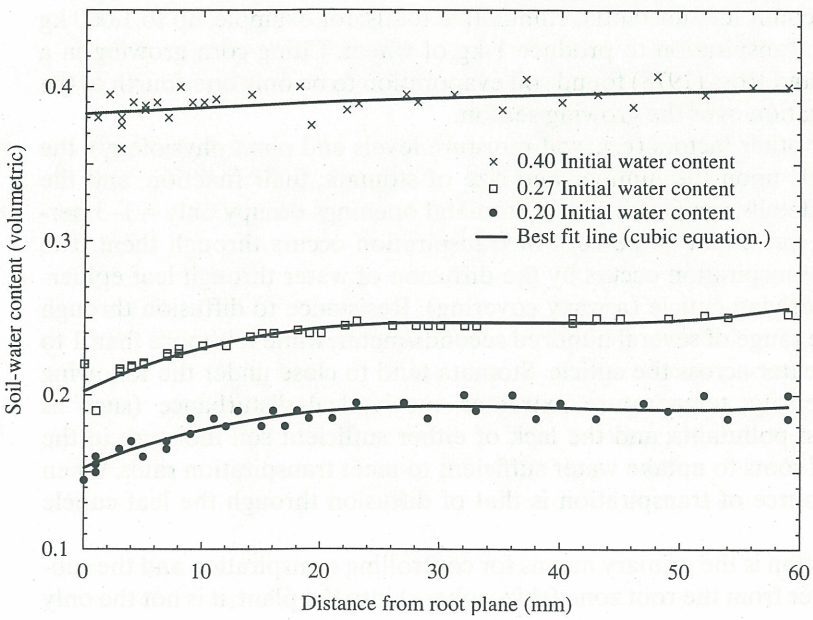

Figure 9.28 Soil-moisture distribution of a sandy soil in the vicinity of an onion root mat attached to live shoots after 2.5 days. Water content was 42–45 percent (top), 27 percent (middle), and 20 percent (bottom). Data represent measurements from either side of the root mat (data from Dunham and Nye 1973)

where s is the slope of the saturation–vapor-pressure curve at the wet-bulb temperature and γ is the psychrometric constant ($C_p P/\varepsilon L_v$).

A variety of approaches are available for estimating ET, many of which are described in Rosenberg, Bard, and Verma (1983). This chapter focuses on a number of physically derived and semi-empirical models that have global applicability. Some regression (and other, strictly empirical) approaches of ET estimation based on the use of routinely measured climate variables are covered in chapter 12.

Penman model A model proposed by Penman (1948) was derived from energy-balance and aerodynamic equations. This method has been widely accepted in agriculture and hydrology, since few measurements are needed and it usually produces reasonable estimates. Originally derived for open water, evaporation is given by:

$$E = \frac{sR_{nw} + \gamma E_a}{s + \gamma} \tag{9.63}$$

where R_{nw} is net radiation over water. A variety of semi-empirical equations have been used to specify E_a (see Rosenberg, Bard, and Verma 1983), which is a function of wind-speed and the vapor-pressure deficit. Penman (1948) multiplied equation 9.63 by an empirically derived factor to estimate ET, but Thom and Oliver (1977) found a better global application of equation 9.63 by replacing R_{nw} with $(R_n + G)$, without the empirical coefficient.

Priestly–Taylor A semi-empirical formula for ET_p was proposed by Priestly and Taylor (1972):

$$ET_p = \alpha \frac{s}{s + \gamma}(R_n + G) \tag{9.64}$$

where α is an empirically derived constant (conceptually equivalent to ET_p/ET_{eq}), with values ranging from 1.08–1.34 and a mean of 1.26 (Priestly and Taylor 1972). α appears sensitive to surface soil-moisture levels ($\alpha = 1.26$ for wet surfaces). The relation for non-ET_p conditions appears to be inconsistent (Williams et al. 1978; Rosenberg et al. 1983).

Penman–Monteith Monteith (1965) expanded the Penman model to improve simulation of vegetation feedbacks on ET by inclusion of resistance terms (units of s m^{-1}) for the aerial transport of water vapor (r_a) from the canopy, and the resistance to vapor transport through stomata (r_c). This was an important development, since for any land surface covered with vegetation, r_c largely controls the transpiration rate and, consequently, much of $L_v E$. In contrast to previous models, this model predicts actual ET (as $L_v E$; energy) in contrast to ET_p:

$$L_v E = \frac{s(R_n + G) + \rho_a C_p[(e_s - e_a)/r_a]}{(s + \gamma)[(r_a + r_c)/r_a]} \tag{9.65}$$

Difficulties in the practical application of equation 9.65 include obtaining stomatal-resistance data (either through direct measurements or a surrogate). Wind-speed measurements are required for r_a, which varies with vegetation type. Details on the application of the Penman–Monteith model and closely related models—some more sensitive to sparse vegetation canopies than equation 9.65—can be found in Jensen, Burman, and Allen (1990) and Stannard (1993). An important finding by Stannard was that, when r_c must be estimated (i.e., when measurements are not available), the Penman model predicted measured-ET better than the Penman–Monteith model.

Water-budget ET is one of the key elements of the hydrologic cycle (or water budget) of a land surface (Garratt 1992):

$$\rho_w\left(P_R - d\frac{\partial\theta}{\partial t}\right) = ET + D + R \tag{9.66}$$

where all terms are kg m^{-2} s^{-1}. Terms on the left side of equation 9.66 account for water in a soil layer of depth (d). P_R is the precipitation rate, m s^{-1}, and θ is soil-water content. These terms are balanced by the "loss" terms on the right, where D is drainage (or water loss) through the bottom of the soil layer and R is surface run-off. Assuming the budget is closed, ET can be estimated as a residual term in equation 9.66, provided all other terms are measured accurately.

9.6 MEASURING ENERGY BUDGET TERMS

Soil heat flux Knowing a temperature profile and thermal conductivity, soil-heat flux can be calculated by applying equation 9.34. In practice, conductivity is a difficult parameter to obtain in the field, made more complex by the temporal variability of water content and soil compaction. Soil-heat flux plates (see figure 9.29) allow flux to be measured directly. Heat-flux plates consist of differential thermopiles (or multiple thermocouple junctions) embedded in the top and bottom of a substance with a known thermal conductance (usually $\simeq$1.2 W m^{-2}); chosen to be similar to that of typical soil, so that the naturally occurring thermal gradient in their vicinity is minimally distorted. They are usually made of a material with low heat-capacity and kept small to enable them to respond quickly to temperature changes. The small size of the soil-heat flux plates also minimizes latent-heat exchanges, due to the condensation or vaporization of water caused by differential heating or cooling that results from their presence. Although the plate's thermal conductivity is representative of that of many soils, it can differ substantially from that of the soil at the measurement site. Thus, the plates cannot be positioned at or near the surface, since their presence can substantially alter heat flux in this region of very strong temperature gradients. Typically, they are instead placed at a depth of 5 to 10 cm, where thermal gradients are smaller and the distortion of these gradients is less. However, short-term fluctuations in heat flux cannot be measured with this placement, because they are damped-out in the top few centimeters of soil.

The combination method (Stannard et al. 1994) offers a means by which soil-heat flux (at some depth) can be measured with heat-flux plates, and combined with a measurement of change in heat storage in soil above the plate:

$$G_{\text{Tot}} = G_x + G_{\text{stor}} \tag{9.67}$$

G_x is the heat flux measured by a heat-flux plate; G_{stor} is calculated by measuring soil temperature at a number of depths, averaging the temperatures, and then multiplying the result by the specific-heat capacity of the soil layer above the plate, determined from specific mea-

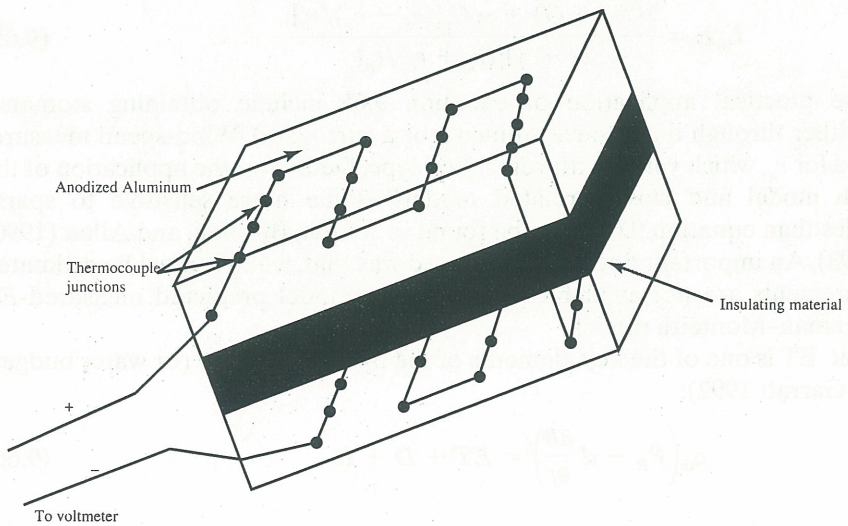

Figure 9.29 Schematic diagram of a soil-heat flux plate. The model consists of a differential thermopile with thermocouples embedded in substrates near the top and bottom surfaces of the instrument. Magnitude of the difference between thermocouple (in series) on the top of the plate versus those (in series) on the bottom is proportional to heat flux (plate thickness exaggerated to show detail).

surements of soil density, composition and moisture. Temperature can be measured at equidistant points above the heat-flux plate, or if the depth is greater than several centimeters, at logarithmic spacing (densest sampling near the surface), to capture the non-linear temperature profile. Another problem that may need to be addressed is properly accounting for latent-heat transport, related to the movement of water vapor. If significant, the soil-moisture profile would need to be measured concurrently.

Some practical problems with field measurements of soil-heat flux include: disruption of the natural soil profile (its structure and moisture) when installing sensors; installing enough sensors for measuring the soil-temperature profile; and sampling heat flux at enough locations to avoid spatial bias due to soil heterogeneities—either inherent in the soil, slope, or with vegetative cover.

Net radiation As shown in section 9.2, net radiation is the difference of incoming radiation minus that of outgoing. Net radiometers are identical, in the principle of operation, to soil heat-flux plates, where thermopiles are embedded in both upper and lower portions of a substrate of known thermal properties. The upward- and downward-facing surfaces that intercept radiation are painted with a high-emissivity black paint, simulating blackbody emissivity. Transparent domes cover the radiometers' sensing surfaces to shield them from dust and moisture, which could modify radiative characteristics (absorptivity and emissivity) of these surfaces (see Rosenberg, Bard, and Verma 1983 for more details).

Sensible and latent-heat fluxes These surface fluxes are typically measured with micrometeorological methods: gradient; aerodynamic; Bowen-ratio-energy-balance (BREB); or eddy covariance. Ideally, all micrometeorological methods require a homogeneous (in terms of surface roughness and flux), flat surface area upwind of the point of measurement. This surface area is referred to as the flux footprint, and the linear distance of its upwind leading edge to the instruments is called the fetch. The depth of the atmosphere that is in equilibrium with the surface area (the equilibrium boundary layer, lying at the bottom of the surface layer) increases at about 1 m per 100 m of fetch. Considering limitations of current instrumentation for flux measurement and characteristics of atmospheric turbulence over vegetation it is generally desirable to install instruments 1–2 m above ground level over short vegetation (e.g., grass, wheat), and at least twice the plant height over tall vegetation such as forests. Thus, the decision regarding site selection for micrometeorological flux measurements primarily must weigh fetch (being aware of both wind direction and speed variability), instrumentation limits, and surface characteristics. For small areas or plots, latent-heat flux can be derived from weighing lysimeters that directly measure the amount of water lost to evaporation. Details of these methods may be found in Rosenberg, Bard, and Verma (1983), Verma (1990), and Daamen et al. (1993). For the sake of brevity, our present review of methods will focus on the BREB and eddy-covariance methods, which are used most often in the field for flux estimates from large areas (on the order of several hectares or more).

BREB The BREB method provides a robust and low-cost means of obtaining H and L_vE. This method relies on the assumptions of energy-budget closure and similarity in the turbulent transport of sensible and latent heats. Energy-budget closure is expressed as:

$$R_n + G + H + L_vE = 0 \tag{9.68}$$

In applying equation 9.68, we assume that there is no energy storage above the soil surface (such as within a vegetation canopy). Expressions for H and L_vE in terms of thermal and vapor gradients in the atmosphere's turbulent surface layer (see figure 9.5) are:

$$H = \rho C_p K_h \frac{\partial \overline{T}}{\partial z} \tag{9.69}$$

$$L_vE = L_v\rho \frac{\varepsilon}{P} K_v \frac{\partial \overline{e}}{\partial z} = L_v K_v \frac{\partial \overline{\rho_v}}{\partial z} \tag{9.70}$$

where C_p is specific heat of air at constant pressure (~1.005 kJ kg^{-1} K^{-1}), ε is the ratio of molecular weights between water and dry air (0.622), P is atmospheric pressure [kPa], z is height above ground, and K is the turbulent-exchange coefficient, or eddy diffusivity [m^2 s^{-1}]. Subscripts (h and v) refer to heat and water vapor, respectively; overbars indicate a time average. The BREB method assumes that $K_v = K_h$. While this can be true under neutral thermal stability (windy daytime conditions in the presence of small (~0) air-to-surface temperature gradients), it is only an approximation under other conditions. Substituting equations 9.69 and 9.70 into 9.68, solving for K, and assuming eddy diffusivities are equivalent, we find

$$K_h = K_v = -\frac{(R_n + G)}{\rho\left(C_p \frac{\partial \overline{T}}{\partial z} + L_v\left(\frac{\varepsilon}{P}\frac{\partial \overline{e}}{\partial z}\right)\right)} \tag{9.71}$$

By substituting equation 9.71 into 9.70, we obtain:

$$L_v E = -\frac{R_n + G}{1 + \beta} \tag{9.72}$$

where β is the Bowen ratio $H/L_vE = \gamma(d\overline{T}/d\overline{e})$.

The beauty of the BREB method is that no wind-speed measurements are needed, and the equipment required for taking the measurements is robust and relatively inexpensive. Typically, only an aspirated, wet- and dry-bulb psychrometer system is needed, in addition to radiation and soil-heat flux measurements. However, we need to remember that BREB measurements must be conducted at sites where the inherent assumptions in method development closely approximate reality.

Eddy covariance Increasing in popularity because of its lowered instrument costs, more robust instrumentation, and ease of use, the eddy-covariance (or eddy-correlation) method offers a direct means to measure H and L_vE. The principle of the measurement is to obtain the covariance of the product of fluctuations in vertical velocity and the scalar variable of interest (e.g., temperature, T' or water-vapor density fluctuations, ρ_v'), measured at a distance above the surface

$$H = -\rho C_p \overline{w'T'} \tag{9.73}$$

$$L_v E = -L_v \overline{w'\rho_v'} \tag{9.74}$$

where the deviations (primes) from the means (overbars) in vertical velocity and the entity of interest are defined by: $w = \overline{w} + w'$; $T = \overline{T} + T'$; $\rho_v = \overline{\rho_v} + \rho_v'$. Because of fluctuations in air density, equation 9.74 (actually a simplified result) must be adjusted. Following Webb, Pearman, and Leuning (1980), equation 9.74 becomes:

$$L_v E = L_v \overline{w'\rho_v'} + (1 + 1.61\overline{q})\frac{\overline{\rho_v}}{\overline{T}}\overline{w'T'} \tag{9.75}$$

where q is specific water vapor (defined in equation 9.10).

Key to the success of eddy-covariance measurements are fast-response instruments. A basic deployment of some often-used eddy-covariance instruments is depicted in figure 9.30. Most eddy-covariance sensors are capable of making accurate measurements at a frequency faster than 10 Hz. Sonic anemometers are often chosen for the wind-velocity measurement and some can derive temperature fluctuations from speed-of-sound measurements as well. However, in this case, temperature is virtual temperature, (temperature that dry air would have if it was of the same density as air containing water vapor) and must be converted to kinetic temperature to calculate sensible-heat flux. Other sonic anemometers are outfitted with a fine-wire (~.02 mm) thermocouple for kinetic-temperature measurement. Humidity often

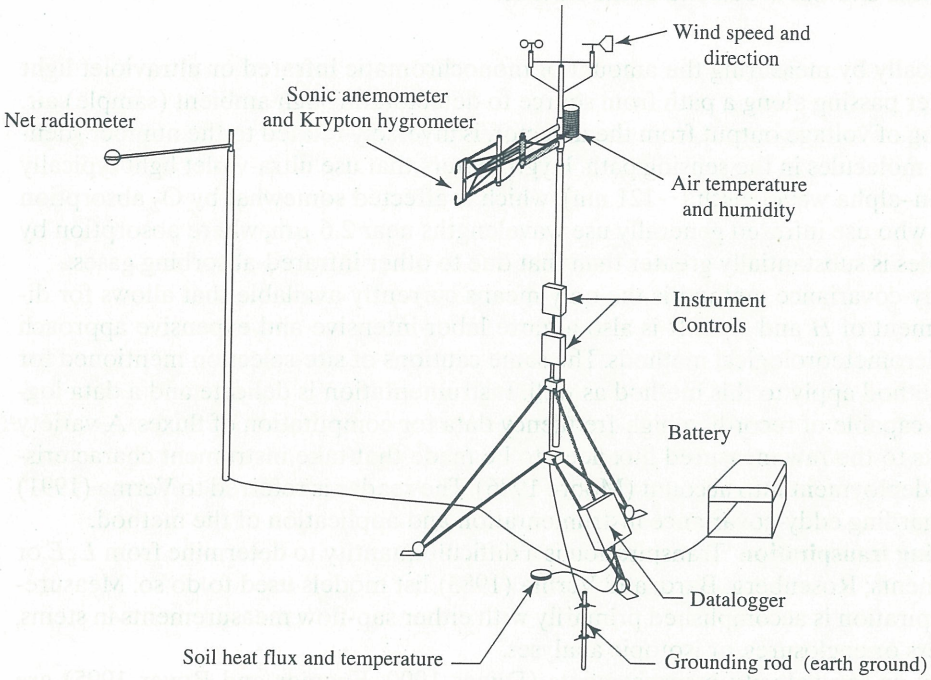

(a)

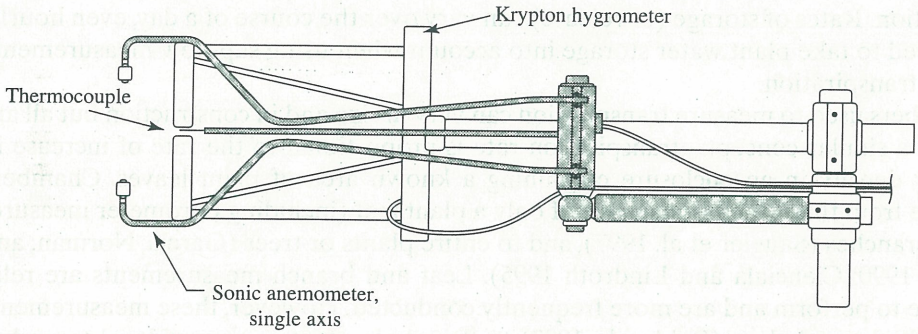

(b)

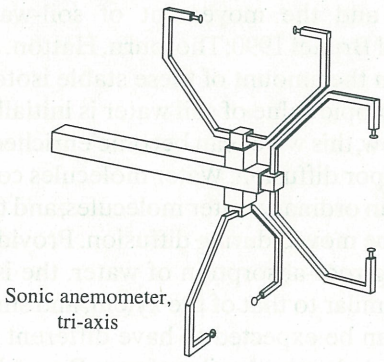

(c)

Figure 9.30 A basic eddy-covariance deployment, providing sensible- and latent-heat flux measurements. A net radiometer and soil-heat flux plates supplement the array to provide measurements of major energy-budget terms (a). Single-axis sonic anemometer (vertical velocity sensing only) outfitted with a fine-wire thermocouple and krypton hygrometer (to sense water-vapor density) is depicted in (b). Tri-axis sonic anemometers (c) provide complete velocity measurement and virtual temperature. Panels (a) and (b) courtesy of Campbell Scientific, Logan, UT; panel (c) courtesy of Applied Technologies, Boulder, CO.

is sensed optically by measuring the amount of monochromatic infrared or ultraviolet light remaining after passing along a path from source to detector, through ambient (sample) air. The natural log of voltage output from the detector, is inversely related to the number (density) of vapor molecules in the sensing path. Hygrometers that use ultra-violet light typically use the Lyman–alpha wavelength (~121 nm), which is affected somewhat by O_2 absorption of UV. Those who use infrared generally use wavelengths near 2.6 μm, where absorption by water molecules is substantially greater than that due to other infrared-absorbing gases.

The eddy-covariance method is the only means currently available that allows for direct measurement of H and L_vE. It is also a more labor-intensive and expensive approach than other micrometeorological methods. The same cautions of site-selection mentioned for the BREB-method apply to this method as well. Instrumentation is delicate and a data logger is needed capable of recording high-frequency data for computation of fluxes. A variety of adjustments to the raw measured flux need to be made that take instrument characteristics and their deployment into account (Moore 1986). The reader is referred to Verma (1991) for details regarding eddy-covariance instrumentation and application of the method.

Measuring transpiration Transpiration is a difficult quantity to determine from L_vE or ET measurements; Rosenberg, Bard, and Verma (1983) list models used to do so. Measurement of transpiration is accomplished primarily with either sap-flow measurements in stems, plant chambers or enclosures, or isotopic analyses.

Sap-flow or sap-velocity measurements (Dugas 1990; Kramer and Boyer 1995) are used to estimate the amount of water traveling through stems. The operating assumption is that the amount of water measured by sap flow is proportional to the amount transpired; however, plants can store (or release) water in sufficient quantity at times, as to invalidate the assumption. Rates of storage (or release) can vary over the course of a day, even hourly. Thus, we need to take plant water storage into account when using sap-flow measurements to estimate transpiration.

Chambers used to measure transpiration can vary in size and in construction but all are based upon a similar concept—transpiration rate is proportional to the rate of increase in water-vapor density in an enclosure containing a known area of plant leaves. Chambers range in size from that which is inclusive of only a plant leaf (including porometer measurements), to branches (Saugier et al. 1997), and to entire plants or trees (Garcia, Norman, and McDermitt 1990; Cienciala and Lindroth 1995). Leaf and branch measurements are relatively simple to perform and are more frequently conducted. However, these measurements must carefully be scaled-up (Baldocchi 1993) to the whole plant or canopy level to understand the significance of transpiration on soil moisture. Successful use of this method requires a well-planned temporal and spatial sampling strategy.

Recently, the stable isotopes deuterium (^{2}H) and oxygen-18 (^{18}O) have been used in attempts to quantify transpiration and the movement of soil-water in the soil–plant–atmosphere continuum (Walker and Brunel 1990; Thorburn, Hatton, and Walker 1993). There is a naturally occurring variability in the amount of these stable isotopes found in the air, foliage, soil, and ground water. The isotopic value of soil water is initially determined by precipitation. At the soil's surface and below, this water can become enriched with ^{2}H and ^{18}O during the processes of evaporation and vapor diffusion. Water molecules consisting of the combination of these isotopes are heavier than ordinary water molecules, and thereby require more energy to reach the vapor phase or to be moved during diffusion. Provided that little isotope-enrichment or depletion occurs during root-absorption of water, the isotopic concentration of transpired water is expected to be similar to that of the xylem, and similar to the soil source of this water. Thus, transpired water can be expected to have different concentrations of stable isotopes than water evaporated from plant and soil surfaces. By evaluating the isotopic ratio of air above canopy vegetation, the relative strength of transpiration to measured evapotranspiration is obtained for a plant canopy. If ET is concurrently measured, then transpiration

can be quantified. The stable-isotope method offers an attractive potential as a means of quantifying transpiration and determining the source of transpired water. However, at this time, it is still undergoing experimental development and field verification.

9.7 SOIL-GAS TRANSPORT

Soil gases move in response to pressure gradients; that is, air moves from a higher pressure potential to a lower one. Additionally, since air is made up of a number of gases, each species can have different concentration gradient that drive individual gases in different directions. Thus, at any time, gas transport can occur in response to the total pressure gradient of air, as well as that of the partial pressure gradients of individual gas species in the air. The objective of this section is to develop an understanding of these and other gas-transport mechanisms operating in soil. Before doing so, a review of basic properties of gases is provided.

General Properties of Gases

Variables of state and ideal gases If we consider a gas as consisting of a number of individual molecules, we could describe it as having a chaotic system of motions and collisions. However, when considered en masse, this same population of chaotic molecules could instead be described by nonchaotic variables of state (the basis of the continuum hypothesis): mass (M), volume (V), pressure (P), temperature (T) and composition. For now, we focus on ideal gases that are stable in time (nonreactive, nondecaying) and do not exhibit a change in phase with a change in temperature. Variables of state can be combined to form specific variables, such as density ($\rho = M/V$) and specific volume ($a = V/M$). In this review, we refer to standard conditions for a gas: pressure (P_o = 101.3 kPa), temperature (T_o = 273 K), and mole-volume (mole = 22.4 liters).

Charles' law In the late 1700s, Jacques Charles and Joseph Gay-Lussac found that an ideal gas, contained in sealed insulated vessels and uniform pressure, undergo a change in temperature corresponding to a change in volume. Thus, at constant pressure (P_o) a gas initially at temperature (T_o) and specific volume (a_o), will have a new temperature (T) when its specific volume has been changed to (a):

$$\frac{a(T, P_o)}{T} = \frac{a_o(T_o, P_o)}{T_o} \tag{9.76}$$

Boyle's law In the 1660s, Robert Boyle adjusted pressure and volume at a constant temperature, and found that pressure is inversely proportional to specific volume

$$Pa = C(T) \tag{9.77}$$

where C is a temperature-dependent constant.

Ideal gas law It was later found that Charles' Law compliments Boyle's Law by providing a means of relating P, T, and a in a powerful relation we call the ideal gas law. From Boyle's Law, we can write (at a fixed temperature)

$$Pa(T, P) = P_o a(T, P_o) \tag{9.78}$$

Using Charles' Law (equation 9.76), we substitute for $a(T, P_o)$ in equation 9.78 to obtain:

$$Pa(T, P) = \frac{P_o a(T_o, P_o)}{T_o} T = RT \tag{9.79}$$

where R is the specific gas constant. Equation 9.79 is the ideal gas law, which can be written in terms of volume if we consider a mass of gas equal to its molecular weight (i.e., a mole of gas)

$$PV = mRT \tag{9.80}$$

where m is molecular weight, and volume is $V = ma$. Equation 9.80, Avogadro's Law states that a mole of ideal gas will occupy the same volume as a mole of any other ideal gas, at the same temperature and pressure. Therefore, a more general form of equation 9.80 is

$$\frac{PV}{T} = mR = R^* \tag{9.81}$$

where R^* is the universal gas constant (8.3144 J mol^{-1} K^{-1}).

Dalton's law The soil-air and atmosphere are a mixture of a number of gases. Dalton's Law of Partial Pressures states that the total pressure (P_{total}) of a gas mixture is equal to the sum of pressures of each gas:

$$P_{\text{total}} = \sum_{i=1}^{n} P_i \tag{9.82}$$

For each ideal gas

$$P_i = \frac{R^*T}{m_i a_i} = \frac{R^* M_i T}{m_i V} \tag{9.83}$$

where M_i is the mass of gas (i). For the gas mixture, we write

$$P_{\text{total}} = \frac{R^*T}{V} \sum \frac{M_i}{m_i} \tag{9.84}$$

Since $V = Ma$, equation 9.84 can be rewritten as:

$$Pa = R^*T \frac{\sum \frac{M_i}{m_i}}{\sum M_i} = \frac{R^*T}{\overline{m}} \tag{9.85}$$

Thus, the specific-gas constant for dry air ($R = R^*/m_d = 287.04$ J mol^{-1} K^{-1}) can be calculated once the mean molecular weight of dry air is found. Weight, $\overline{m}$, is defined more specifically as the mass-weighted harmonic mean of the molecular components that comprise dry air.

Porosity and Permeability

Porosity ϕ is defined as the volume ratio of fluids (gas and liquid) in soil, to the total soil volume (solid and fluid components):

$$\phi = \frac{V_a + V_l}{V_a + V_l + V_s} \tag{9.86}$$

Coarse-textured, sandy soils tend to have the greatest porosity, typically about 35 percent, and have a high V_a (field-air capacity) fraction. Water-filled pores drain quickly, since these soils usually consist of siliconitious, nonhygroscopic particles, and large pores. In contrast, fine-textured soils, which may have a high content of loam or clay, drain slowly and typically, are easily compacted. They tend to be poorly aerated and can have a field-air capacity of only 5 percent. These soils often contain soil macropores and soil aggregates which can exceed 5 mm in diameter. Thus, the soil porosity in these soils can vary greatly in space and time.

In contrast to porosity, air permeability defines the ability of a soil to conduct fluids (air and water) through it via connected interstitial spaces, or pores (Katz et al. 1959). Permeability is determined solely by structure, and hence is also referred to as intrinsic permeability. Changes in permeability occur if the soil structure is altered by water (Marshall and

Holmes 1979), or by compaction. Permeability [Darcys, L^2], and can be calculated from the equation for flux

$$k = -\eta q \left[\frac{dx}{dP}\right] \tag{9.87}$$

where q is flux density (a volume flow-rate per unit area), η is dynamic viscosity [Pa s], x is distance over which a pressure (P) differential [Pa] is measured. Hydraulic conductivity (K), on the other hand, is a function of the fluid properties of viscosity and density, as well as the properties of the medium. The following expresses its relation to permeability:

$$K = \frac{gk}{\nu} \tag{9.88}$$

where g is gravitational acceleration and $\nu\ (= \eta/\rho)$ [$m^2 s^{-1}$] is kinematic viscosity.

QUESTION 9.7

Why would an increase in field air capacity not necessarily show a similar increase in air permeability?

Physical Mechanisms Responsible for Soil-gas Transport

There are three modes of gas transport in the vadose zone that usually operate simultaneously and in parallel (see figure 9.31). Viscous flow (also known as mass, advective, or bulk flow) is caused by a pressure (force per unit area) gradient in a gas mixture that results in mass movement of gas molecules down the pressure gradient. Gas movement by diffusion occurs due to molecular interactions. When a gas is concentrated in one region of a mixture more than another, it is a probabilistic outcome of the random motions of gas molecules that this gas spreads or diffuses into other regions. The molecules of the diffusing gas possess an overall velocity differing from that of the mixture; this is the diffusive flux. Thus, a diffusive flux occurs as a result of a concentration or partial-pressure gradient of individual gases. Generally, viscous and diffusive fluxes are the primary means by which gases move through soil. The third mode of gas transport is surface flow, occurring by nonreactive absorption of gas onto soil surfaces. It is a complex phenomenon, typically of secondary significance (Mason and Milanausksa 1983), and is beyond the scope of this text. The relative significance of the differing modes of transport depends upon the total- and partial-pressure gradients, molar concentration of the gases and their viscosities, and the physical properties of the soil. Small environmental changes can determine the relative significance of transport mechanisms. For instance, Thorstenson and Pollock (1989b) found that a pressure gradient of only 1 Pa m^{-1} in a sandy soil can lead to the development of a viscous flow that exceeds most diffusive flows under most circumstances.

Mechanisms inducing viscous (mass) flow Viscous flow is facilitated by the presence of a pressure gradient or potential. To equalize pressure, a mass of air travels from a region of higher pressure and density to a lower one. The air flowing from region to region through soil experiences a resistance to movement from the rough surfaces of pore walls; specifically, momentum of the moving gas molecules is lost to the stagnant pore walls. We call this resistance friction. The efficiency of momentum-transfer from the gas to the walls grows with increasing viscosity of the gas, and is much higher if flow is turbulent. Viscous transport within soil pores is ordinarily well-organized, (laminar) because flow velocities are low and soil-pore sizes are small. In contrast, turbulent flow, dominating atmospheric transport, is characterized by random motions of air.

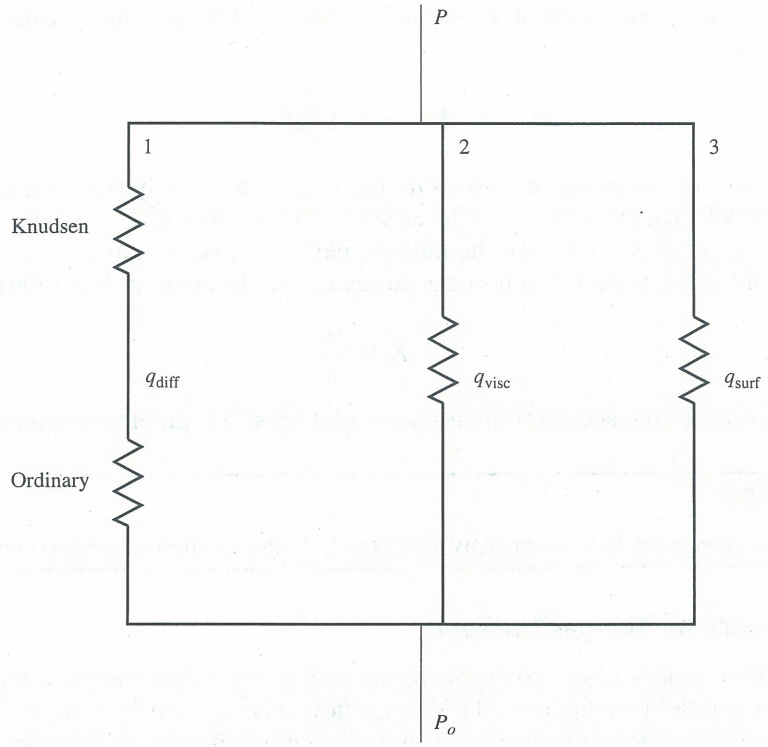

Figure 9.31 Conceptual diagram using an electrical analog to illustrate the relations between fluxes (q) and their associated resistances (jagged symbol) to the transport of gases in soil. Diffusive, viscous, and surface fluxes operate in parallel (independently), responding to the difference ($P_o - P$). Their sum is the total flux. For simplicity, non-equimolar flux is not shown, since it can be a positive or negative contribution to total diffusive flux. If it were included, it would appear in some unique form in branch 1.

1: Diffusive flow branch
2: Viscous flow branch
3: Surface flow branch

The nondimensional Reynolds number provides us with a convenient means for determining whether flow is laminar or turbulent, based on basic properties of the fluid and the medium containing it:

$$Re = \frac{Uk^{1/2}}{\nu} \tag{9.89}$$

This nondimensional quantity is applicable to any fluid (gas or liquid) in soil, and is comprised of the mean-flow velocity of the fluid (U) [m s^{-1}], gas permeability (k) [m^2], and kinematic viscosity of the gas (ν), which is a function of the molecular properties and density of the gas. Equation 9.89 has been adapted from classical fluid-dynamic studies of pipe flow, where a characteristic length (such as diameter) is used in place of $k^{1/2}$; Ward (1964) shows how $k^{1/2}$ is related to characteristic length. In soil, fluid flows with Reynolds' numbers below about 1 are laminar. They are transitional in the 1–200 range and fully turbulent above 200 (Ward 1964). Equation 9.89 is similar to equation 6.17, except that the latter assumes an equivalence between grain and pore size for the characteristic-length dimension.

Mechanisms initiating mass flow are varied and can be linked to either density (thermal) or pressure-induced changes occurring above or within soil. Differential soil heating creates thermal gradients and consequently, density-driven mass (viscous) flow. However, it only accounts for ≃0.1–0.5 percent of soil-gas exchange (Romell 1922). In contrast, pressure fluctuations associated with large-scale weather patterns that occur with periods from many hours to many days, can penetrate well into soil and can enhance movement of gases significantly, particularly if the unsaturated zone is deep (Buckingham 1904; Nilson et al. 1991).

This mechanism is referred to as "barometric-pumping." The depth of influence and impact on soil-gas exchange of this phenomenon varies with the amplitude of the pressure change at the surface, its period, soil-water content of the unsaturated zone and its depth, and with soil porosity. Over a 10-hour period Weeks (1978) found a change of 20 Pa in soil-air pressure at a 32-m depth in soil due to an atmospheric-pressure change of $\simeq$100 Pa at the surface. Clements and Wilkening (1974) studied ^{222}Rn efflux in an arid region, and found a 20–60 percent increase in gas-exchange rates with changing synoptic weather patterns that were responsible for a 100–200 Pa surface pressure change in a day. In contrast to deep, dry soils, barometric pressure changes above shallow soils ($\leq$ 15 m above a high-water table) have little effect on total soil-gas exchange (Kimball 1983).

Soil-gas exchanges are also induced by pressure fluctuations of a more-minute scale (on the order of several Pa in soil), that occur as turbulent wind gusts pass over a rough surface. This mechanism is referred to as "wind-pumping." The associated pressure fluctuations have a duration on the order of fractions-of-a-second to minutes. As a consequence of their high frequency and viscous damping in soil pores, they have a much shallower penetration into soil than those related to barometric-pumping. Kimball and Lemon (1971) found that wind-pumping strongly diminishes from the soil-atmosphere interface downward, becoming negligible below several centimeters, even in coarse, sandy soils. Wind-pumping occurs in two parts. Ahead of an approaching wind gust, air pressure is slightly higher than the time-average and some air is forced downward, into the soil. With the gust's passage, pressure decreases and air moves upward, out of the soil. Shaw et al. (1990) document the creation of coherent, well-defined, turbulent structures penetrating from the top of a forest to the forest floor, thereby inducing pressure fluctuations. Baldocchi et al. (1991) found that these pressure fluctuations at the soil's surface measurably increased flux of CO_2 from the forest floor (litter and soil). Although there is typically little net effect on gaseous exchanges in the entire soil-air volume (Romell (1922) estimates about 0.1 percent of soil-gas is exchanged this way), the rate of soil-atmosphere exchanges in the uppermost portion of soils can be affected greatly (Farrell, Greacen, and Gurr 1966; Kimball and Lemon 1971). Wind-pumping can substantially enhance the local rate-of-drying of the top layer of soil (Baldocchi and Meyers 1991), which includes mulches and humus. Kimball and Lemon (1971) report that soil evaporation in a 2-cm layer of coarse sand proceeded at a rate about double that attributable to diffusion alone. With increasing soil-water content, soil-gas exchanges initiated by wind-pumping rapidly diminish.

Wind flow over topography (mountains), or topographic flow, can produce pressure gradients between upwind and downwind exposures that can induce mass flow through the unsaturated zone. Weeks (1993) documented an example of this flow through highly fractured rock, deep within Yucca Mountain (a prospective nuclear-waste repository). Flow was in response to a combination of atmospheric-pressure changes and wind-induced pressure patterns over the mountain.

Pressure-induced viscous flow also occurs with the infiltration of rainfall and snowmelt that initiate mass flow by displacing air-filled pore space ahead of the wetting front. As water moves downward, it draws air from the surface into the soil above the drying front. The amount of soil-gas exchange due to infiltration by water can vary widely due to soil porosity, frequency, and intensity of wetting events. Romell (1922) estimated that overall, about 7–9 percent of soil–atmosphere gas-exchange was attributable to this mechanism.

QUESTION 9.8

Determine whether viscous flow in a fine, sandy soil is laminar or turbulent. We know that $\nu \sim 10^{-6}\ \mathrm{m^2\ s^{-1}}$, $U \sim 10^{-4}\ \mathrm{m\ s^{-1}}$, $K \sim 10^{-5}\ \mathrm{m\ s^{-1}}$.

Mathematical Description of Gas Transport

Equations describing physical properties and transport of soil gases will be introduced now, including both viscous and diffusive modes. The examination of diffusive transport will begin with Fickian diffusion but later considers non-Fickian modes as well. A model incorporating viscous and diffusive modes of transport is presented last.

Vicous flow and the pressure field Viscous flow responds to pressure potential of air while diffusion occurs in response to concentration gradients or partial pressures of gases in the air mixture. Dynamic pressure originates from varying atmospheric pressure, infiltrating water, a change in water table depth, or pressure changes created by chemical or bio-physical activities within soil. Examples of the latter include biological generation of gas through decomposition, phase changes of water, or, thermal expansion or contraction of soil-air. The flux density of air due to dynamic pressure is:

$$q = \frac{k}{\eta} \nabla P \tag{9.90}$$

Although we are presently concerned with the movement of air, this equation is equally applicable to the flux of water (eqn. 7.5). Soil permeability to air (k) is a function of soil water content, porosity, and the connectivity and tortuosity of pores (related to soil structure). To solve for q, gas permeability (k) must be determined. Ordinarily this is done under stable, steady state conditions such as in an environmentally controlled chamber. If a liquid is used in the determination of k, Corey (1986) points out that while the intrinsic permeability of soil under saturated conditions should be equivalent to k, many times it may not. Usually k is underestimated if a liquid such as water is used in its determination. It appears that air as a fluid behaves differently in soil than a liquid due to slippage of flow along pore surfaces (the Klinkenberg effect, discussed in more detail later in this section). Also because of interactions between water and soil solids (particularly clayey soils) permeability may be further reduced from what would be representative of air.

Geopotential pressure arises from gravitational pull on an air-mass, much the same as defined for water (eqn. 7.5). The combination of dynamic and geopotential pressures is total pressure (P_{total}):

$$P_{total} = P + \rho g \Delta z \tag{9.91}$$

where the geopotential terms are density (ρ), gravitational acceleration (g), and height ($\Delta z = z - z_0$) above a chosen reference (z_0).

Geopotential pressure differences increase with increasing depth from a reference or datum. For steady-state, isothermal conditions, pressure change with depth is given by the hydrostatic equation:

$$\frac{dP}{dz} = -\rho g \tag{9.92}$$

Applying a finite difference form of equation 9.92, pressure at a 1 m depth is found to be 12 Pa higher than at the surface, at sea level ($\rho = 1.21$ kg m^{-3}, $T = 25$ °C). If pressure is measured over a thick, unsaturated layer, the geopotential component to equation 9.90 should include a density that is a function of depth and temperature. The derivation of an expression for static pressure in terms of temperature may begin with the substitution of the ideal gas law

$$\rho = \frac{P}{RT} \tag{9.93}$$

into equation 9.91; we have, after rearranging terms

$$\frac{dP}{P} = -\frac{g}{RT}dz \tag{9.94}$$

The change in temperature with depth in the soil profile may be written:

$$T = T_R - \zeta z \tag{9.95}$$

Substitution of this into equation 9.91, where ζ is the rate of temperature change with depth, and T_R is temperature at the reference point, $z = 0$, yields

$$\frac{dP}{P} = -\frac{g}{R}\frac{dz}{(T_R - \zeta z)} \tag{9.96}$$

Integrating from the reference point (having P_R, T_R) down, we use

$$\int_{P_R}^{P}\frac{dP}{P} = -\frac{g}{R}\int_{z_R}^{z}\frac{dz}{(T_R - \zeta z)} \tag{9.97}$$

to obtain

$$\ln\left(\frac{P}{P_R}\right) = \frac{g}{R\zeta}\ln\frac{(T_R - \zeta z)}{T_R} \tag{9.98}$$

After taking the antilog of both sides, we find

$$P = P_R\left[\frac{(T_R - \zeta z)}{T_R}\right]^{g/R\zeta} \tag{9.99}$$

If the soil is isothermal, equation 9.99 reduces to

$$\frac{dP}{P} = -\frac{g}{R}\frac{dz}{T} \tag{9.100}$$

with the result

$$P = P_R\exp^{-(gz/RT)} \tag{9.101}$$

Using equation 9.99 or 9.101, geopotential pressure can be subtracted from total pressure to arrive at a dynamic pressure which could drive a viscous flux.

Fluid (gas) flow Theoretical development and mathematical description of gas flow in soil is facilitated with simplifying assumptions regarding soil gases. We assume soil gases behave like ideal gases and that the continuity equation, also known as the conservation-of-mass equation, for a gas (concentration, C) applies:

$$\frac{\partial C}{\partial t} = -\left(u\frac{\partial C_x}{\partial x} + v\frac{\partial C_y}{\partial y} + w\frac{\partial C_z}{\partial z}\right) = -C\nabla\cdot\mathbf{U} \tag{9.102}$$

where u, v, and w are unit velocities along the x, y, and z coordinates, respectively, and $\mathbf{U}$ is the total component velocity vector. Equation 9.102 is analogous to that for temperature (section 9.4) and for water (equation 7.18).

Viscous flow The movement of air (or any other fluid in free space) is described by the equations of motion, also known as the Navier–Stokes equations, established in the 19th century. The relevant terms of the mean-flow equations for a viscous fluid in soil are:

$$\rho\left(\frac{\partial u_i}{\partial t} + u_j\frac{\partial u_i}{\partial x_j}\right) = -\frac{\partial P}{\partial x_i} + \rho g + \eta\frac{\partial^2 u_i}{\partial x_j\,\partial x_j} \tag{9.103}$$

where η is dynamic viscosity (L^2t^{-1}) and subscripts (i and $j, i \neq j$) refer to Cartesian coordinates (x, y, z). The left side of the equation contains the inertia terms that describe the rate of change in momentum of the moving air. This includes the local-time rate of change in fluid motion and the advection of fluid, respectively. The first two terms on the right side are force terms that drive momentum, consisting of the dynamic-pressure gradient and gravimetric- pressure potential. The last group on the right side holds the viscous terms through which momentum is lost to internal friction. In soils, the inertial terms are dropped, since velocities are very low. Under steady-state conditions and hydrostatic equilibrium, equation 9.103 reduces to

$$\frac{\partial P}{\partial x_i} - \rho g = \eta \frac{\partial^2 u_i}{\partial x_j \partial x_j} \tag{9.104}$$

Assuming density is a constant, the force terms on the left side of equation 9.104 can be combined (for details, see Corey 1977), and referred to as total (or piezometric) pressure. As mentioned earlier, the contribution of the hydrostatic term is only effective in the vertical dimension, and is very small over short vertical distances. Solutions of equation 9.104 are given in Corey (1977).

We generally consider pore space in soils to be a three-dimensional maze of interconnected channels. Conceptually, we can think of the tortuous flow-path through pores as having an effective (or actual) length (l_e), which corresponds to a straight-line distance (l) (see figure 9.32). The square of the ratio of the effective length of the pathway traveled by air to the straight-line distance traveled (l) is the tortuosity (details in Chapter 7):

$$\tau = \left[\frac{l}{l_e}\right]^2 \tag{9.105}$$

Bear (1972) notes that $\tau < 1$ and is typically about $(0.4)^{1/2}$, or about $2/\pi$, with a usual range of 0.5 to 0.8. We expect τ to decrease as liquid soil-water content increases. Tortuosity reduces

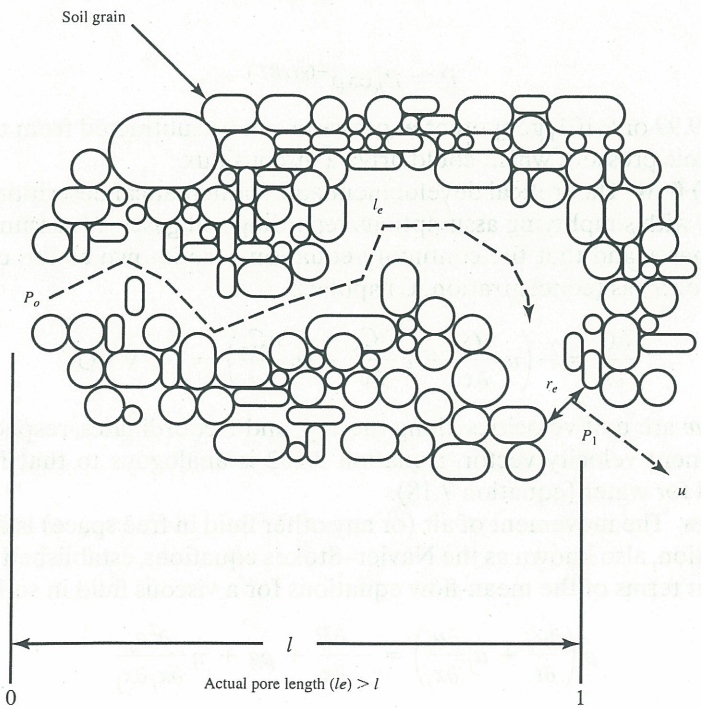

Figure 9.32 Conceptual diagram of tortuosity and its effect on gas movement in dry soil. Flow velocity (u) through the pore of radius (r_e) is in response to a pressure differential ($P_0 - P_1$) between points of reference, (0) and (1). Actual pore length (l_e) is longer than the straight-line distance (l) between the two reference points.

mean-mass flow velocity through soil as shown by Corey's (1977) derivation of the mean velocity for a fluid passing through soil:

$$u_{\mathbf{i}} = -\frac{r_e^2}{s_k \tau \eta} \frac{\partial P}{\partial x_{\mathbf{i}}} \tag{9.106}$$

where $u_{\mathbf{i}}$ is velocity of flow in the direction of a unit vector ($\mathbf{i}$) through a channel of effective radius (r_e), and s_k is a nondimensional geometrical-shape factor. The average (or effective) hydraulic radius of the channel carrying the air is defined as the internal volume of the channel divided by its internal surface area. Note, too, that flow velocity decreases with increasing viscosity.

Fickian diffusion The focus of our discussion now turns to gaseous diffusion—an omnipresent phenomenon, regardless of the mechanism that forces gas transport. Adolf Fick, following work on diffusion by Thomas Graham in the late 1820s, first formulated a law of diffusion in 1855, establishing that the rate of diffusion of a solute in any direction is proportional to the concentration gradient in that direction. Similar to gradients in potential that drive fluid flow (as described by Darcy's law), and analogous to Fourier's law of heat conduction, Fick's law defines a gaseous flux (q) driven by a concentration gradient:

$$q = -D_{ij}(x, y, z)\, \nabla C \tag{9.107}$$

where C is gas concentration (in density units, when a mass flux is desired). D_{ij} [$m^2\ s^{-1}$] is the binary gas diffusion coefficient (for gas (i) in gas (j)), that ordinarily varies in both horizontal and vertical directions due to variable soil composition, presence of water, and soil compaction. Since, in most cases, vertical transfer of gas is dominant, equation 9.107 reduces to

$$q = -D_{ij} \frac{\partial C}{\partial z} \tag{9.108}$$

where D_{ij} is assumed constant. The binary diffusion coefficient controls diffusive flow in a system composed of two gases. Diffusive flow of a gas in one direction (due to a partial pressure gradient) must be balanced by the flow of the other gas in the opposite direction in response to the development of a pressure potential, thereby reattaining an equilibrium. The value of D_{ij} has to be determined experimentally; it varies with temperature and pressure as described below

$$D_{ij}(T, P) = D_{ij}(T_o, P_o)\left(\frac{T}{T_o}\right)^n \left(\frac{P_o}{P}\right) \tag{9.109}$$

where subscript (o) refers to standard conditions. Values of n vary, with $n = 1.823$ for nonpolar gas pairs (Bird, Stewart, and Lightfoot 1960). D_{ij} in soils is affected by soil porosity and soil moisture. It may be estimated from measured binary diffusivity in free air, D_a (see table 9.6 for selected gases):

$$D_{ij} = \tau_f D_a \tag{9.110}$$

The gas tortuosity factor (τ_f) is specific to a soil with known porosity, volumetric air (θ_a) and water content. An often-used relation expressing τ_f in terms of θ_a and porosity (ϕ) was derived by Millington and Quirk (1961):

$$\tau_f = \frac{\theta_a^{10/3}}{\phi^2} \tag{9.111}$$

A few other models of τ_f can be found in Jury, Letey, and Collins 1991.

We emphasize the distinction between τ and τ_f. Tortuosity is typically applied to viscous-flow problems, since fluid velocity through a soil column decreases as τ increases. While it can include some effects of tortuosity, τ_f is usually determined empirically from diffusion experiments where a number of transport processes can be simultaneously involved in gas transport.

Fickian–diffusive gas transport Fick's law describes a flux due to diffusion of a gaseous constituent, in response to a partial-pressure or concentration-gradient. If we require conservation of mass in a soil volume, equation 9.108 can be inserted into equation 9.102 to obtain an equation that describes gas transport due to diffusion (Fick's second law):

$$\alpha \frac{\partial C}{\partial t} - D_{ij} \frac{\partial^2 C}{\partial z^2} - S(z, t) = 0 \tag{9.112}$$

where, again, D_{ij} is assumed constant, α is a volumetric-air constant, and a source/sink term was added for completeness. D_{ij} can be calculated, under steady-state, homogeneous conditions, if gas flux and the concentration profile is known. Tindall, Petrusak, and McMahon (1995) discuss laboratory measurements of soil-gas flux and concentration gradients from confined soil columns, from which D_{ij} is determined.

QUESTION 9.9

Calculate the concentration profile of O_2 through the rhizosphere (the layer of soil containing roots) from the surface ($z = 0$) to maximum rooting depth ($z = \delta$). Assume that there is no source or sink of O_2 below the roots, that there is a steady rate of consumption of O_2 in the rhizosphere with depth, and that O_2 concentration at the surface remains constant.

Diffusion involving point and line sources (or sinks) Thus far, only planar transport has been considered, in which diffusion has been expressed in Cartesian coordinates. In natural settings, gaseous diffusion often involves point or line sources and sinks. In these instances, the problems are better-posed in polar coordinates. Roots, with associated microbes, can be considered line sources of CO_2 and sinks for O_2. The governing equation for diffusion to (or from) roots is described in cylindrical coordinates:

$$\alpha \frac{\partial C}{\partial t} = \frac{1}{r}\left[\frac{\partial}{\partial r}\left(rD_{ij}\frac{\partial C}{\partial r}\right) + \frac{\partial}{\partial \theta}\left(\frac{D_{ij}}{r}\frac{\partial C}{\partial \theta}\right) + \frac{\partial}{\partial z}\left(rD_{ij}\frac{\partial C}{\partial z}\right)\right] \tag{9.113}$$

where the coordinates are radius (r), length (z), and arc (θ). Cylindrical coordinates are related to Cartesian coordinates in the following way: $x = r\cos\theta, y = r\sin\theta, z = z$, for a vertically oriented cylinder.

Diffusion to (or from) a point or sphere (perhaps a soil aggregate or microsite), expressed in spherical coordinates, is

$$\alpha \frac{\partial C}{\partial t} = \frac{1}{r^2}\left[\frac{\partial}{\partial r}\left(r^2 D_{ij}\frac{\partial C}{\partial r}\right) + \frac{1}{\sin\theta}\frac{\partial}{\partial \theta}\left(D_{ij}\sin\theta\frac{\partial C}{\partial \theta}\right) + \frac{\partial}{\partial \theta}\left(\frac{D_{ij}}{\sin^2\theta}\frac{\partial^2 C}{\partial \phi^2}\right)\right] \tag{9.114}$$

where ϕ is azimuth angle. Expressions relating spherical coordinates to Cartesian coordinates are: $x = r\sin\theta\cos\phi, y = r\sin\theta\sin\phi, z = r\cos\theta$.

Analytical solutions and suggestions for numerical methods to solve equations 9.113 and 9.114 are given in Carslaw and Jaeger (1959). Although this reference concerns itself with heat flow, the solutions for heat and gas transport are analogous, other than a change of coefficients.

Non-Fickian diffusion: non-equimolar and Knudsen Historically, the Fickian model has been assumed to represent diffusion problems in soil adequately. However, Thorstenson

and Pollock (1989a, b), Baehr and Bruell (1990), Abu-El-Sha'r and Abriola (1997) have shown that this model can grossly underestimate fluxes. Baehr and Bruell (1990) document that the underestimates can be of significant practical importance when modeling transport of hydrocarbon vapors. Fickian diffusion considers only the movement of gas in response to the partial-pressure potential driving it, and the resistance to this movement by intermolecular collisions of gas molecules. Actually, there are four different types of diffusion (including Fickian), that can simultaneously occur (at differing levels of significance) in soil:

1. Ordinary molecular
2. Knudsen
3. Nonequimolar
4. Surface flow

Ordinary diffusion, most closely represented by Fickian models, refers to the movement of molecules from a region of higher, to lower concentration. Resistance to diffusion comes from momentum loss due to intermolecular collisions and, to a lesser extent, losses to collisions with pore walls. In this instance, pore dimensions are much larger than the mean free path of travel—the distance a gas molecule travels before colliding with another gas molecule. The molecular free path decreases with increasing gas density, as the probability of a gas molecule colliding with another molecule (within a given travel distance) increases.

If, in contrast to the conditions above, the molecular free path of diffusing gas molecules was equal to or greater than the dimensions of pores, Knudsen diffusion would occur. In this instance the only collisions are those of gas molecules and pore walls.

Nonequimolar diffusion occurs when gases of differing molecular weight diffuse into one another. A lighter molecular-weight gas will diffuse into a heavier one at a higher rate than in the reverse process (see Mason and Malinauskas (1983) for details). Gas flux resulting from non-equimolar diffusion can cause a compensating viscous flow to develop that can move gas in the opposite direction to the diffusive flux. To explain this event conceptually, consider a two-bulb experiment involving two initially pure gases under isothermal and isobaric (constant pressure) conditions (see figure 9.33). Gas in bulb A has a lighter molecular weight and higher thermal energy than that in bulb B. Consequently, the lighter gas in bulb A diffuses into bulb B faster than the gas in bulb B diffuses into bulb A, causing an initially higher total pressure to build in bulb B. This pressure differential leads to a viscous flow from bulb B to bulb A. Following the diagram, for the system to reach equilibrium, the piston shown in the diagram must move toward bulb A.

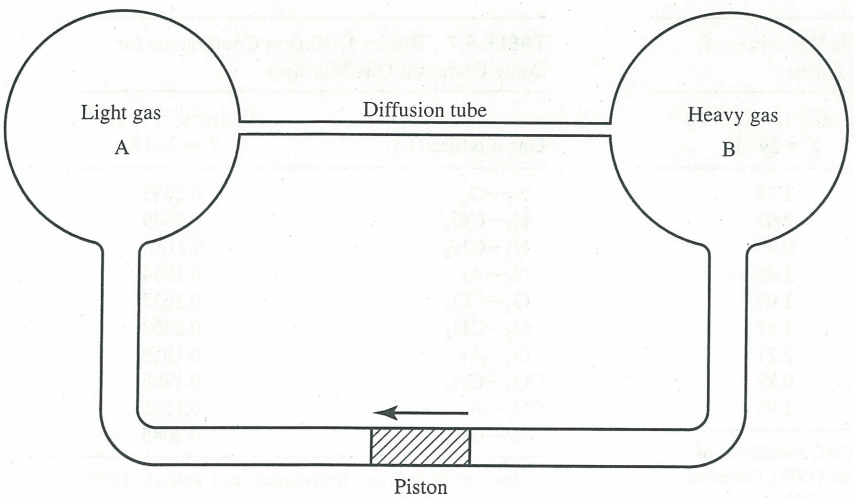

Figure 9.33 A two-bulb experiment illustrating nonequimolar flux due to differential diffusion of a lighter gas into a heavier one. Lighter gas flux into bulb B results in a higher pressure in the gas mixture in bulb B. Viscous flow attempts to equilibrate pressures, moving the piston toward bulb A. Reproduced from Thorstenson and Pollock 1989b, published by the American Geophysical Union

Diffusion through pores having sizes of the same order of magnitude as the molecular free path may include ordinary, Knudsen, and non-equimolar diffusion. Under the conditions of this transitional regime and with the presence of a bulk-pressure gradient, viscous flow occurs, as is expected. However, Klinkenberg (1941), found that measured flux is greater than that predicted by permeability considerations alone, due to viscous slip of gas through pore space. Now known as the "Klinkenberg effect," this property of flow is used to determine Knudsen-diffusion coefficients, needed to predict diffusive flow (Thorstenson and Pollock, 1989a).

The fourth type of diffusion—surface-flow—refers to the non-reactive absorbence of gas molecules onto solid-soil surfaces and their subsequent transport down the sorbed phase concentration gradient (Cunningham and Williams, 1980). It is distinctly different from the other forms of diffusion, therefore it is listed as another mode of transport. Ordinarily, it is of secondary importance with respect to other modes of transport, and is beyond the scope of this chapter.

The dusty-gas model for combined gas transport The dusty-gas model, first described by Mason, Malinauskas, and Evans (1967), combines viscous and diffusive gas-transport mechanisms. Conceptually, the model considers the solid components of soil to be giant dust molecules. Consequently, one can think of the model as applying to a gas mixture that includes dust particles as a component of the mixture. The governing equations for transport of gas component (i) in a mixture of (l) number of gases are:

$$\sum_{j=1;j\neq i,p}^{l} \frac{X_i F_j - X_j Q_i}{D_{ij}} + \frac{Q_i}{D_i^k} = \frac{\nabla P_i}{RT} + \frac{k P_i \nabla P}{D_i^k \eta RT} \tag{9.115}$$

where X_i is the mole fraction of gas (i) having a partial pressure P_i, Q_i is its molar flux (mol $L^{-2}\,t^{-1}$), D_i^k is its Knudsen-diffusion coefficient, P is air pressure of the mixture, k is permeability (L^2) of the media to air, and η is the dynamic viscosity of the gas mixture (m$L^{-1}\,t^{-1}$ = Pa s). Dynamic viscosity of common gases are given in table 9.6 and binary-diffusion coefficients for common gas pair mixtures are listed in table 9.7. The first term in equations 9.115 represents molecular transfer among gas species (classical Fickian-type diffusion). By not summing over p (particles) in the first term, the system of equations are independent of one another. Proceeding through the equation, the second term represents Knudsen diffusion; the third term (first one right of the "equals" sign) is the partial-pressure contribution to diffusion; and the last term is the viscous-flow contribution to flux. Details of the model are given in Mason and Malinauskas (1983) and Cunningham and Williams (1980).

TABLE 9.6 Dynamic Viscosities of Some Common Soil Gases

Gas	Viscosity (Pa s) × 10^{-5} T = 293 K
N_2	1.75
O_2	2.03
H_2O	0.95
CO_2	1.46
CH_4	1.09
N_2O	1.47
Ar	2.21
H_2	0.87
He	1.94

Source: Data from CRC Handbook of Chemistry and Physics (1972), Chemical Rubber Co., Cleveland, OH.

TABLE 9.7 Binary Diffusion Coefficients for Some Common Gas Mixtures

Gas mixture (i, j)	D_{ij} ($m^2\,s^{-1}$) × 10^{-4} T = 293 K
N_2—O_2	0.2083
N_2—CO_2	0.1649
N_2—CH_4	0.2137
N_2—Ar	0.1954
O_2—CO_2	0.1635
O_2—CH_4	0.2263
O_2—Ar	0.1928
CO_2—CH_4	0.1705
CO_2—Ar	0.1525
Ar—CH_4	0.2045

Source: Data from Thorstenson and Pollock, 1989a.

Thorstenson and Pollock (1989a, b) examined gas transport using a form of equation 9.115. They considered an example of CH_4 flux, constant with depth (0–10 m) and time, as ideally can occur in the soil overlying a landfill. They also assumed that the primary gases (N_2, O_2) were stagnant—that is, they were not being generated or consumed in the soil column. Soil-gas concentration gradients for the numerical experiment depict strong nonlinearity with depth (see figure 9.34). Referring to the figure and with only Fickian-diffusion in mind, we can expect to find a downward flux of N_2, and no CH_4 flux below $\simeq$5 m. However, an interesting story is told by examining components of total flux (figure 9.35), computed from equation 9.115. Ordinary or Fickian-type diffusive flux of CH_4 is upward. Because CH_4 is much lighter than N_2 and O_2, its non-equimolar flux becomes a large upward flux, nearly one-third that of ordinary diffusion. The flux due to Knudsen diffusion alone was not determined, but relative to ordinary diffusion, it is believed to be small. Thus, the combined total diffusive-flux is upward. Viscous flux of CH_4 is also upward, becoming an increasing component of total flux with increasing depth. For example, at 10 m it is responsible for all the flux, while at 1 m it is comparable in size with diffusive flux. Turning now to N_2, we find a diffusive flux of N_2 into the soil. However, without a sink for N_2 in the soil, why should a downward flux occur? On closer inspection, we find that net flux of N_2 is indeed zero (figure 9.35), but only because diffusive flux into the soil is precisely balanced by viscous and non-equimolar flux out of the soil. Thorstenson and Pollock (1989b) note that in this example, viscous flux accounts for 65–90 percent of total CH_4 flux, driven by a pressure gradient of only 24 Pa m^{-1}.

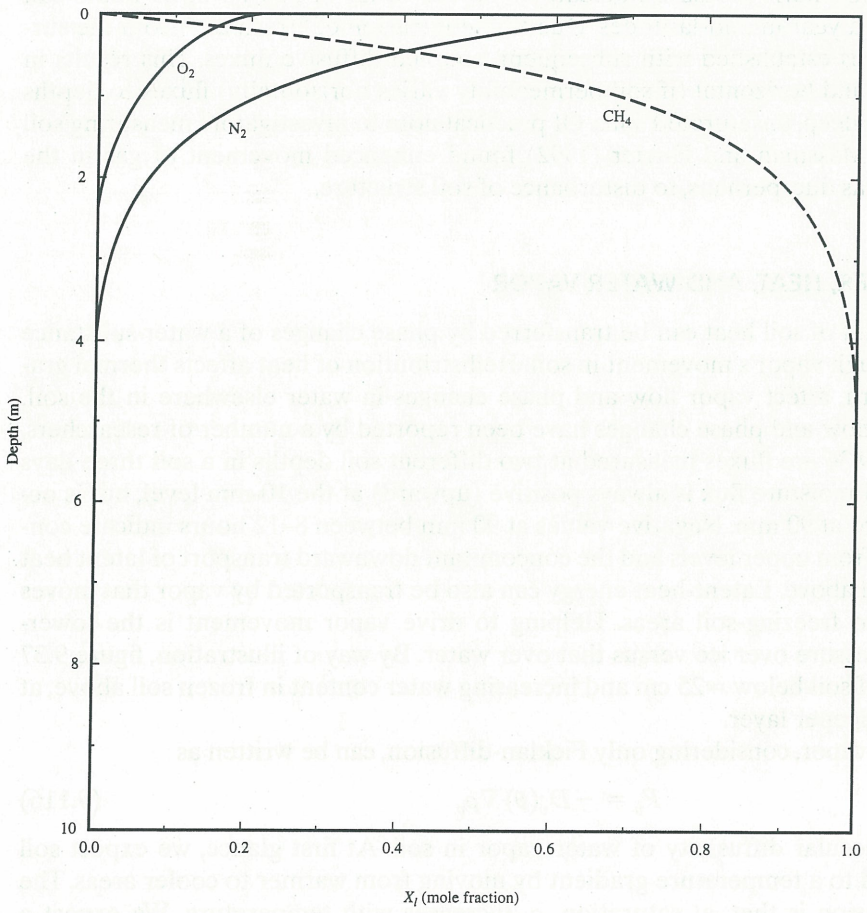

Figure 9.34 Hypothetical gas concentration profiles in soil; concentration is expressed as a molar fraction (X_i). These profiles were used in a dusty-gas model simulation of soil-gas flux. Reproduced from Thorstenson and Pollock, 1989a, copyright by the American Geophysical Union

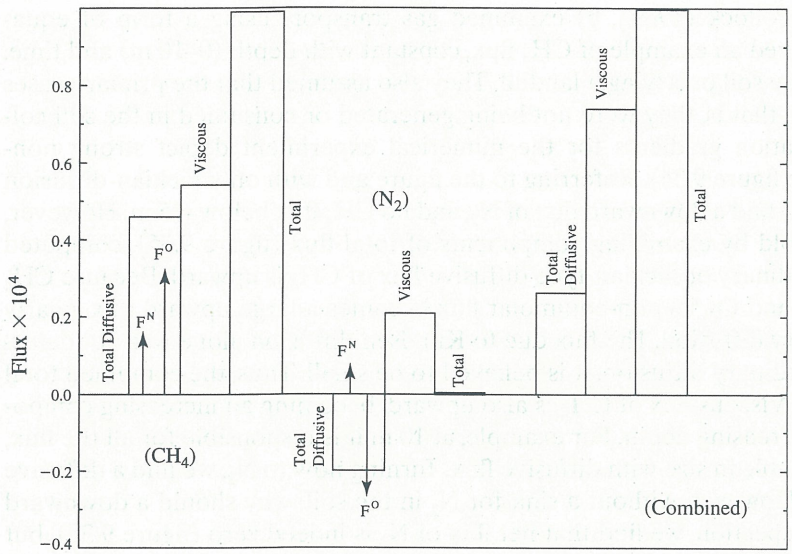

Figure 9.35 Relative magnitudes and directions of CH_4, N_2, and total combined gas fluxes. F^N is non-equimolar flux and F^O is ordinary diffusive flux. Reproduced from Thorstenson and Pollock, 1989a, copyright by the American Geophysical Union

The extent to which pressure fluctuations in soil derived from atmospheric weather affect soil-gas transfer in the dusty-gas model was examined by Massman and Farrier (1992). They note that atmospheric-pressure fluctuations on the order of 200 Pa in 24 hours can occur several times a year in mid-latitudes. Due to the intrusion of "fresh air" from the surface, a viscous flow is established with subsequent, coupled diffusive fluxes. This results in substantial vertical and horizontal (if soil permeability varies horizontally) fluxes to depths of several meters in deep, unsaturated soils. Of practical note to investigators measuring soil gases with probes, Massman and Farrier (1992) found enhanced movement of gas in the vicinity of probes was due, perhaps, to disturbance of soil structure.

9.8 COUPLED TRANSPORT OF WATER, HEAT, AND WATER VAPOR

A substantial amount of soil heat can be transferred by phase changes of a water-substance (liquid or gas) through vapor's movement in soil. Redistribution of heat affects thermal gradients, which, in turn, affect vapor flow and phase changes in water elsewhere in the soil. Evidence of vapor flow and phase changes have been reported by a number of researchers. Depicted in figure 9.36 are fluxes measured at two different soil depths in a soil three days after irrigation. Soil-moisture flux is always positive (upward) at the 10-mm level, but is occasionally downward at 90 mm. Negative values at 90 mm between 8–12 hours indicate condensation of vapor from upper levels and the concomitant downward transport of latent heat energy from the soil above. Latent-heat energy can also be transported by vapor that moves from evaporating to freezing-soil areas. Helping to drive vapor movement is the lower-saturation vapor pressure over ice versus that over water. By way of illustration, figure 9.37 depicts the drying of soil below ≈25 cm and increasing water content in frozen soil above, at the expense of the deeper layer.

Flux of water vapor, considering only Fickian-diffusion, can be written as

$$F_v = -D_v(\theta)\,\nabla\rho_v \tag{9.116}$$

where $D_v(\theta)$ is molecular diffusivity of water vapor in soil. At first glance, we expect soil moisture to respond to a temperature gradient by moving from warmer to cooler areas. The basis of this conclusion is that, at saturation, ρ_v increases with temperature. We expect a

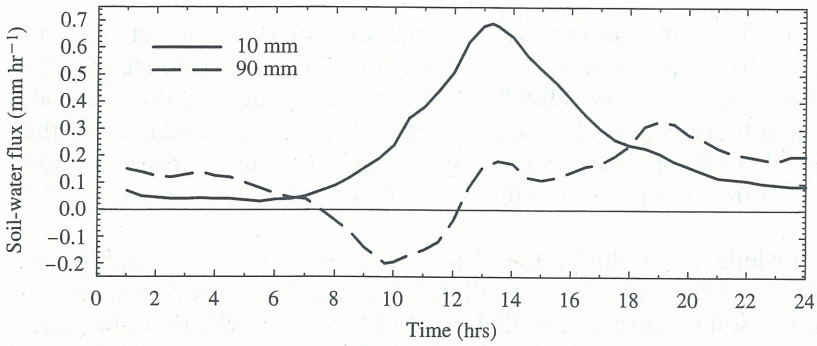

Figure 9.36 Soil-water flux measured at 10-mm and 90-mm depths, three days after irrigation (data from Jackson et al. 1973). Upward flux is positive.

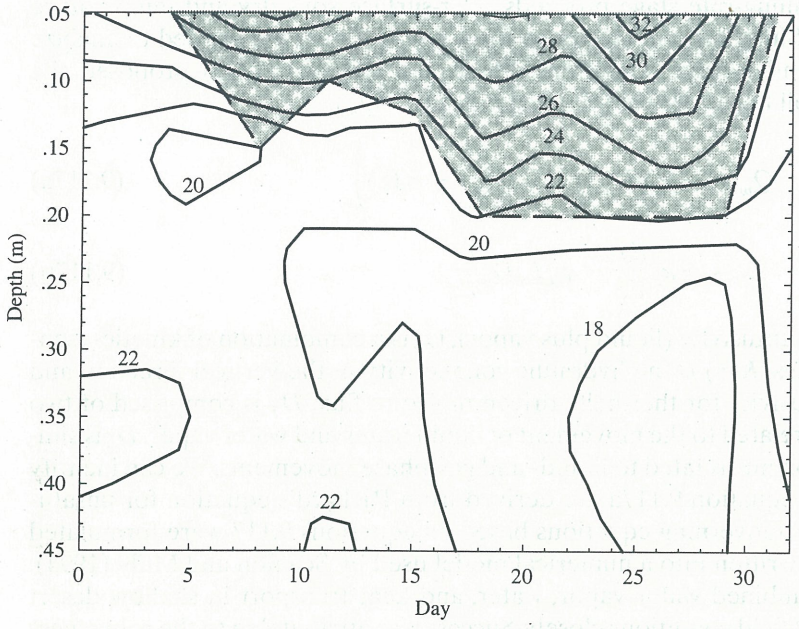

Figure 9.37 Soil-water content (percent volumetric) in a cold soil, with an intermittently frozen surface (data from Geiger 1965). Frozen soil is shaded.

vapor-pressure gradient in the direction from cool (low saturated vapor density) to warmer (high saturated vapor density) areas in soil and, therefore, for a flux (equation 9.116) of water to move down this gradient, from high (warm) to cool (low).

With the presence of both liquid and vapor, the net-overall transport of water in a multi-phase problem becomes more complex. Gravitational effects aside (for the moment), due to the temperature dependence of matric potential, the net flow of liquid water is from warm to cool areas. However, citing the work of others using closed-horizontal soil columns, Marshall and Holmes (1979) point out that in the presence of liquid-vapor phase changes, just the opposite occurs; that is, net flow of water will be from cool to warm. The explanation is that, initially, vapor flux is in the direction of the temperature gradient (from warm to cool), resulting in the condensation of water in the cool area. Next, the increasing liquid-water content that results from the condensation of vapor flux leads to the development of a water-content gradient in the opposite direction to that just created by the thermal gradient. Thus, the matric-potential gradient from liquid water becomes greater than that caused by the thermal gradient. As a result of the difference in potentials, water moves from the cooler to warmer areas of soil in this instance.

Philip and deVries (1957) found another way in which dual phases of water can lead to enhanced-water flux due to soil physical structure. They proposed the existence of a migrating, sharp temperature gradient across individual soil particles. Under unsaturated conditions, water condensing onto a soil particle releases heat. This energy is conducted to the other side of the particle where it vaporizes water. Responding to the vapor-pressure gradient, water vapor moves forward from this site to the next site of condensation, repeating the scenario.

It is generally acknowledged that during the constant-rate stage and early falling-rate stages of drying, the isothermal flow equation (equation 9.54) adequately predicts moisture transport and, consequently, soil evaporation (Hillel, 1980). The reason why the flow equation holds for other than constant-rate stage drying (under isothermal conditions), is that the nonlinear form of the vapor-diffusivity equation is similar to that for liquid water (Hillel 1980). However, as the falling-rate stage proceeds, near-surface soils dry and temperature gradients become larger. Simultaneous equations for water and heat are needed to analyze soil-moisture transport under these conditions. Philip and deVries (1957) proposed the following equations for soil fluxes of heat (G_c) and moisture (Q_w):

$$Q_w = -\rho_w\left(D_T\frac{dT}{dz} - D\frac{d\theta}{dz} - K(z)\right) \tag{9.117a}$$

$$G_c = -\kappa_c\frac{dT}{dz} - \rho_w L_v D_v\frac{d\theta}{dz} \tag{9.117b}$$

where D is total-moisture diffusivity (liquid plus vapor); G_c is a combination of kinetic- (sensible) and latent-heat fluxes; $K(z)$ is the hydraulic conductivity in the vertical direction and D_T [$m^2\ s^{-1}\ °C^{-1}$] is a diffusivity for thermally driven moisture flux. D_T is comprised of two components, individually related to the movement of liquid water and water vapor. D_v is similarly comprised of components related to liquid- and gas-phase movements. We can identify that the last two terms in equation 9.117a are derived from Richard's equation for unsaturated flow (see chapter 8). Governing equations based on equations 9.117 were formulated by Milly (1982; 1984) and written into a numerical model used by Scanlon and Milly (1994). Model simulations for combined water vapor, water, and heat transport in shallow desert soils were found to predict field conditions closely. Success was attributable to the robustness of thermal calculations. Main sources of uncertainty in simulations centered on estimated hydraulic conductivity.

9.9 MULTI-PHASE TRANSPORT OF VOLATILE COMPOUNDS IN SOIL

Volatile compounds can also exist in liquid and vapor phases in soil. Additionally, some solutes may be adsorbed onto surfaces of solids. Thus, concentration of a solute in soil may exist as a combination of absorbed solute (C_s),dissolved solute (C_l), or as a vapor (C_g). These concentrations may be expressed on a per-mass basis by multiplying by bulk density (ρ_b), volumetric water content (θ), or volumetric air content (θ_a), yielding $\rho_b C_s$, θC_l, and $\theta_a C_g$, respectively. The governing equation for multiphase transport of the solute within a specific volume is

$$\frac{\partial}{\partial t}(\rho_b C_s + \theta C_l + \theta_a C_g) - \frac{\partial}{\partial z}\left(D_g\frac{\partial C_g}{\partial z}\right) + \frac{\partial}{\partial z}\left(D_e\frac{\partial C_l}{\partial z}\right) - \frac{\partial Q_w C_l}{\partial z} - S(z,t) \tag{9.118a}$$

where the effective dispersion coefficient (D_e) is the combination of the liquid diffusion coefficient and the hydrodynamic dispersion coefficient (viz.; $D_e = D_l + D_{lh}$), $D_g$is diffusivity of the vapor phase, and Q_w is the liquid water flux. The term on the left describes the local time rate of change in total solute concentration due to the transport and production/decay terms

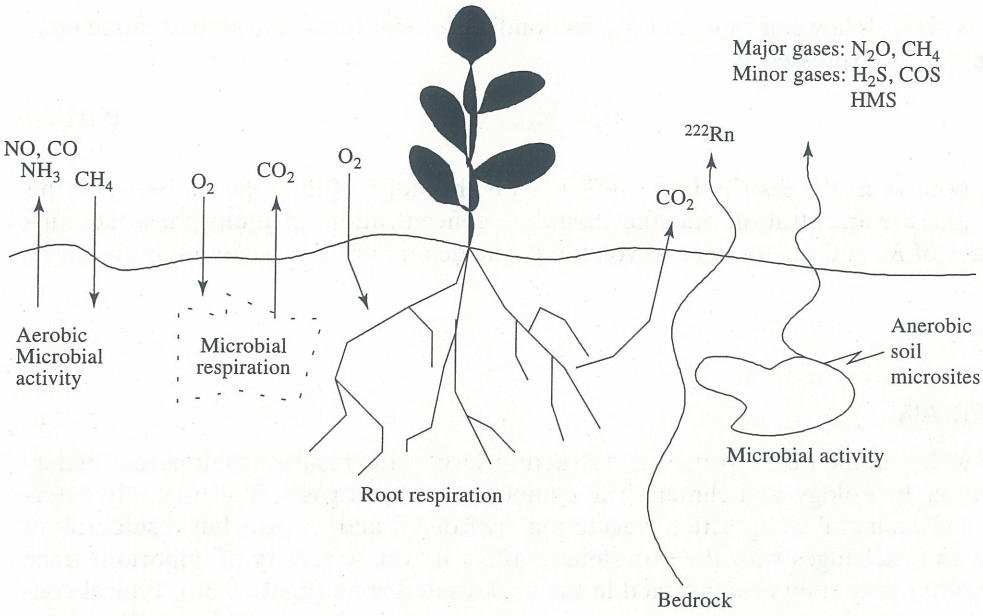

Figure 9.38 Schematic of trace gas fluxes in unsaturated soil and associated sources and sinks

TABLE 9.8 Nondimensional Henry's Law and Distribution Coefficients of Selected Volatile Pesticides and Organic Compounds (at 20 °C)

Compound	K_H	K_S [cm^3 g^{-1}]
Atrazine	2.5×10^{-7}	1.6
Benzene	1.77×10^{-1}	
Bromacil	3.7×10^{-8}	0.7
Carbon disulfide	5.82×10^{-1}	
Chloromethane	3.9×10^{1}*	
Cis-1, 2-Dichloroethane	3.7×10^{-1}	
DBCP	8.3×10^{-3}	1.3
DDT	2.0×10^{-3}	2400
Lindane	1.3×10^{-4}	13
MTBE (methyl tert-butyl ether)	1.69×10^{2}	
Napthalene	1.74×10^{2}	
Chloroform (trichloromethane)	1.2×10^{-1}	
Toluene	2.28×10^{-1}	
Phorate	3.1×10^{-4}	6.6

Source: Data from Jury, Gardner, and Gardner (1991), Howard (1991), Mackay and Shui (1981), and Robbins (1993).
*This value determined at 25 °C

on the right: Fickian diffusive transport of the vapor phase (first term on the right), the convective—dispersive transport in the liquid phase (second term), mass liquid water flux, and the production/decay term (S), which is spatially and temporally variant.

To utilize equation 9.118a, a relation is needed reducing the number of unknowns (C_s, C_l, and C_g) to one. An approach used by Jury, Gardner, and Gardner is to describe the left side of 9.118a in terms of C_l. Applying Henry's law and the Ideal Gas law, a phase-partitioning law is derived:

$$C_g = k_H \frac{C_l}{\rho_w R_v T} = K_H C_l \tag{9.118b}$$

where k_H is Henry's law constant, and K_H, its nondimensional form. The sorbed phase concentration may be expressed as

$$C_s = K_S C_l \tag{9.118c}$$

where K_S (known as the distribution coefficient) is the slope of the relation between the adsorbed phase concentration and the dissolved concentration, at multi-phase equilibrium. Values of K_S and K_H for several volatile pesticide and organic compounds are given in table 9.8.

9.10 COMPOSITION OF SOIL-AIR

Soils vary widely in their composition and structure, largely the result of their parent material, vegetation, hydrology, and climate. The composition of soil gases is also largely determined by soil's mineral composition, vegetation, hydrology, and climate, but resident flora and fauna and exchanges with the atmosphere affect it, too. A variety of important trace gases are either generated or consumed in the unsaturated zone (figure 9.38). Typical concentrations of the primary gaseous components of soil-air are given in table 9.9. The abundance of N_2 in soil is due to equilibration of soil-air with the atmosphere.

Some soil-gas concentrations differ from atmospheric levels. Concentrations can vary both horizontally and vertically within the soil, as determined by the distribution of their sources and sinks. Since the composition of soil-air is influenced by biological activity, concentrations vary temporally in response to changes in soil temperature, water content, nutrient availability, and soil aeration. O_2 and CO_2 are good examples of contrasts in gas concentrations between the atmosphere and within soils. O_2 is generated primarily by photosynthesis above-ground, while a large quantity of this gas is consumed by below-ground respiring soil organisms. As a result, in most ecosystems its concentration is higher in the atmosphere than in the soil. Just the opposite is true for CO_2, which is respired by roots and soil organisms but consumed in photosynthesis.

TABLE 9.9 Constituents of Clean Air, and Soil

Constituent	Atmosphere (percent volume or as indicated)	Conditions regarding soil environment	Soil-air (percent volume or as indicated)
Nitrogen	78.08		78
Oxygen	20.95	Variable due to respiration	19
Argon	0.93		0.93
Carbon Dioxide[G]	350 ppm_v	Variable due to respiration	400–10,000 ppm_v
Water vapor[G]	0–3	Usually near saturation	0–3
Methane[G]	1.8 ppm_v	Variable due to soil source/sinks	0–20 ppm_v
Nitrous oxide[G]	320 ppb_v	Variable due to soil source/sinks	0.3–134 ppm_v
Hydrogen	0.5 ppm_v	Variable due to sources (bedrock, biological)	0–0.5 ppm_v
Radon	0.1–1 pC L^{-1}	Range is function of bedrock composition (granitic is highest)	100–100,000 pC L^{-1}

[G]Indicates a greenhouse gas.

Source: Data compiled from Williamson (1972); Denmead (1991), Lal et al. (1995), Otton Gunderson, and Schumann (1993).

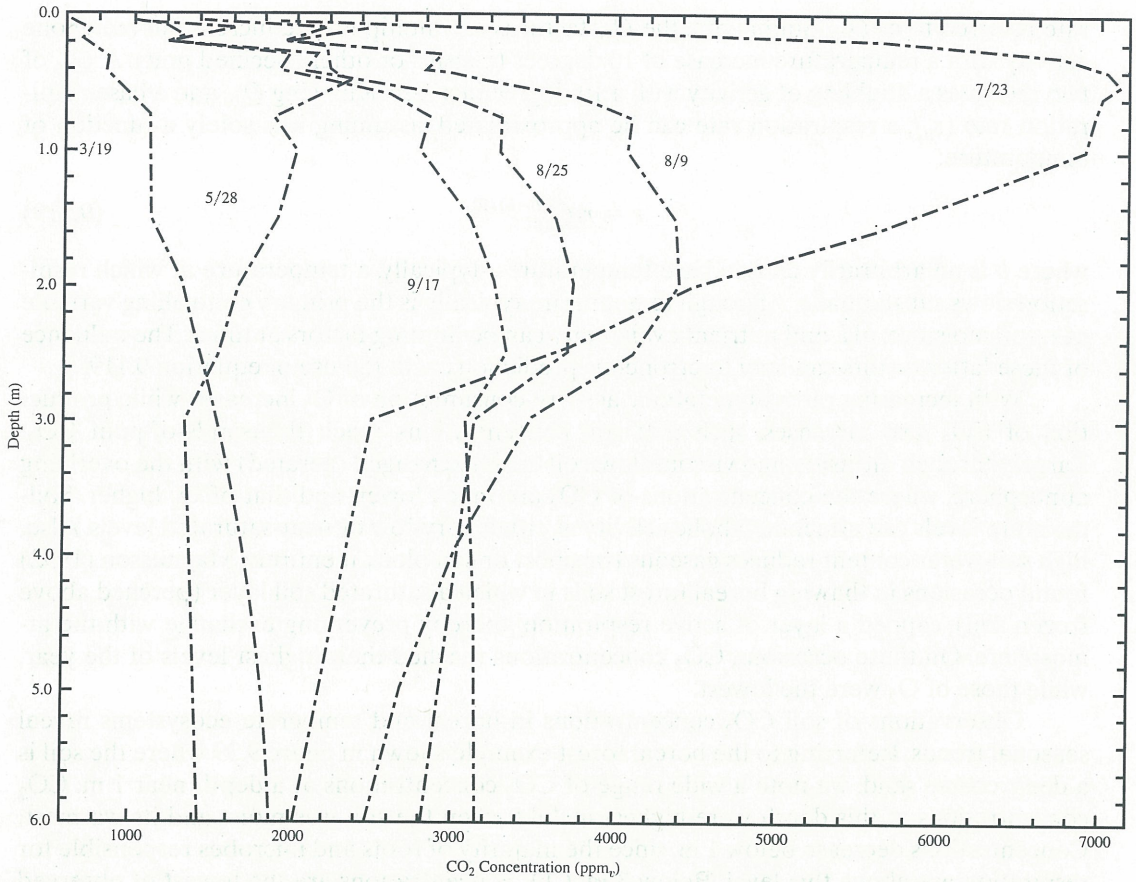

Figure 9.39 CO_2 concentration profiles measured in sandy soil beneath a boreal jack pine forest in central Canada. Month and day given alongside individual profiles (data from Wickland and Striegl, 1997)

Due to its agricultural and climatological significance, CO_2 is the most commonly studied of soil gases. CO_2 is generated by plant roots, fauna, and soil microbes (bacteria and fungi) as a result of respiration. This process involves the consumption of carbohydrates and oxygen, and the release of combustion energy, along with CO_2 and water vapor as by-products. Energy acquired through respiration is utilized to conduct metabolic activity, some of which is related to plant growth and decomposition. Both fauna and microbes are involved with decomposition. The former mechanically reduce organic structures, while microbes in both aerobic and anaerobic soils reduce complex organic-carbon molecules to simple carbohydrates. In turn, these carbohydrates can be utilized to attain energy through respiration.

It is difficult to determine the relative significance of plant-root and soil-microbial contributions to soil CO_2. Field studies by Bowden et al. (1993) indicate that for a temperate hardwood forest, roots contribute about one-third of the total respired flux of CO_2. Near-surface soil microbes, largely consuming litter-fall, also generate about one-third, as do deep-soil microbes. Studies of other ecosystems indicate a greater contribution (up to 50 percent) by roots (Behera, Joshi, and Pati 1990; Nakane et al. 1983).

Responding to daily and seasonal temperature- and moisture-patterns in soils, the rates of decomposition by soil microbes and respiration by plant roots and microbes change at a

rate referred to as Q_{10}. Simply put, the Q_{10} factor is the multiplicative increase in metabolic activity with a temperature increase of 10 degrees (Celsius or other specified unit). A Q_{10} of two indicates a doubling of activity with a 10-degree increase. Knowing Q_{10} and a base respiration rate (r_b), a respiration rate can be approximated, assuming it is solely a function of temperature:

$$r = r_b Q_{10}^{(T-b)/10} \tag{9.119}$$

where b is an arbitrarily chosen base-temperature—typically, a temperature at which respiration slows substantially. Although temperature typically is the primary controlling variable of r, soil moisture, pH, and nutrient availability can be limiting factors at times. The influence of these latter factors can lead to erroneous predictions with the use of equation 9.119.

With increasing rates of metabolic activity, consumption of O_2 increases while production of CO_2 also increases, such that soil concentrations reach thousands-of-ppm CO_2. Largely through diffusion and viscous flow, soil-air is exchanged (aerated) with the overlying atmosphere, where the concentrations of CO_2 are much lower, and that of O_2 higher. Soil-moisture levels can affect metabolic activity at either very-low or near-saturated levels. Also, high soil-water content reduces gaseous transport or can block it entirely. Magnusson (1992) found occasions in thawing boreal forest soils in which a saturated soil layer (perched above frozen soil), capped a layer of active respiration, thereby preventing exchange with the atmosphere. On these occasions, CO_2 concentrations reached their highest levels of the year, while those of O_2 were the lowest.

Observations of soil CO_2 concentrations in boreal and temperate ecosystems reveal seasonal trends. Referring to the boreal forest example shown in figure 9.39 where the soil is a deep, coarse sand, we note a wide range of CO_2 concentrations at a depth near 1 m. CO_2 concentrations at this depth were highest in July, when the soil was moist and its warmest. Concentrations decrease below 1 m, since the majority of roots and microbes responsible for respiration are above this level. Below 3 m, CO_2 concentrations are the lowest of observed levels on May 28, likely the result of the penetration of the seasonal temperature wave. Temperatures at 3 m were the coldest of the entire profile in early June (see figure 9.20). In contrast to this soil, larger CO_2 concentrations are often found in agricultural soils (Rosenberg, Blad, and Verma 1983) or other settings where soils are rich in organic carbon and fixed nitrogen, that support greater rates of biological activity.

Other gases produced by biological activity in soils that have a substantial influence on the atmosphere's radiation balance (through the greenhouse effect) are nitrous oxide (N_2O), nitric oxide (NO) and methane (CH_4). Additionally, biological activity in soils may produce smaller amounts of other gases (see figure 9.38), including NH_3 (ammonia), CO (carbon monoxide), H_2S (hydrogen sulfide), COS (carbon monosulfide) and DMS (dimethyl sulfide) (Conrad 1995). All of these gases (CH_4, N_2O, H_2S, COS, DMS) are typically produced under anoxic conditions, which generally occur in saturated soils. In some instances, substantial amounts of certain of these gases, such as N_2O, have been measured from generally unsaturated soils (Rosswall 1989). It appears that saturated soil aggregates (microsites) within the drier soil media provide the needed anoxic environment for gas production.

N_2O and NO are released during nitrification and denitrification processes associated with reduction and oxidation reactions involving nitrate-reducing bacteria and, on occasion, by fungi in acidic forest soils (Rosswall, 1989). Nitrification is a major source of N_2O production in soils following the application of urea- or ammonium-based fertilizers. Mineral-N (nitrogen) availability increases with the application of N-based fertilizers or in the absence of plant N uptake. With the occasion of plant root die-off, the large increase in organic C availability intensifies denitrification, leading to increased N_2O production. In general, N_2O and NO production are highest under conditions of intermediate soil water content, high

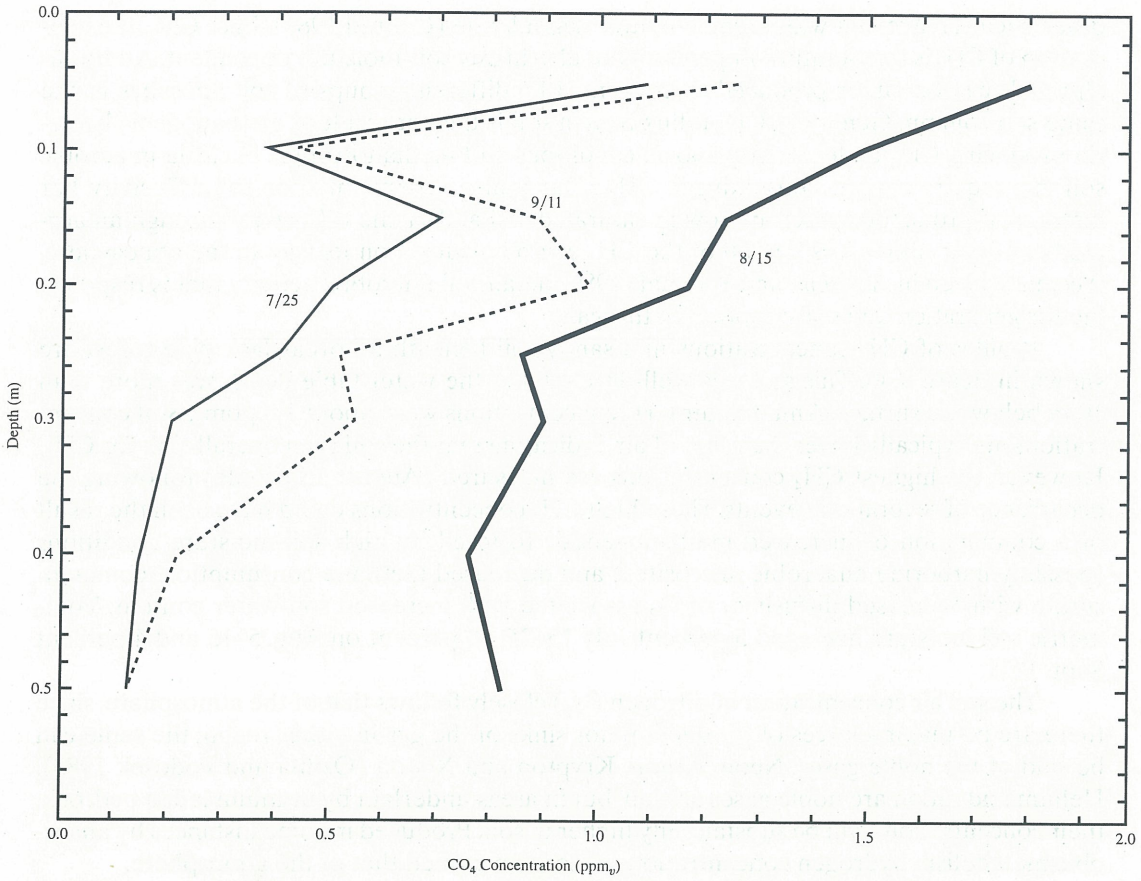

Figure 9.40 CH_4 concentration profiles measured at the same location as for data in figure 9.39 (data from Wickland and Striegl, 1997)

mineral-N availability, and warm temperatures (Rosswall 1989). Coincident soil characteristics are high fertility (making sufficient N available) and low O_2 levels, thereby resulting in anaerobic microsites. Generation and transport of NO and N_2O are largely controlled by soil texture. For instance, anaerobic metabolism resulting in NO and N_2O by-products is fostered by numerous dense-soil aggregates while gas-transport depends largely on diffusion through soil. Anaerobic conditions are more prevalent in saturated soils, but since diffusion of gas is more than 3 to 4 orders of magnitude slower in water than it is in air, there is an optimum soil-water content that facilitates anaerobic processes within saturated microsites while simultaneously facilitating gaseous transport through soil. Bouwman et al. (1993) present a general algorithm and model, simulating N_2O production for a variety of soils. Disturbed soils such as those put to agricultural uses exhibit strong seasonal emissions of N_2O following tillage, as well as strong consumption of CH_4 as a consequence of mechanical aeration (Mosier et al. 1997; Powlson et al. 1997).

CH_4 and CO_2 are produced by methanogenic bacteria under strictly anoxic conditions where organic matter (e.g., cellulose, hexose) is degraded into gaseous by-products

$$C_6H_{12}O_6 \rightarrow 3CO_2 + 3CH_4 \qquad (9.120)$$

Equation 9.120 is a simplification of a number of reactions. Methanogenic bacteria are not solely responsible for the above reaction, and are the recipients of by-products from three

other bacteria involved with organic-matter degradation (Conrad 1989). Like CO_2, the generation of CH_4 is temperature-dependent but also highly soil-moisture dependent. Additionally, CH_4 can be either produced or consumed by different groups of soil microbes in the same soil column. Generally, CH_4 efflux from a soil is the net result of methanogenic bacteria producing CH_4 under strictly anoxic conditions and methanotrophic bacteria in aerobic soil that require oxygen, consuming it. CH_4 efflux is also dependent upon soil diffusivity. For instance, if production rates are low in saturated soil and/or the diffusivity through an aerated soil-layer above it is low, all of the CH_4 can be oxidized on its way to the atmosphere. Accounts given in Andreae and Schimel (1989) detail soil microbial activity that is responsible for generation and consumption of this gas.

Profiles of CH_4 concentrations in a sandy soil beneath a boreal Jack pine forest are shown in figure 9.40. This soil was well-drained and the water-table depth was more than 10 m below the surface. Ambient air CH_4 concentrations were about 1.8 ppm_v. Soil concentrations are typically lower than that of air, indicating that the soil is an overall sink for CH_4. However, the highest CH_4 concentrations are measured (August 15 profile) following the occurrence of several rain events. These high CH_4 concentrations could have been the result of a combination of increased methanogenesis fostered by high soil-moisture conditions (possibly harboring anaerobic microsites) and decreased methane consumption, commensurate with decreased diffusivity of O_2 associated with increased soil-water content. Volumetric soil moisture averaged 5 percent July 15–25, 10 percent on Aug. 5–15 and 4 percent Sept. 1–11.

The soil air concentration of nitrogen (N_2) closely follows that of the atmosphere, since there are no major sources of production nor sinks of the gas in either realm; the same can be said of the noble gases: Neon, Argon, Krypton and Xenon (Ozima and Podosek 1983). Helium and radon are noble gases as well, but in areas underlain by uranium laden bedrock, their concentrations will be substantially higher in soil. Produced in some instances by anaerobic metabolism hydrogen concentrations in soil can exceed that of the atmosphere.

Water-vapor concentration varies (particularly in the upper soil layers) on daily to weekly time-scales due to variability in temperature and infiltrating water. Vapor concentrations are typically higher in soils than in the overlying atmosphere for the same location. This is because soils generally contain water (at some depth) and resistance to diffusive transport of vapor is large in contrast to transport in the atmosphere above the surface. Relative humidities in soils are seldom below 90 percent, even in arid regions. As a result, vapor density or concentration is strongly determined by soil temperature.

Naturally occurring radioisotopes Transport of radon (^{222}Rn) gas in soils—and from soils into buildings—has become a subject of practical importance to homeowners, building contractors, and to workers exposed to air in enclosed, poorly ventilated, subterranean environments. Radon is the product of successive disintegrations of uranium (^{238}U), and follows radium (^{226}Ra) in the decay sequence. Its occurrence and abundance is directly linked to area geology. Rocks having a relatively high uranium content include those that are either: of volcanic origin; of granitic composition; sedimentary rocks containing phosphates; or metamorphic rocks derived from rock types in this list. Radon decomposes into a series of unstable isotopes of polonium, bismuth, and lead; these are known as "radon daughters." Disintegration ends with the stable lead isotope (^{206}Pb). During the decay, a series of alpha and beta particles are emitted, sometimes coincident with gamma radiation. Radon gas contributes only about 5 percent of the combined alpha emissions from radon and radon 'daughters.'

Radon and its decay products present a public-health risk when inhaled, since its radioactive decay results in the release of alpha particles into lung tissue. The radioactive half-life (time for a substance to lose one-half of its radioactivity) of ^{222}Rn is 3.8 days. Typically, then, it is exhaled before large amounts of alpha particles are emitted. However, some radon-

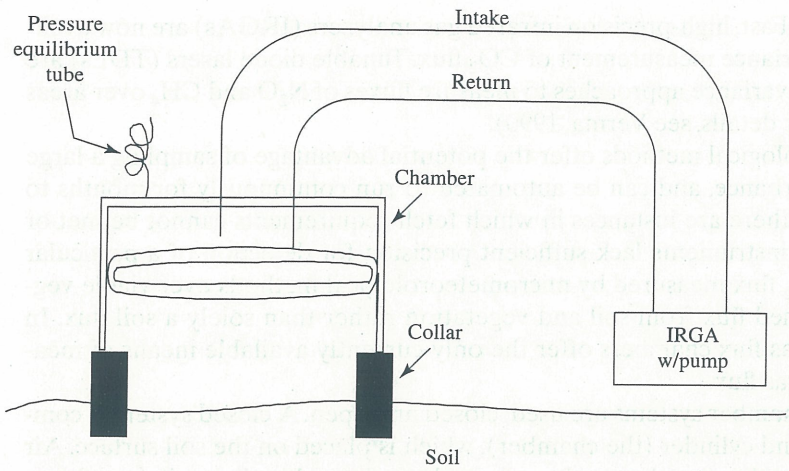

Figure 9.41 Schematic of chamber method of measurement of atmsophere–soil gas fluxes

daughter products posing substantial health risks have much shorter half-lifes. These atoms can also become embedded into dust, and after inhalation, accumulate in lung tissue. Radon daughter product, polonium, is that most linked to lung cancer (Miller and Dalzell, 1982).

The migration of radon from parent material occurs mostly by diffusion through rock fractures and soil pores in overlying soil. In addition to parent bedrock, radon can be transported from areas with decaying radium in the soil. In many regions, radium is found in concentrations on the order of picograms per gram of dry soil (Clements and Wilkening 1974). The flux of radon to the atmosphere varies by region from 0.1 to 2.5 atoms $cm^2\ s^{-1}$, and averages 0.75 (Wilkening, Clements, and Stanley 1974). Only about 10–50 percent of the radon generated in subsurface soil and rock ever reaches the surface. A substantial amount of radon is driven into soil-mineral grains or water-filled pore space due to the recoil of particles when radium decays. Radon transport in dry soil can be as much as 3 m within its half-life, but only about 0.02 m in wet soil over the same interval. Radon transport may be enhanced by barometric-pumping by the atmosphere (Kraner, Schroeder, and Evans 1964).

Buildings that are situated on dry and highly permeable soils, fractured bedrock, hillsides, bottoms of canyons, or on coarse glacial debris will have high-indoor radon levels unless precautions are taken during construction. Radon moves into buildings because of pressure differences that enable transport by mass flow and diffusion between soil and the interior of these buildings. Pathways for radon to enter a building are through unfinished basements or crawl-spaces, cracks in walls or floors and, around the subterranean entrances of water, sewer and electrical lines (Nazeroff et al. 1987). The simplest preventative measure against radon's intrusion into buildings is to back-fill loose stone and gravel during construction of concrete footings, foundation walls, and floors poured over disturbed soils. Back-fill tends to be much more permeable than the surrounding soil and rock, thereby facilitating gas transport around the foundation. Sometimes, ventilated porous tubing is embedded in the fill to enhance movement of gas away from footings and foundations (Otton, Gunderson, and Schumann 1993).

9.11 MEASURING SOIL-GAS FLUX

Soil–Atmosphere Exchanges

There are two categories of approaches used to measure gas flux between the soil and atmosphere: micrometeorological approaches, and surface chambers. We examined micrometeorological approaches in section 9.6, where means of measuring evapotranspiration and

heat flux where discussed. Fast, high-precision infrared gas analyzers (IRGAs) are now available that allow eddy-covariance measurement of CO_2 flux. Tunable diode lasers (TDLs) are also being used in eddy-covariance approaches to measure fluxes of N_2O and CH_4 over areas where fluxes are large (for details, see Verma, 1990).

While micrometeorological methods offer the potential advantage of sampling a large area with negligible disturbance, and can be automated to run continuously for months to years (Wofsy et al. 1993), there are instances in which fetch requirements cannot be met or fast-response gas-sensing instruments lack sufficient precision for detection of a particular gas flux. Additionally, CO_2 flux measured by micrometeorological methods over viable vegetation provides a combined flux from soil and vegetation rather than solely a soil flux. In these situations, surface gas-flux chambers offer the only currently available means of measuring soil—atmosphere gas flux.

Two basic types of chamber systems are used: closed and open. A closed system is comprised of a single closed-end cylinder (the chamber), which is placed on the soil surface. Air can be circulated between the chamber and a gas analyzer in a closed-circuit (see figure 9.41), or be extracted from the chamber with syringes for measurement off-site. Gas flux is determined by first measuring the rate of change of concentration with time; flux can then be calculated from the following equation

$$q_i = \left(\frac{V}{A}\right)\frac{d\rho_i}{dt} = h\frac{d\rho_i}{dt} \tag{9.121}$$

where ρ_i is the density of gas (i), V is volume of the air space enclosed by the chamber, A is the enclosed soil area, and h is the mean height of the top of the chamber above the soil's surface. Gas flux is expressed in moles (or mass) per unit area per unit time. The key to accurate flux measurement is to keep sampling duration as short as possible and to minimize soil disturbance when conducting the measurement. It is particularly important to strive for minimal disturbance if the gas has a significant near-surface source or sink, as is the case for CO_2. The closed-chamber method is intended for diffusive flux measurement only. It is criticized for creating an artificial environment in which atmospheric-turbulent transport is eliminated, and for allowing gas concentrations to increase above ambient levels. Increasing above soil concentrations diminishes the natural concentration gradient and can lead to flux underestimates. Methods to estimate flux missed by employing chambers are given in Nakayama (1990) and Healy et al. (1996). A variety of other effects can introduce bias errors in either the positive or the negative. Using CO_2 flux measurement as an example, placing a closed-chamber on the surface forces atmospheric air into the soil, which can decrease measured flux by reducing the near-surface CO_2 gradient. On the other hand, forcing the chamber wall into the soil compacts it, possibly enhancing flux. Also, forcing chamber walls into the soil can provide pathways for enhanced exchange, increasing flux. To help avoid some problems related to the effects of soil disturbance, a collar (see figure 9.41) may be placed into the soil's surface some time before measurements are to be made; a chamber may then be attached to the collar at the time of measurement.

Open-chamber systems have the advantage of continuous measurement with minimal soil disturbance, preservation of the natural air-soil concentration gradient, and allowing (for the most part) naturally occurring atmospheric-turbulent exchange. Flux is determined by measuring the gas concentration entering (ρ_{in}) and leaving (ρ_{out}) the chamber, and accurately measuring the flow rate (v) through the chamber. Applying the following formula, a flux is calculated:

$$q_i = \frac{v}{A}\left[\rho_{in} - \rho_{out}\right] \tag{9.122}$$

Accurate measurements are made by keeping the concentration difference small by adjusting v and accurately measuring v. Open-chamber systems are much more difficult to operate than closed chambers however, and critics argue that pressure fluctuations associated with air flow through them can enhance flux estimates.

In the field, chamber measurements offer a comparatively low-cost means of measuring flux. Often, if the flux or the gas concentration is small, they offer the only means of measuring flux currently available. Beyond the disadvantages mentioned above, sampling density and frequency are often highly variable with site characteristics (physical and biological), potentially introducing some bias into measurements.

Gas Flux within Soil

It is very difficult to accurately determine gas flux from one region to another within soil. A typical approach would be to determine diffusivity of the specific gas in the soil and make gas concentration and water content measurements along the path of interest. Since gas permeability is much lower through water-filled than dry pores, permeability used in the determination of diffusivity must be carefully adjusted for a known soil moisture level. Using Fick's law (equation 9.107), we may attempt to estimate flux from:

$$q_i = -D_{ij}\left(\frac{\partial C}{\partial x}\right) + S(x, t) \tag{9.123}$$

Beyond soil measurement of gas concentrations and determination of diffusivity (D_{ij}), knowledge is needed of the spatial and temporal character of the source/sink term, $S(x, t)$. Often, investigators refer to laboratory measurements of D_{ij} and $S(x, t)$ in moisture and temperature controlled environments. Once a model has been generated from laboratory data, field measurements of soil moisture, temperature and other parameters relevant to the source or sink are taken to predict D_{ij} and $S(x, t)$. To obtain soil gas concentrations, many investigators insert a small, stainless steel tube (about 2 mm diameter) with a sealed insertion tip into soil. Small inlet ports are manufactured near the tip or sealed-end through which soil-air may be drawn for analysis. It is important to keep the extracted sample volumes as small as possible to avoid significant alteration of the natural concentration profile of the gas. Field application of this method is increasingly difficult with depth in drier, low porosity soils since tube insertion is difficult and new gas flow paths, particularly along the outside of the tube, are created.

SUMMARY

We have shown that the movement of heat, water vapor, and other gases through the soil, and between soil and the atmosphere is an important influence on life dependent on the soil for sustenance (both directly and indirectly), as well as an important influence on the world's climate. Incoming radiation was shown to influence not just surface heating of soil, but the heating of the entire soil column. Additionally, we showed that incoming radiation received at the Earth's surface differs, according to a variety of factors: season; latitude; slope and aspect of the surface; and vegetative cover. This energy is partitioned into heating the soil as well as the air above it, and evaporating water (at the surface, within soil, and within plants). Methods of quantifying these fluxes of energy and mass were examined, including models and instrumentation.

The composition of soil air was reviewed, as well as the importance of atmospheric exchanges and biological activity in determining its make-up. The generation of radon and its transport were also discussed as were the mechanisms responsible for the movement of soil

gases and exchanges with the atmosphere. Key mathematical models used to quantify soil-gas transport were reviewed as well, and field methods to measure them were briefly described. Although—due to its complexity—coupled-transport of gases, heat, and water (liquid and vapor) is given only brief mention in this chapter, it is important to realize that understanding this phenomenon is the next step essential for fully understanding heat and gas transport in the unsaturated zone.

ANSWERS TO QUESTIONS*

9.1. Referring to figure 9.1, we find that the saturation vapor pressure over water is greater than that over ice. Water migrates down the potential gradient to the region of lower pressure (the cold end).

9.2. Using the definition of rH (see equation 9.7), $rH = e/e_s$ and the relation between e_s and temperature, we see that an increase in temperature leads to an increase in e_s, which decreases rH if e is constant.

9.3. At 20 °C, $I_{20} = (0.949)(5.67 \times 10^{-8}\ W\ m^{-2}\ K^{-4})(293\ K)^4 = 396.6\ W\ m^{-2}$. $I_{22} = 407.5\ W\ m^{-2}$. The net difference is a 10.9 W m^{-2} increase.

9.4. Total energy received by the surface is 146 (100 from incoming longwave +46 absorbed shortwave). The surface loses 31 percent (of incoming solar energy) to sensible- and latent-heat fluxes. Therefore, 146 − 31 percent = 115 percent leftover energy to radiate upward.

9.5. First, let us determine the damping depth of the diurnal temperature wave. Referring to figure 9.18, we find the following:

Depth (m)	T max (°C)	T min (°C)
0.05	20.0	10.4
0.37	15.2	13.8

Eqn. 9.45 can be applied to find maximum and minimum temperature with depth.

$$T_{max}(z) = T_a + A_o \exp\left(-\frac{z}{Z_D}\right);\ \sin\left(\omega t - \frac{z}{Z_D}\right) \rightarrow 1$$

$$T_{min}(z) = T_a - A_o \exp\left(-\frac{z}{Z_D}\right);\ \sin\left(\omega t - \frac{z}{Z_D}\right) \rightarrow -1$$

At depths z_1 and z_2:

$$[T_{max}(z_1) - T_{min}(z_1)] = \Delta T(z_1) = 2A_o \exp\left(-\frac{z_1}{Z_D}\right)$$

$$\Delta T(z_2) = 2A_o \exp\left(-\frac{z_2}{Z_D}\right)$$

We can eliminate A_o and solve for Z_D using the ratio

$$\frac{\Delta T(z_1)}{\Delta T(z_2)} = \frac{\exp\left(-\frac{z_1}{Z_D}\right)}{\exp\left(-\frac{z_2}{Z_D}\right)} = \exp\left(\frac{z_2 - z_1}{Z_D}\right)$$

*Before answering these questions, the reader may wish to refer to the conversion factors in appendix 3.

and

$$Z_D = \frac{z_2 - z_1}{\ln\left[\frac{\Delta T(z_1)}{\Delta T(z_2)}\right]}$$

Plugging in values to calculate damping depth:

$$Z_D = \frac{0.37 - 0.05\ \text{m}}{\ln\,(9.6/1.4)} = 0.166\ \text{m}$$

We can solve for thermal diffusivity now that Z_D is known

$$Z_D = \left[\frac{2D_h}{\omega}\right]^{1/2}$$

For the diurnal damping depth ($\tau = 1$ day):

$$D_h = \frac{\pi Z_D^2}{\tau} = 1.0 \times 10^{-6}\,\text{m}^2\,\text{s}^{-1}$$

9.6 Taking the derivative of equation 9.56, we have

$$E = \frac{dE_{\text{cum}}}{dt} = (\theta_i - \theta_f)\left(\frac{\overline{D}}{\pi t}\right)^{1/2}$$

where E is the evaporative flux.

In the second part of this question, we are to find $\overline{D}$ given $\theta_o = 0.35$ and $E_{\text{cum}}/t^{1/2} = 2.5\ \text{cm/day}^{1/2}$. Following the accompanying text we rearrange equation 9.56 and set $\theta_a = 0$:

$$\text{slope} = \frac{E_{\text{cum}}}{t^{1/2}} = 2\theta_o\left[\frac{\overline{D}}{\pi}\right]^{1/2}$$

$$\overline{D} = \pi\left[\frac{\text{Slope}}{2\theta_o}\right]^2 = \left(\frac{40.1\ \text{cm}^2}{\text{day}}\,\frac{1\text{m}^2}{10000\ \text{cm}^2}\right)\left(\frac{1\ \text{day}}{86400\ \text{s}}\right) = 4.6 \times 10^{-8}\,\text{m}^2\,\text{s}^{-1}$$

9.7 We are given U, ν, and K (hydraulic conductivity). To determine whether a flow is turbulent or not we will use the Reynolds number. To do so we need k, which can be solved from equation 9.88:

$$k = \frac{K\nu}{g} = \frac{1 \times 10^{-5}\,1 \times 10^{-6}}{9.8} = 1 \times 10^{-12}\,\text{m}^2$$

Now using equation 9.89:

$$Re = \frac{(1 \times 10^{-4}\,\text{m s}^{-1})\,(1 \times 10^{-12}\,\text{m}^2)^{1/2}}{1 \times 10^{-6}} = 1 \times 10^{-4}$$

Since $Re \ll 1$, this flow is laminar.

9.8 Field-air capacity is a measure of the volume of air in soil (including entrapped air), while permeability only relates to the connectivity of air-filled pores.

9.9 We are given that, below rooting depth δ the flux of O_2 (q_{O_2}) = 0, that steady-state conditions exist ($dC/dt = 0$), the sink for O_2 is constant in time and depth ($S(z, t) = \text{S}$), and that the concentration at the surface (C_o) is constant. From equation 9.112, we have

$$D_{ij}\frac{d^2C}{dz^2} = \frac{dq_{O_2}}{dz} = -\overline{S}$$

Applying boundary conditions and integrating:

$$\frac{d^2C}{dz^2} = \frac{dq_{O_2}}{dz} = -\overline{S}$$

$$\int_0^{F_{O_2}} dq_{O_2} = -\overline{S}\int_{+\delta}^{z} dz$$

Solving, we find:

$$q_{O_2} = -\bar{S}(z - \delta)$$

Substituting for q_{O_2}:

$$-D_{ij}\frac{dC}{dz} = -\bar{S}(z - \delta)$$

Rearranging:

$$dC = -\frac{\bar{S}}{D_{ij}}(z - \delta)\,dz$$

and after integration

$$\int_{C_o}^{C} dC = \frac{\bar{S}}{D_{ij}}\int_{o}^{z}(z - \delta)\,dz$$

we find the profile equation

$$C - C_o = \frac{\bar{S}}{D_{ij}}\left(\frac{z^2}{2} - \delta z\right)$$

ADDITIONAL QUESTIONS

9.10. Confirm that a water potential measured as -2000 J kg^{-1} converts to -2.0 MPa.

9.11. Calculate the heat content of 1 kg of wet ($\theta = 0.4$), sandy soil at 20 °C.

9.12. Calculate the relative humidity in a soil where $\psi = -4000$ J kg^{-1}, $T = 10$ °C.

9.13. **(a)** Find the soil-heat flux at the surface for a soil having the following composition: 40 percent mineral solids, 15 percent organic solids, and 20 percent volumetric water content. A heat flux plate at a 5-cm depth sensed a heat flux of -30 W m^{-2} and thermocouples within the upper 5 cm of soil were used to calculate an average temperature increase of 2 °C in a hour.

(b) What would be the heat flux if half of the soil moisture was ice? (Assume the ice is randomly distributed.)

9.14. **(a)** Find the total evaporation (over the course of a day) from a soil column with initial volumetric water content 15 percent and surface volumetric content of 5 percent. Assume a sandy soil (from question 9.2, use a mean value of $D = 0.265$ cm^2 min^{-1}), and a constant soil temperature.

(b) Assuming that the only energy available for evaporation is derived from net radiation at the surface, calculate the average 24-hour net radiation needed.

9.15. **(a)** Convert 350 ppm$_v$ CO_2 to mg m^{-3} and mmol m^{-3} units when $T = 20$ °C and P = 900 mb.

(b) Compare this result with that calculated for a -10 °C temperature.

9.16. **(a)** Steady-state soil respiration generates CO_2 uniformally from the surface ($z = 0$) to rooting depth ($z = \delta = 1$ m). Assuming that atmospheric concentration at the surface ($C_o = 350$ ppm$_v$) is constant and that there is no sink or source of CO_2 below the roots, derive the CO_2 profile from $z = 0$ to δ.

(b) Assuming that the parameters of respiration rate equation are: $Q_{10} = 3$, $b = 15$, $r_b = 7$ μ · mol m^{-3} s^{-1}, calculate soil CO_2 concentrations in ppmv at the 0.5-m depth when soil temperature is 20 °C, and also when it is 10 °C. Assume that soil temperature is uniformly distributed and is constant, and that the soil-air is a mixture of CO_2 and N_2. Use the Millington-Quirk method to find an equivalent diffusivity in soil with $a = 0.35$ and $\phi = 0.55$.

9.17. Calculate CO_2 flux from the CO_2 concentration measurements obtained from a closed-chamber (cylindrical shape: radius = 15 cm, height = 20 cm) placed on the soil surface. Initial concentration is 360 ppm$_v$; average ambient temperature is 20 °C and pressure is 90 kPa. Calculate flux in μmol m^{-2} s^{-1} and mg m^{-2} s^{-1} units. The IRGA used in the concentration measurements reported the amount of time between 1 ppm$_v$ increases in CO_2 concentration. Here are the times between the 1 ppm$_v$ increases, beginning immediately after chamber placement (in seconds): 1.0, 0.9, 1.3, 0.8, 1.6, 2.4, 3.4, 1.5, 3.0, 4.2.